ON NONLINEAR FINITE ELEMENT ANALYSIS OF SHELL STRUCTURES

by

EDUARDO NATALIO DVORKIN

ING., Universidad Nacional de Buenos Aires
(1974)

S.M. in M.E., Massachusetts Institute of Technology
(1982)

SUBMITTED TO THE DEPARTMENT OF
MECHANICAL ENGINEERING IN PARTIAL FULFILLMENT
OF THE REQUIREMENTS FOR THE DEGREE OF

DOCTOR OF PHILOSOPHY

at the

MASSACHUSETTS INSTITUTE OF TECHNOLOGY

February 1984

© Massachusetts Institute of Technology, 1984

Signature of Author _____
Department of Mechanical Engineering, February 1984

Certified by _____
Klaus-Jürgen Bathe
Thesis Supervisor

Accepted by _____
Warren Rohsenow
Chairman, Departmental Committee on Graduate Studies
Department of Mechanical Engineering

JUL 17 1984 Archives

ON NONLINEAR FINITE ELEMENT ANALYSIS OF SHELL STRUCTURES

by

Eduardo Natalio Dvorkin

Submitted to the Department of Mechanical Engineering on February 1, 1984 in partial fulfillment of the requirements for the Degree of Doctor of Philosophy.

ABSTRACT

A short review of current limitations of methods for nonlinear shell analyses is presented.

A new four-node (non-flat) general quadrilateral shell element for geometric and material nonlinear analysis is presented. The element is formulated using three-dimensional continuum mechanics theory and it is applicable to the analysis of thin and moderately thick shells. The formulation corresponds to the use of a mixed variational principle. The element stiffness matrix is calculated using "full" numerical integration and does not contain spurious zero energy modes.

Also, an algorithm for the automatic incremental solution of nonlinear finite element equations in static analysis is presented. The procedure is designed to calculate the pre- and post-buckling response of general structures. The algorithm includes an eigensolution for calculating linearized buckling loads and associated buckling mode shapes used to impose initial imperfections.

The new shell element is used with the automatic stepping algorithm to analyze various simple to complex shell structures. A study is performed to identify the characteristics of the element regarding convergence, distortion sensitivity and applicability to thin and moderately thick shells. It is demonstrated that the element is very effective both in linear and nonlinear analyses.

Thesis Committee: Prof. K.J. Bathe (Chairman)
Prof. M.P. Cleary
Prof. J.E. Meyer

ACKNOWLEDGEMENTS

I want to express my deep appreciation to Professor Klaus-Jürgen Bathe for his continuous interest, encouragement and guidance throughout this research; working with him has been a most challenging and enjoyable experience.

I also want to thank the other two members of my thesis committee, Professor M.P. Cleary and Professor J.E. Meyer for their very valuable comments and suggestions.

I am very grateful to the people of my country, Argentina, for providing for my early education in our public schools and Universities, to the Organization of American States for their fellowship during 1981-82; and to the ADINA Users Group for their economic support during 1983 and for providing computer time for my research.

I am also very grateful to Ms. Eugenia Model for the accurate typing of this thesis.

Finally, I want to thank my parents and sister for their continuous encouragement and my wife, Elena, for her patience and support. I dedicate this thesis to our daughter, Cora, and to all those who in my country dreamt dreams, even at the price of their lives.

TABLE OF CONTENTS

	PAGE
ABSTRACT	2
ACKNOWLEDGEMENTS	3
TABLE OF CONTENTS	4
LIST OF TABLES	8
LIST OF FIGURES	9
NOTATION	12
1. INTRODUCTION	13
2. CONTINUUM MECHANICS BASED SHELL ELEMENTS FOR GENERAL NONLINEAR ANALYSIS	18
2.1 Element formulation	18
2.2 The element locking problem	24
2.2.1 Four-node element under constant bending moment	26
2.2.2 Simply-supported plate model	27
2.2.3 Curved cantilever	29
2.3 Remedies for the locking problem	29
2.3.1 Reduced and selective integration in the cantilever plate under constant bending moment	31
2.3.2 Reduced integration in the simply-supported plate model	32
2.3.3 Reduced integration in the curved cantilever case	32

TABLE OF CONTENTS (Continued)

PAGE

2.3.4 The element distortion affects the number of zero energy modes obtained when using reduced integration 32

2.4 Final observations on the 3D degenerated shell element . . 34

3. A NEW CONTINUUM MECHANICS BASED FOUR-NODE SHELL ELEMENT FOR GENERAL NONLINEAR ANALYSIS 37

3.1 Basic considerations 37

3.2 Total Lagrangian formulation 47

3.3 Some remarks on the presented element 55

4. SOLUTION OF NONLINEAR FINITE ELEMENT EQUATIONS 56

4.1 Incremental solution algorithm 56

4.1.1 Incremental solution algorithm using modified Newton iterations 58

4.1.1.1 Load constraints 58

4.1.1.2 Iterations within a load step 61

4.1.1.3 Some general remarks 70

4.1.2 Incremental solution algorithm using full Newton iterations 70

4.2 Linearized buckling analysis 71

4.3 Some sample solutions 75

4.3.1 Structure with snap-through characteristic 75

4.3.2 Structures with stiffening characteristics 78

4.3.3 Structure with snap-back characteristic 78

4.3.4 Structures with collapse characteristics 78

TABLE OF CONTENTS (Continued)

	PAGE
4.3.5 Linearized buckling analysis of a circular ring	81
4.3.6 Thermal buckling of a rectangular plate	81
5. NUMERICAL TESTS AND PROBLEM SOLUTIONS	87
5.1 Convergence check	88
5.2 Some simple problems in linear analysis	90
5.2.1 Cantilever linear analysis	90
5.2.2 Linear analysis of simply-supported plate	94
5.3 Linear analysis of a cylindrical (Scordelis-Lo) shell	94
5.4 Linear analysis of a pinched cylinder	98
5.5 Some simple problems of nonlinear analysis	98
5.5.1 Large deflection analysis of a cantilever	98
5.5.2 Analysis of a rhombic cantilever	105
5.6 Geometric nonlinear response of a shallow spherical shell	107
5.7 Linear buckling analysis and large deflection response of a simply-supported stiffened plate	107
5.8 Analysis of elasto-plastic response of a circular plate	109
5.9 Large deflection elastic-plastic analysis of a cylindrical shell	111
5.10 Dynamic analysis of a simply-supported elasto-plastic plate	115
5.11 Circular plate with constant temperature gradient through the thickness	115

TABLE OF CONTENTS (Continued)

		PAGE
6. CONCLUSIONS		119
REFERENCES		121
APPENDIX 1:	An interpretation of reduced integration . . .	130
APPENDIX 2:	An example where the use of reduced integration in nonlinear analysis leads to incorrect results	137
APPENDIX 3:	The new four-node shell element does not contain spurious zero energy modes	140
APPENDIX 4:	Matrices used in the new 4-node shell element	143
APPENDIX 5:	Specialization of the new 4-node shell element for a linear plate element . . .	148

LIST OF TABLES

TABLE		PAGE
1	$t^{\tilde{1}}_{B\ 0^-NL}$	144
2	$t^{=1}_{K\ 0^-NL}$	146
3	$t^{=2}_{K\ 0^-NL}$	147

LIST OF FIGURES

FIGURE		PAGE
2.1	Isoparametric (degenerate) nine-node shell element . . .	19
2.2	Local Cartesian coordinate system used	22
2.3	Cantilever beam under constant bending moment	27
2.4	Analysis of simply-supported plate model	28
2.5	Analysis of a curved cantilever model	30
2.6	Spurious zero energy modes in 8-node shell element . . .	33
3.1	Four-node shell element	38
3.2	Interpolation functions for the transverse shear strains	41
4.1	Maximum ${}^{t+\Delta t}W$ to be used in a step	69
4.2	Analysis of a simple arch structure using updated Lagrangian formulation	76
4.3	Large displacement analysis of a cantilever using total Lagrangian formulation	79
4.4	Analysis of a structure with snap-back characteristic using updated Lagrangian formulation . .	80
4.5	Analysis of a thick-walled elastic-perfectly-plastic cylinder using materially-nonlinear-only or updated Lagrangian formulation	82
4.6	Analysis of a triangular truss structure using updated Lagrangian formulation	83
4.7	Analysis of a 7-bar truss using updated Lagrangian formulation	84
4.8	Analysis of a circular ring under constant pressure	85

LIST OF FIGURES (Continued)

FIGURE		PAGE
4.9	Thermal buckling of a rectangular plate	86
5.1	Patch tests	
5.2	Cantilever subjected to tip bending moment	89
5.3	Response of a cantilever subjected to transverse tip load	91
5.4	Linear analysis of a simply supported plate	92
5.5	Linear analysis of a cylindrical shell subjected to dead weight	95
5.6	Linear analysis of a pinched cylinder	97
5.7	Large deflection analysis of a cantilever using non-distorted elements	99
5.8	Large deflection analysis of a cantilever using distorted elements	101
5.9	Response of a rhombic cantilever subjected to constant pressure	104
5.10	Geometric nonlinear response of a spherical shell	106
5.11	Nonlinear response of a stiffened plate	108
5.12	Response of elastic-perfectly-plastic circular plate subjected to a concentrated load, P, at its center	110 112
5.13	Large deflection elastic-plastic analysis of a cylindrical shell	114
5.14	Dynamic analysis of elastic-plastic plate	116
5.15	Circular plate with constant temperature gradient through the thickness	118

LIST OF FIGURES (Continued)

FIGURE		PAGE
A2.1	Plane structure in nonlinear analysis	137
A2.2	Response of the structure of figure A2.1	139
A5.1	Notation used for Mindlin/Reissner plate theory	150
A5.2	Conventions used in formulation of 4-node plate bending element	152

NOTATION

All notation is defined in the text when used first.

1. INTRODUCTION

The analysis of shell structures, that is to say, the prediction of their load carrying capacities, of their deformations under a given load, the stability limits, and of the effects of manufacturing imperfections on the above, has been for a large number of years an important field of applied work and research for engineers as well as mathematicians [18].

Nowadays, many branches of technology require extremely light and dependable shell structures; this has brought about the requirement for efficient and reliable techniques for general shell structural analyses. In some cases, as in the aeronautical industry, the objective is to analyze thin shell structures, in their pre- and post-buckling regimes; in other cases, as in the nuclear industry, interest lies in the analysis of moderately thick shells, with accidental conditions giving rise to extensive areas of plasticity.

Even for shells with very simple geometric and load configurations, in a static linear-elastic regime, it is frequently not possible to obtain an analytical solution to the differential equations that govern the shell structural behaviors [6-8]. Therefore, the solution for stability limits or complete nonlinear responses involving large displacements, rotations and/or nonlinear material behavior represents a most challenging task.

Usually, when confronting a shell structural analysis, in particular a nonlinear one, the analyst has to resort to a numerical method. The broad development of the finite element method for linear and nonlinear structural analysis, its generality and good numerical characteristics [27-37] has rendered this method the most suitable one for general analysis of

structures.

The purpose of this thesis is to enhance the available capabilities to perform general nonlinear structural analysis of shells including pre- and post-buckling responses, stability calculations, the study of the effects of initial imperfections on the nonlinear response and elastic-plastic regimes.

For efficiently performing a reliable nonlinear finite element analysis of shell structures, there are two main ingredients to be considered:

- The formulation of appropriate shell elements.
- The development of numerical algorithms for solving the equations of motion.

Regarding the first topic, it has been a very active field of research for a large number of years [28, 44]; curved and flat shell elements have been developed, especially for linear analysis, the first ones usually based on deep or shallow shell theories [45, 48-54], the latter ones usually based on plate theory [27, 28, 44]. The applicability of different variational principles corresponding to different finite element formulations has also been extensively investigated [32, 33, 47-49, 71, 80, 81].

During recent years it has become apparent that two approaches for the development of shell elements are very appropriate:

- The use of simple flat elements based on the discrete-Kirchhoff approach for the analysis of thin shells [64, 69, 70].
- The use of degenerated isoparametric elements for the analysis of thin and moderately thick shells, in which fully three-dimensional stress and strain conditions are degenerated to shell behavior.

This approach was introduced for linear analysis in Ref. [55] and implemented in general nonlinear formulations in Refs. [59, 60, 62, 63].

The latter approach has the advantage of being independent of any particular shell theory, being therefore of very general applicability. The element reported in Refs. [62,63] has been employed very successfully when used with 9 or in particular 16 nodes. However, the 16-node element is quite expensive, and although it is possible to use in some analyses only a few elements to represent the total structure, in other analyses still a fairly large number of elements needs to be employed (see Chapter 2 and Ref. [66]).

Considering general shell analyses, much emphasis has been placed onto the development of a versatile, reliable and cost-effective 4-node shell element [71, 73-76, 82, 86]. Such element would complement the above high-order 16-node element and may be more effective in certain analyses. The difficulties in the development of such element lie in that the element should be applicable in a reliable manner to thin and thick shells of arbitrary geometries for general nonlinear analysis.

In Chapter 3, we present a simple 4-node general shell element with the following properties [67]:

- the element is formulated using three-dimensional stress and strain conditions without the use of a specific shell theory;

- the element is applicable to model thin and moderately thick shells of arbitrary geometry, and is non-flat;

- the element is applicable to the conditions of large displacements

and rotations, but small strains, and can be used effectively in material nonlinear analysis.

The formulation of the element is based on continuum mechanics theory, and has good predictive capabilities without containing spurious zero energy modes or numerically adjusted factors. In Chapter 5, we present numerical solutions obtained using our new element.

As mentioned above, the nonlinear finite element analysis of structures requires the use of accurate and reliable finite element models and, of equal importance, the use of efficient procedures for the solution of the incremental equations of motion. The equation solution procedures are efficient when, for a given solution accuracy, the computer cost of solution is low and the solution is obtained in a reliable manner with a minimum amount of effort by the analyst.

In Chapter 4, we describe an algorithm [90] for the automatic solution of the nonlinear equations of static equilibrium. The algorithm is used in Chapter 5 for the solution of nonlinear shell problems.

When analyzing structures that, due to their material constitutive relation and/or large displacements and/or strains, present a nonlinear static equilibrium path in the load-displacement space [15], the engineer usually seeks to determine the location of the critical points (bifurcation and limit points) and sometimes to continue the analysis beyond these points (post-buckling analysis [13]). Using a load-controlled incremental algorithm [29, 89] the existence of critical points must be inferred from error messages printed by the finite element program (which can require significant experience on the part of the analyst to interpret), and to

carry on the analysis through the critical points, some special methods have to be used (e.g. artificial springs [93]). However, those methods require some advanced information about the equilibrium path that is being sought and also some post-processing work by the analyst.

The algorithm we present in Chapter 4 can automatically trace static nonlinear equilibrium paths in general finite element structural analyses.

The above algorithm is very general but, although effective, can still lead to a high solution cost because an incremental solution is performed. In some analyses for which the pre-collapse displacements are negligible, it is valuable to calculate only an estimate of the buckling load of the structure, without going through a solution for the complete nonlinear response. This may, for some structures, be achieved economically by a linearized buckling analysis [12, 14]. In Chapter 4, we present an algorithm for calculating linearized buckling loads of a general finite element model [90], and in Chapter 5, we apply this algorithm to shell problems. The main features of the linearized buckling algorithm that we present are:

- it is easy to implement in an existing nonlinear finite element code, and

- numerically, it can handle eigenproblems where positive and negative eigenvalues are present.

The new four-node shell element, used in conjunction with the algorithms described above, enables us to perform efficient and reliable general nonlinear shell structural analysis.

2. CONTINUUM MECHANICS BASED SHELL ELEMENTS FOR GENERAL NONLINEAR ANALYSIS.

In this chapter we first briefly review the formulation of the shell element presented in Refs. [62, 63], and then investigate its locking problem, that renders this element (especially in its low order versions), sometimes ineffective for the analysis of thin shells [66].

This investigation will lead us into the development of a new shell element, to be presented in Chapter 3.

2.1 Element formulation

For an element with q midsurface nodes, the position vector, $\underline{x}$, of any interior particle with convected (natural) coordinates r_i at a given time t, is assumed to be (see Fig. 2.1),

$$ {}^t\underline{x} = \sum_{k=1}^{q} h_k(r_1, r_2)\, {}^t\underline{x}_k + \frac{r_3}{2} \sum_{k=1}^{q} a_k h_k(r_1, r_2)\, {}^t\underline{V}_n^k \qquad (2.1) $$

where:

- ${}^t\underline{x}_k$: position vector of the nodal point k, at time t;
- $h_k(r_i)$: interpolation function corresponding to node k, (see Ref. [29, Fig. 5.5]);
- ${}^t\underline{V}_n^k$: unit director vector at nodal point k, at time t, this director vector is not necessarily normal to the midsurface of the element;

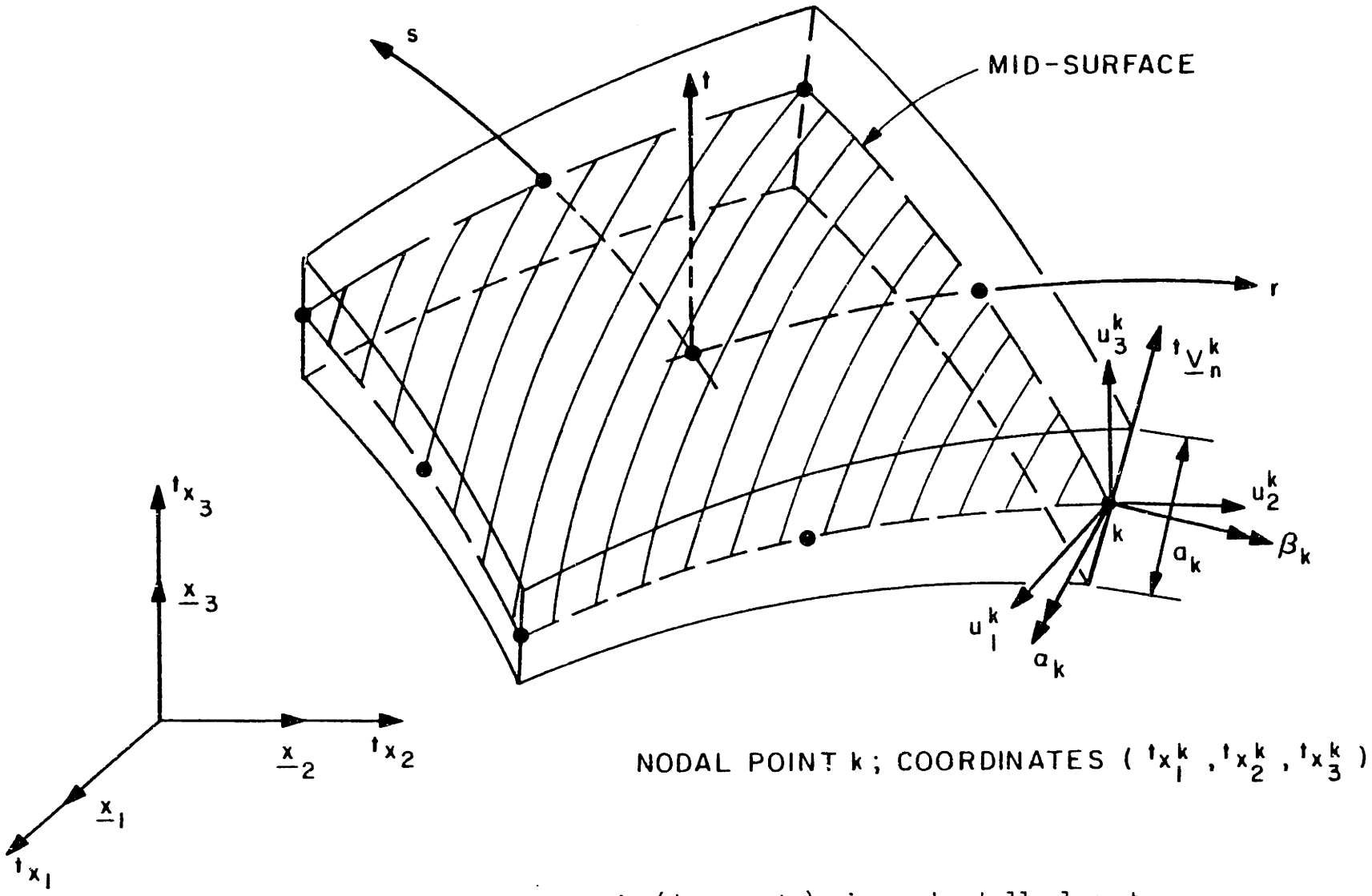


Figure 2.1 Isoparametric (degenerate) nine-node shell element

a_k : thickness of the element at node k, measured along ${}^t\underline{V}_n^k$.

Note that Eq. (2.1) describes a variable thickness shell element.

The displacement of an arbitrary particle at time t, measured from the reference configuration at time 0, is

$$ {}^t\underline{u} = {}^t\underline{x} - {}^0\underline{x} \tag{2.2-a} $$

$$ {}^t\underline{u} = \sum_{k=1}^{q} h_k(r_1, r_2)\, {}^t\underline{u}_k + \frac{r_3}{2} \sum_{k=1}^{q} h_k(r_1, r_2)\, a_k\, ({}^t\underline{V}_n^k - {}^0\underline{V}_n^k) \tag{2.2-b} $$

where ${}^t\underline{u}_k$ is the displacement vector corresponding to the node k.

The kinematic description of Eqs. (2.1) and (2.2) incorporates the following assumptions:

a) The director vectors remain straight during the deformations.

b) The thickness of the element, measured along a director vector remains constant during the deformations.

These are the only kinematic assumptions introduced; therefore, the description is very general, incorporating also shear deformations.

Similarly, for any particle, the incremental displacement measured from the configuration at time t is

$$ \underline{u} = \sum_{k=1}^{q} h_k(r_1, r_2)\, \underline{u}_k + \frac{r_3}{2} \sum_{k=1}^{q} a_k\, h_k(r_1, r_2) \tag{2.3} $$

$$ (-{}^t\underline{V}_2^k \alpha_k + {}^t\underline{V}_1^k \beta_k) $$

where:

$$ {}^{t}\underline{V}_1^k = \frac{\underline{e}_2 \times {}^{t}\underline{V}_n^k}{|\underline{e}_2 \times {}^{t}\underline{V}_n^k|} \tag{2.4-a} $$

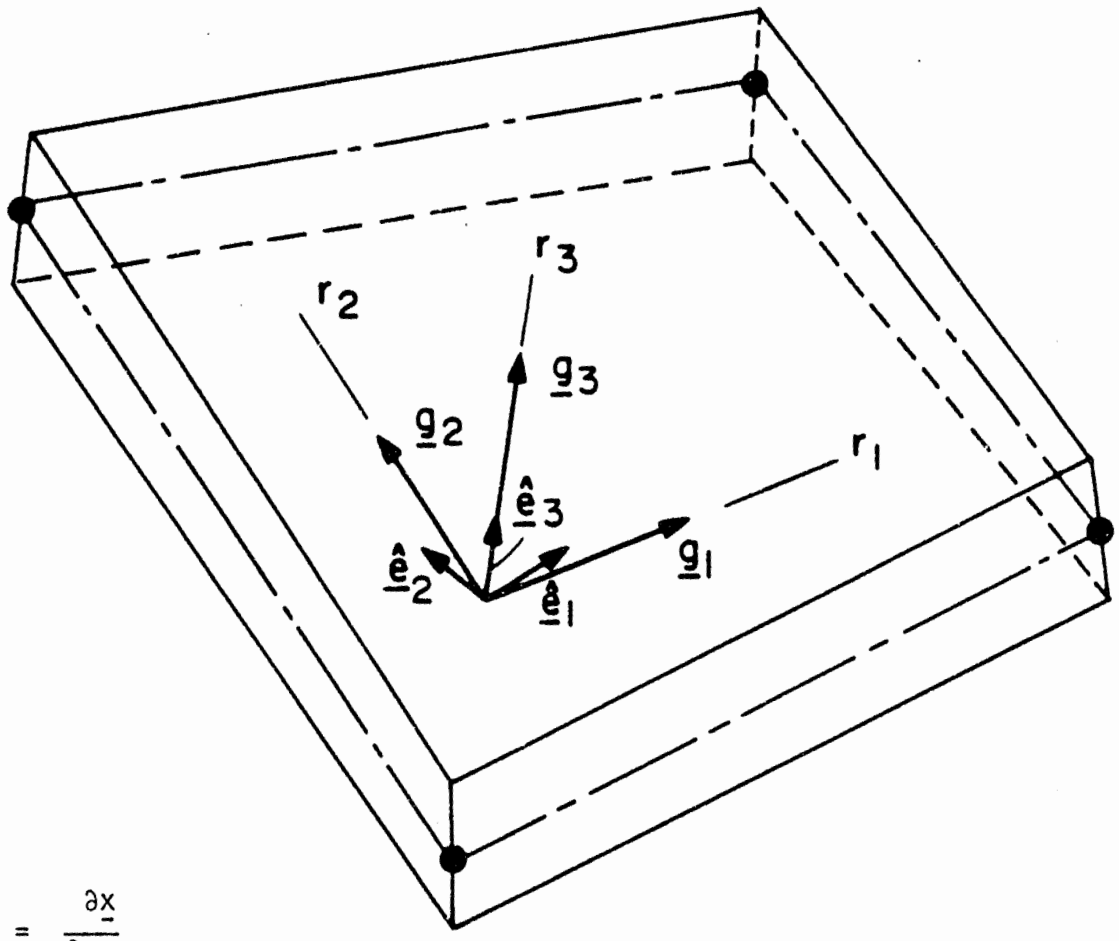
$$ {}^{t}\underline{V}_2^k = {}^{t}\underline{V}_n^k \times {}^{t}\underline{V}_1^k \tag{2.4-b} $$

and α_k, β_k are the incremental rotations about the above vectors.

Since the kinematics of the element has been totally described, we will focus our attention on the constitutive relations. Defining the local Cartesian system $\hat{\underline{e}}_i$ of Fig. 2.2, the incremental consitutive tensor ${}_0\underline{C}$ [29] must reflect the shell assumption ${}^{t}\tau^{33} = 0$ [6-8]; therefore as shown in [29, 62, 63], the constitutive tensor is formed in the $\hat{\underline{e}}_i$ system, representing the above assumption, and then rotated to the global Cartesian system.

In the standard manner shown in [29, 62, 63], the equation for the linearized incremental step from time t to time t+Δt is formulated, for a total Lagrangian (T.L.) formulation [29], as

$$ ({}_0^{t}\underline{K}_L + {}_0^{t}\underline{K}_{NL})\,\underline{U} = {}^{t+\Delta t}\underline{R} - {}_0^{t}\underline{F} \tag{2.5} $$



$$\underline{g}_i = \frac{\partial \underline{x}}{\partial r_i}$$

$$\hat{\underline{e}}_3 = \frac{\underline{g}_3}{|\underline{g}_3|} \quad ; \quad \hat{\underline{e}}_1 = \frac{\underline{g}_2 \times \hat{\underline{e}}_3}{|\underline{g}_2 \times \hat{\underline{e}}_3|} \quad ; \quad \hat{\underline{e}}_2 = \hat{\underline{e}}_3 \times \hat{\underline{e}}_1$$

Figure 2.2 Local Cartesian coordiante system used

where

${}^{t}_{0}\underline{K}_{L}$ and ${}^{t}_{0}\underline{K}_{NL}$ are the incremental linear and nonlinear stiffness matrices;

$$\underline{U}^{T} = [\, U_1^1 \; U_2^1 \; U_3^1 \; \alpha_1 \; \beta_1 \; \ldots\ldots \; U_1^q \; U_2^q \; U_3^q \; \alpha_q \; \beta_q \,] \qquad (2.6)$$

and

${}^{t+\Delta t}\underline{R}$: external nodal load vector acting at time $t+\Delta t$;

${}^{t}_{0}\underline{F}$: vector of nodal forces equivalent to the stresses at time t.

Equation (2.5) represents a linearized approximation to the step; in order to obtain an equilibrium configuration at time $t+\Delta t$, equilibrium iterations must be performed, see Ref. [29, Chapter 8]. It must also be stated that since finite rotations are not vectors [1], each incremental step can only represent infinitesimal rotations, finite rotations are to be accomodated in the equilibrium iterations.

In Refs. [62, 63] also the matrices corresponding to an updated Lagrangian (U.L.) formulation [29] have been presented.

It must be noted that this element can be employed in the following analysis conditions:

a) Arbitrary large displacements/large rotations, but small strains.

Since the thickness of the element is not updated during the solution, the element is only applicable to small strain analysis [88, Appendix A]. With this restriction, the T.L. formulation is particularly

attractive; namely, since the components of the second Piola-Kirchhoff stress and Green-Lagrange strain tensors are invariant under rigid body motions [1, 5, 29], for small strains, the second Piola-Kirchhoff stress tensor and Green-Lagrange strain tensor can be used in the constitutive relations without having to consider the element fiber rotations [29]. Also, as the element will only be used to represent small strain deformations, the assumption ${}^{t}_{0}S_{33} = 0$ can be used, instead of the more natural one ${}^{t}\tau_{33} = 0$ when deriving the constitutive relations [29, 109]. Note that ${}^{t}_{0}S_{33}$ is the normal second Piola-Kirchhoff stress component at time t, referred to the configuration at time 0, in the ${}^{0}\hat{e}_{3}$ direction.

b) The element is formulated with 5 degrees of freedom per mid-surface node, but in some applications (e.g. when connecting with isobeam elements [29], to model stiffened shells) it is convenient to use instead of α_K and β_K three rotations about the global coordinate axes. In this case, we simply transform the obtained stiffness matrices and equivalent nodal force vectors in the standard manner [29].

c) The element is formulated including shear effects (as in a Mindlin-Reissner type of shell theory [9, 10]), although these are only included assuming a constant shear stress over the element thickness. Therefore the element is applicable to the analysis of moderately thick shells. Many results obtained with this element can be found in Refs. [62, 63, 65, 66].

2.2 The element locking problem

To discuss the locking problem [56, 57, 65, 66], let us consider

first an elastic plate element; the expression of its total potential energy can be written [29] as

$$\Pi = \frac{h^3}{2}\left[\int_A \underline{\chi}^T \underline{C}_b \underline{\chi}\, dA + \alpha \int_A \underline{\gamma}^T \underline{C}_s \underline{\gamma}\, dA\right] \tag{2.7}$$

where

$$\underline{\chi} = \begin{bmatrix} \beta_{1,1} \\ -\beta_{2,2} \\ \beta_{1,2} - \beta_{2,1} \end{bmatrix} \; ; \quad \underline{\gamma} = \frac{1}{L}\begin{bmatrix} U_{3,2} - \beta_2 \\ U_{3,1} + \beta_1 \end{bmatrix} \tag{2.8}$$

$$\underline{C}_b = \frac{E}{12(1-\nu^2)}\begin{bmatrix} 1 & \nu & 0 \\ \nu & 1 & 0 \\ 0 & 0 & (1-\nu)/2 \end{bmatrix} \; ; \quad \underline{C}_s = \frac{E\,k}{2(1+\nu)}\begin{bmatrix} 1 & 0 \\ 0 & 1 \end{bmatrix} \tag{2.9}$$

and

E : Young's modulus;

ν : Poisson's ratio;

k : shear correction factor [29];

U_3 : transverse displacement of the plate;

β_i : section rotation about x_i ;

L : characteristic length of the element;

h : thickness of the plate (assumed constant);

$$\alpha = \left(\frac{L}{h}\right)^2 \xrightarrow[h \to 0]{} \infty$$

The second term on the right hand side of Eq. (2.7) can be regarded as a penalty term [29, 39, 40] for imposing the condition

$$\underline{\gamma} \xrightarrow[h \to 0]{} \underline{0} \tag{2.10}$$

that is to say, for imposing the Kirchhoff-Love condition for thin shells [6-8].

The locking problem appears because, in some cases, $\underline{\gamma} \equiv \underline{0}$ cannot be represented by the trial functions that span the finite element solution space.

In what follows, we will consider some examples that illustrate the locking problem.

2.2.1 Four node element under constant bending moment

For this first example let us consider a very narrow cantilever plate element, so the problem can be formulated, as shown in Fig. 2.3, with only two degrees of freedom (isobeam element [29]).

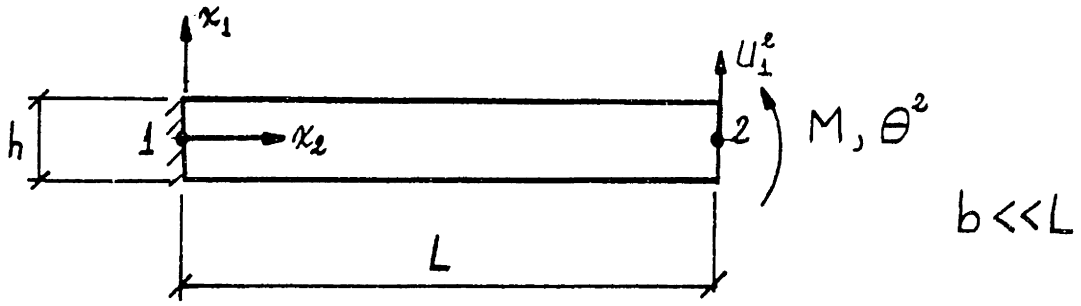


Figure 2.3. Cantilever beam under constant bending moment.

Invoking $\delta \Pi = 0$ and comparing with the analytical solution for a cantilever beam, we get:

$$\frac{\theta_{FE}^2}{\theta_{AN}^2} = \frac{1}{1 + \frac{Gk}{E}\left(\frac{L}{h}\right)^2} \tag{2.11}$$

For thick elements, $(L/h) \longrightarrow 0$, therefore $(\theta_{FE}/\theta_{AN}) \longrightarrow 1$.

For very thin elements, $(L/h) \longrightarrow \infty$, therefore $(\theta_{FE}/\theta_{AN}) \longrightarrow 0$;

and we say that the thin element locks.

2.2.2 Simply-supported plate model

We analyze the problem shown in Fig. 2.4 in which one 16-node element models one quarter of a simply-supported square plate subjected

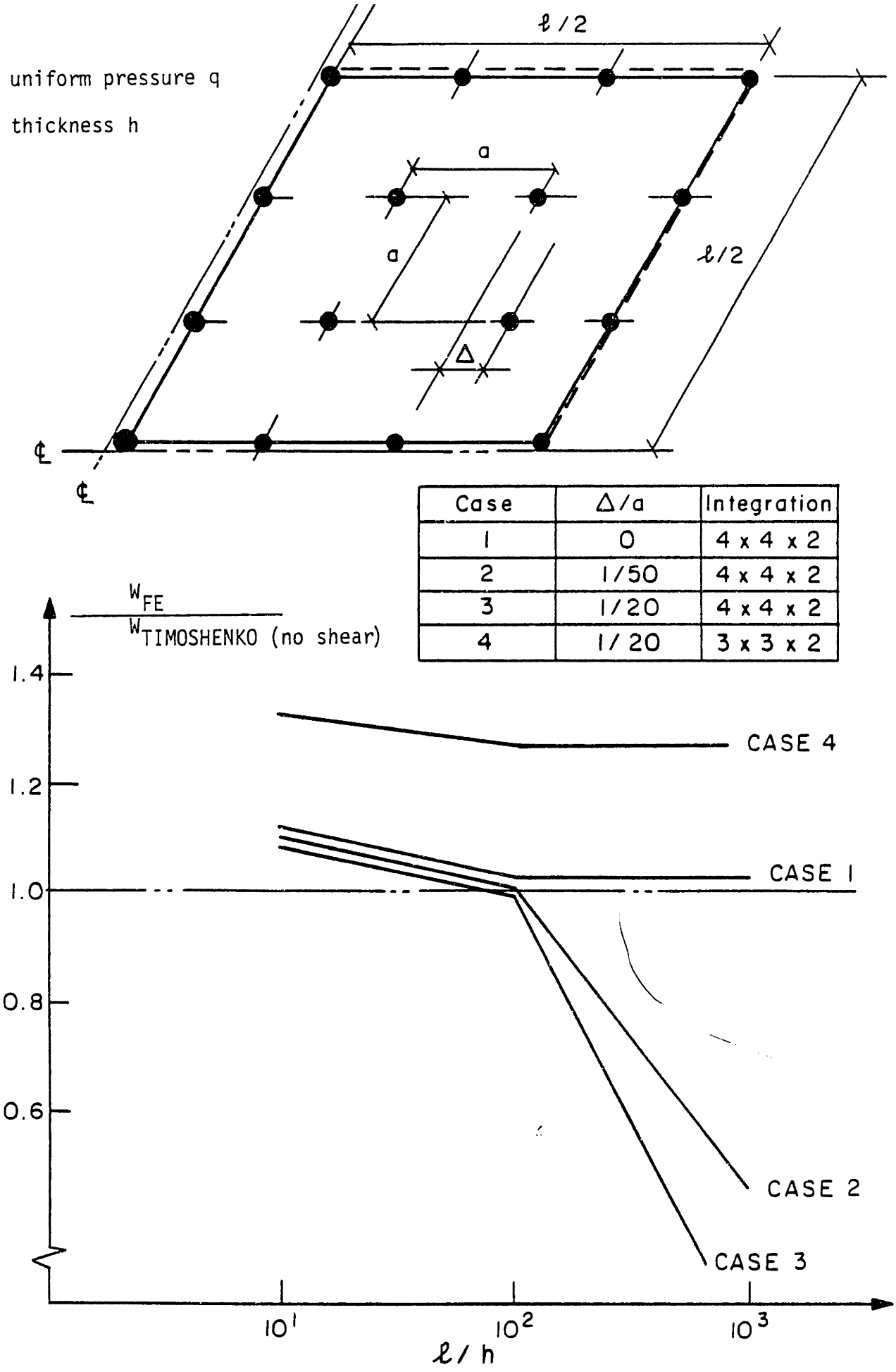


Figure 2.4 Analysis of simply-supported plate model

to a constant pressure load. Figure 2.4 shows that when using normal numerical integration and if the element is distorted as in Cases 2 and 3 (the Jacobian is not constant), the element locks for (l/h) > 100.

2.2.3 Curved cantilever

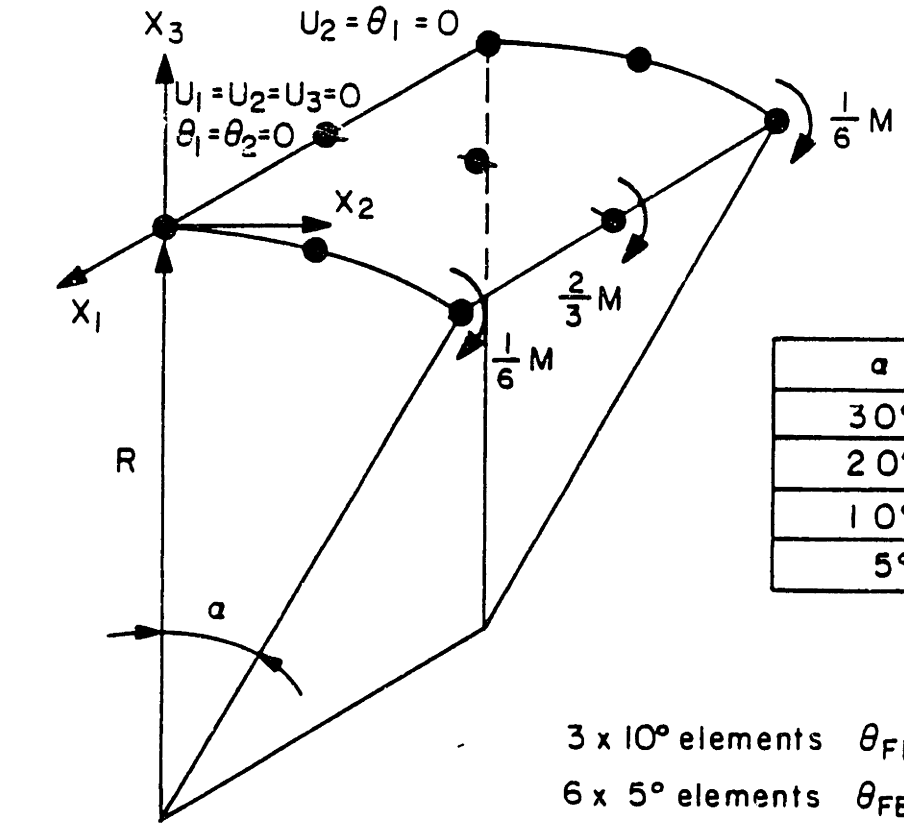
Figure 2.5 shows a curved cantilever modeled using one single parabolic element and the results obtained using a high integration order. We observe that for larger angles spanned by the element the results rapidly deteriorate. However, the locking phenomenon is an element property so that with 6 elements to model the 30° bend reasonable results are obtained. Figure 2.5 also shows that the cubic element behaves considerably better than the parabolic element, but this element behavior deteriorates when the element is distorted in its mid-surface.

Note that, as expected, the element behavior becomes less sensitive to distortion when the element thickness increases. For example, when one parabolic element is used to model the 30° bend for a thickness h=1.2, the value for $\theta_{FE} / \theta_{TH}$ is 0.46.

2.3 Remedies for the locking problem

The matrices in Eq. (2.5) are calculated using numerical integration, usually the Gauss rule [29]. If the number of Gauss integration stations is enough to exactly evaluate the integrals, complete numerical integration is being used; if not, reduced numerical integration is being used [28, 29].

It has been observed that when the matrices in Eq. (2.5) are calculated using either uniform reduced numerical integration or selective

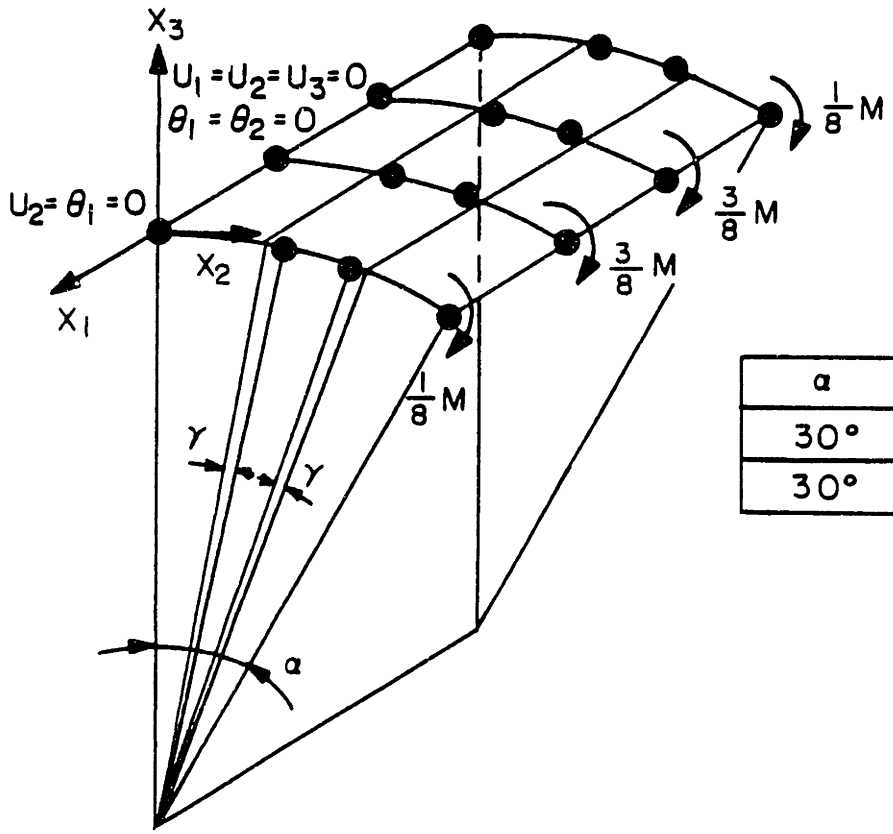


R = 20
h (thickness) = 0.2
E = 2.1×10^6
ν = 0.3
Int = 4x4x2

α	θ_{FE}/θ_{TH}
30°	0.02
20°	0.09
10°	0.62
5°	0.96

3 x 10° elements $\theta_{FE}/\theta_{TH} = 0.61$

6 x 5° elements $\theta_{FE}/\theta_{TH} = 0.96$



R = 20
h (thickness) = 0.2
E = 2.1×10^6
ν = 0.3
Int = 4x4x2

α	γ	θ_{FE}/θ_{TH}
30°	0°	0.91
30°	4°	0.01

Figure 2.5 Analysis of curved cantilever model
(Note that the figure is not to scale)

reduced numerical integration on the shear terms [56, 57, 66, 73-75], the element does not lock. After the first pragmatic approaches to reduced integration, researches have linked it to different variational formulations [38, 80, 81]. In Appendix 1, we identify reduced integration with a mixed formulation in which strains are interpolated, and show that, if the exactly integrated element is complete, the element formulated using reduced integration is also complete. The important problem that the usage of reduced integration presents is that reduced integration can result into rank deficiency of the stiffness matrix; that is to say, it can give rise to spurious zero energy modes.

Let us now analyze the effects of using reduced integration on the examples presented in Section 2.2.

2.3.1 Reduced and selective integration in the cantilever plate under constant bending moment

In this particular case, the use of uniform reduced or selective reduced integration on the shear terms does not produce spurious zero energy modes [80].

Using selective and uniform reduced integration along the axial direction we get:

$$\frac{\theta_{SI}}{\theta_{AN}} = 1. \qquad (2.12\text{-a})$$

$$\frac{\theta_{RI}}{\theta_{AN}} = 1. \qquad (2.12\text{-b})$$

Hence, using either selective or uniform reduced integration along the axial direction 1-2, the locking problem is removed. As can be seen from Eqs. (2.12), in this case selective integration provides the same solution than uniform reduced integration.

2.3.2 Reduced integration in the simply supported plate model

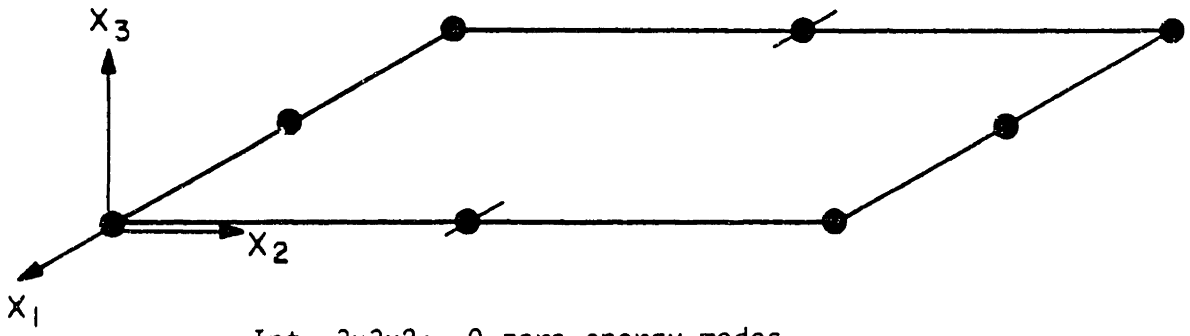
Figure 2.4 shows that for the plate problem the usage of reduced integration over the mid-surface remedies the locking problem, even in the case with higher element distortion; although it provides a too flexible model (Case 4).

2.3.3 Reduced integration in the curved cantilever case

The use of reduced integration does not help in the solution of this model. Gauss integration of order 2x2 and 3x3 over the mid-surface for the parabolic and cubic element models, respectively, results into spurious zero eigenvalues preventing the solution of the governing equations. That is different from the solution of the model used in the analysis of the simply supported plate, for which reduced integration gives much improved results when the element is distorted.

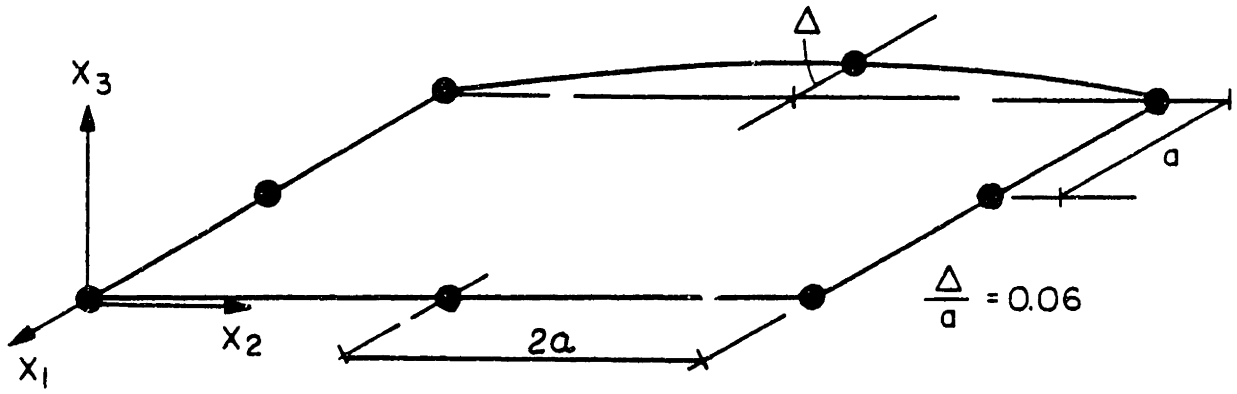
2.3.4 The element distortion affects the number of zero energy modes obtained when using reduced integration

Figure 2.6 illustrates the effect of distortions on an 8-node shell element. We observe that the in-plane element distortion does not reduce the number of spurious kinematic modes, whereas the out-of-plane distortion eliminates these modes.



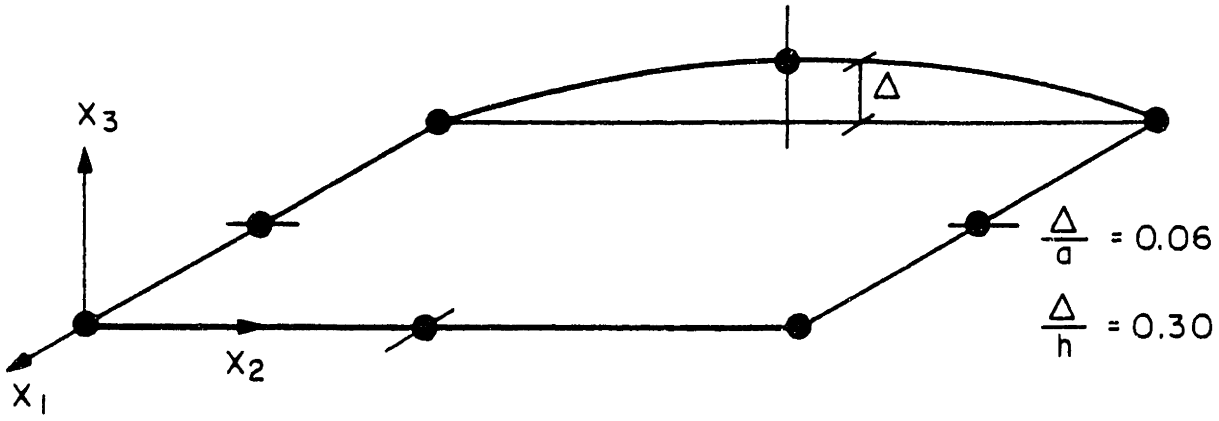
Int. 3x3x2: 0 zero energy modes
Int. 2x2x2: 2 zero energy modes

a) No Distortion



Int. 2x2x2: 2 zero energy modes

b) In-Plane Distortion



Int. 2x2x2: 0 zero energy modes

c) Out-of-Plane Distortion

Figure 2.6 Spurious zero energy modes in 8-node shell element

2.4 Final observations on the 3D degenerated shell element

Considering the isoparametric shell element, the appropriate number of nodal points and the appropriate Gauss integration order must be chosen. For the discussion of these issues we distinguish between the analysis of moderately thick plates/shells and thin plates/shells.

a) Moderately thick plates and shells

These structures can be analyzed using the isoparametric element with any of its nodal configurations, but the Lagrangian quadratic and cubic elements are usually most effective. The integration schemes frequently best for these elements are 3x3 and 4x4 Gauss integration over the mid-surface but the uniform reduced integration 2x2 and 3x3 may be of advantage, when the elements are distorted (as discussed below). The order of Gauss integration through the element thickness depends on whether an elastic (2 point integration) or elastic-plastic (4 point integration or more) analysis is performed.

b) Thin plates and shells

The constraint to be satisfied in the analysis of very thin plates and shells is that of negligible transverse shear deformations. In general, the shell element displacement interpolations will not be able to represent the constraint of zero shear strains through the element, and reduced/selective integration can be used as we have discussed above.

As guidelines for using these shell elements, we suggested in Ref. [66]:

- The locking of an element is an element property and hence the

element aspect ratio (length/thickness) and element distortion must be kept a minimum. If these conditions are met, high order integration (3x3 Gauss integration for the quadratic and 4x4 Gauss integration for the cubic element) provides a reliable solution.

- To establish an appropriate mesh for the analysis of a shell, it may be useful to test a single element with the typical thickness and curvature of the shell. The analysis of the element (which would have typical dimensions to be used in the actual shell analysis) subjected to a bending moment would display whether the element is too large and locks.

In the above, we have emphasized the use of uniform reduced integration rather than selective integration. The reason is that selective integration has the same disadvantage of uniform reduced integration, that is the presence of spurious rigid body modes, and its implementation is more complicated when general nonlinear material models have to be considered [75].

We believe that in a general nonlinear analysis, the presence of spurious rigid body modes, at the element level, is not desirable, even if for the configuration at time 0 the element assemblage prevents those modes from manifesting themselves. This has also been mentioned in Ref. [61].

In Appendix 2, we present a very simple case, in which when using reduced integration, the spurious kinematic modes are restrained in the configuration at time 0; but, during the nonlinear analysis, they are freed, and the model predicts a wrong collapse load.

Many efforts have been reported in the literature to develop plate and shell elements without spurious zero energy modes and with no locking problem [73-84]; but there is still room for improved methods, in particular when considering nonlinear analysis.

3. A NEW CONTINUUM MECHANICS BASED FOUR-NODE SHELL ELEMENT FOR GENERAL NONLINEAR ANALYSIS

In this chapter we present the theoretical formulation of a new 4-node shell element, based on continuum mechanics theory and a mixed finite element formulation [67].

3.1 Basic considerations

The formulation of the 4-node shell element represents an extension of the shell element discussed in the previous chapter, and we therefore use the same notation. Also, to focus attention onto some key issues of the formulation, we consider in this first section only linear analysis conditions.

The geometry of the element, see Fig. 3.1 and Eq. (2.1), is described using

$$ {}^{t}x_i = \sum_{k=1}^{4} h_k \, {}^{t}x_i^k + \frac{r_3}{2} \sum_{k=1}^{4} a_k h_k \, {}^{t}V_{ni}^k \qquad (3.1) $$

where,

${}^{t}x_i$: Cartesian coordinates of any point in the element;

${}^{t}x_i^k$: Cartesian coordinates of nodal point k.

The left superscript is zero for the initial geometry of the element and is equal to 1 for the deformed element geometry. Note that the thickness of the element varies, and the element is in general non-flat.

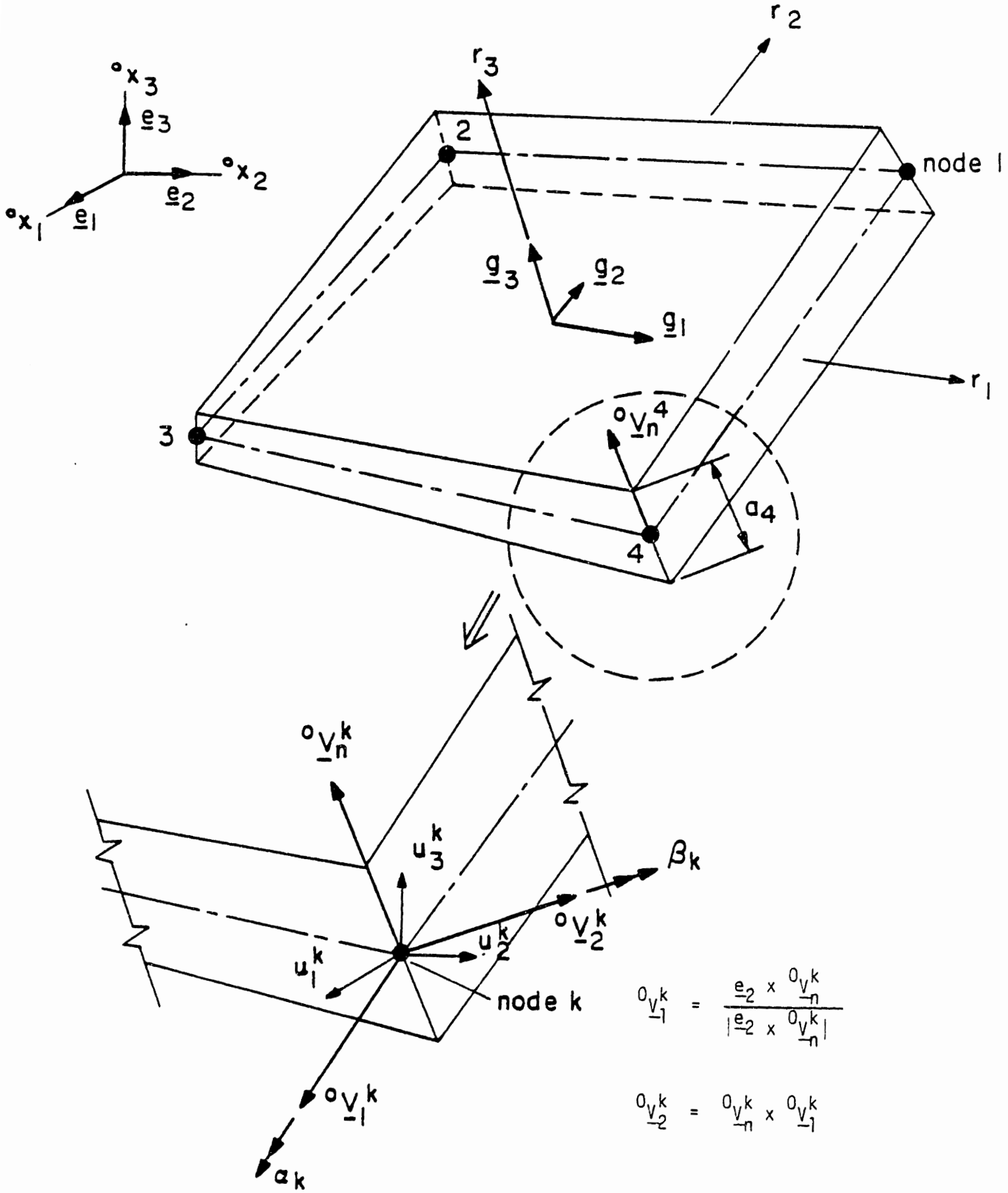


Figure 3.1 Four-node shell element

The displacements of any particle, with natural coordinates r_i , inside the shell element, in the stationary Cartesian coordinate system are (see Eq. (2.3)):

$$u_i = \sum_{k=1}^{4} h_k u_i^k + \frac{r_3}{2} \sum_{k=1}^{4} a_k h_k (-{}^{\circ}V_{2i}^k \alpha_k + {}^{\circ}V_{1i}^k \beta_k) \qquad (3.2)$$

A basic problem inherent in the use of the above interpolation of the displacements, and the derivation of the strain-displacement matrices therefrom, as seen in the previous chapter, is that the element locks when it is thin. This is due to the fact that with these interpolations the transverse shear strains cannot vanish at all points in the element, when it is subjected to a constant bending moment. Hence, although the basic continuum mechanics assumptions contain the Kirchhoff-Love shell assumptions, the finite element discretization is not able to represent these assumptions rendering the element not applicable to the analysis of thin plates and shells.

Considering our element formulation — because the problem lies in the representation of the out-of-surface shear strains — we proceed to not evaluate these shear strains from the displacements in Eq. (3.2), but to introduce separate interpolations for these strain components, using therefore a mixed finite element method [29, 32-34].

Since we consider non-flat shell elements, the separate interpolations are performed effectively in a convected coordinate system [2-4].

Note that in Refs. [29, 62, 63], the shell element formulation is discussed in the global stationary coordinate system, because all displacement components are interpolated in the same way. To emphasize that we use here stress and strain tensor components measured in the convected coordinate system, we place a curl ($\sim$) over these quantities.

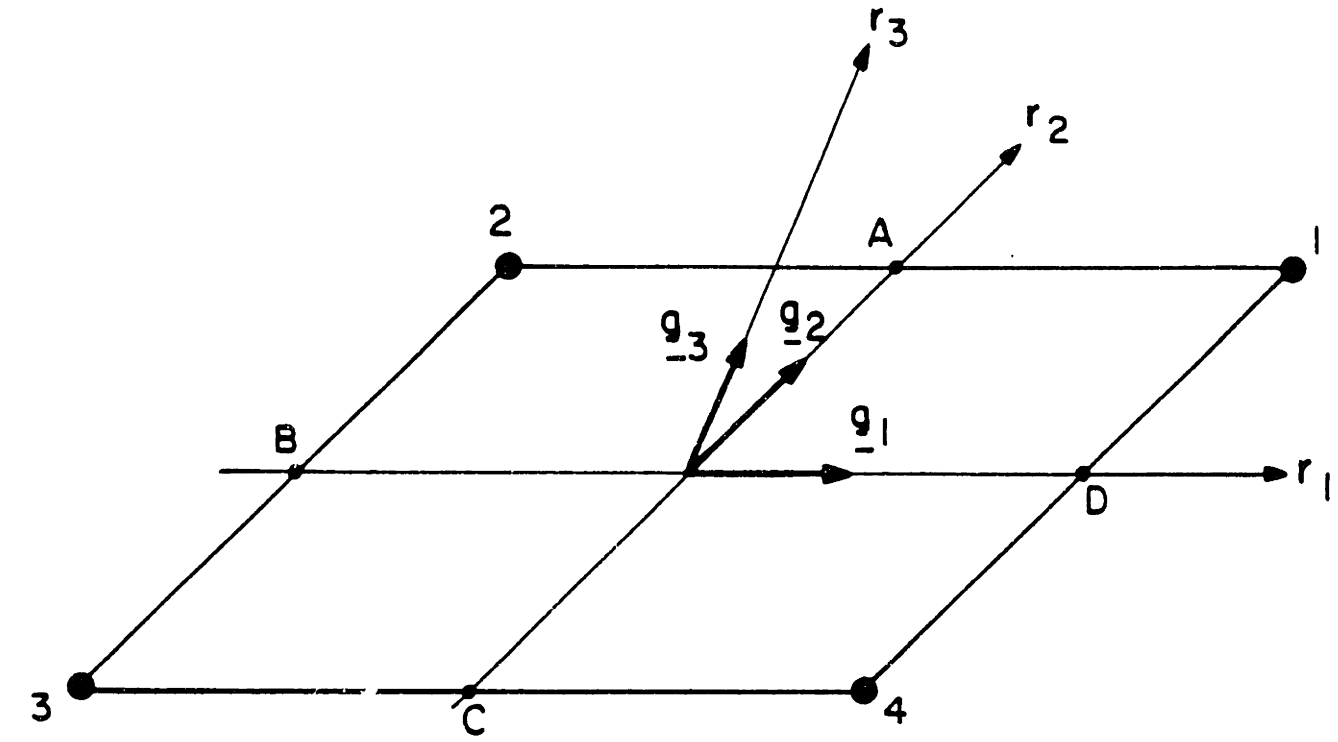
The choice for the interpolation for the transverse shear strain components is the key assumption in our element formulation, because adequate coupling between the element displacements and rotations must be introduced and the element should not exhibit any spurious zero energy modes. For our element, we use, see Fig. 3.2,

$$\begin{aligned}\tilde{\epsilon}_{13} &= \frac{1}{2}(1+r_2)\,\tilde{\epsilon}^{A}_{13} + \frac{1}{2}(1-r_2)\,\tilde{\epsilon}^{C}_{13}\\ \tilde{\epsilon}_{23} &= \frac{1}{2}(1+r_1)\,\tilde{\epsilon}^{D}_{23} + \frac{1}{2}(1-r_1)\,\tilde{\epsilon}^{B}_{23}\end{aligned} \tag{3.3}$$

Since the kinematic relations for the above shear strains are not satisfied using Eq. (3.3), we impose them using Lagrange multipliers [3, 29] to obtain the following functional for the modified potential energy:

$$\Pi^{*} = \frac{1}{2}\int_V \tilde{\tau}^{ij}\,\tilde{\epsilon}_{ij}\,dV + \int_V \lambda^{13}(\tilde{\epsilon}_{13}-\tilde{\epsilon}^{DI}_{13})\,dV$$

$$+\int_V \lambda^{23}(\tilde{\epsilon}_{23}-\tilde{\epsilon}^{DI}_{23})\,dV - W^{\sigma} \tag{3.4}$$





$\tilde{\epsilon}_{13}$ interpolation



$\tilde{\epsilon}_{23}$ interpolation

Figure 3.2 Interpolation functions for the transverse shear strains

where the $\tilde{\tau}^{ij}$ are the contravariant tensor components of the Cauchy stress tensor [2, 4], the $\tilde{\epsilon}_{ij}$ are the covariant tensor components of the infinitesimal strain tensor, the λ^{13} and λ^{23} are the Lagrange multipliers, the $\tilde{\epsilon}^{DI}_{13}$ and $\tilde{\epsilon}^{DI}_{23}$ are the transverse shear strain evaluated using the displacement interpolations in Eq. (3.2), and W^{ϕ} is the potential of the external loads. For the Lagrange multipliers we choose the following interpolations:

$$\lambda^{13} = \lambda^{A}\,\delta(\Gamma_1)\,\delta(1-\Gamma_2) \;+\; \lambda^{C}\,\delta(\Gamma_1)\,\delta(1+\Gamma_2)$$

$$\lambda^{23} = \lambda^{D}\,\delta(\Gamma_2)\,\delta(1-\Gamma_1) \;+\; \lambda^{B}\,\delta(\Gamma_2)\,\delta(1+\Gamma_1) \tag{3.5}$$

where $\delta(\cdots)$ is the Dirac-delta function. This represents a weakening of the Lagrange multiplier constraint in Eq. (3.4) [41].

In order to introduce a physical interpretation of Eqs. (3.5), we can think of two independent systems:

- the mid-surface of the element,
- the director vectors;

These two systems have to be linked in order to avoid the presence of spurious rigid body modes in the element. When they are linked at every point in the element (as in the formulation discussed in Chapter 2), the locking problem is encountered; therefore, our aim is to impose a constraint between those two systems, that while preventing the presence of spurious

zero energy modes, does not produce locking. Equations (3.5) can be regarded as representing the localized shear stress introduced by idealized springs acting at A, B, C, D between the above two systems.

This discrete representation of the shear deformations inside an element is only valid because even for moderately thick shells, the shear deformations are a small percentage of the total deformations. If this is not the case, a fully three-dimensional analysis should be performed, rather than considering the structure as a shell.

Substituting from Eq. (3.5) into Eq. (3.4) and invoking that $\delta \Pi^* = 0$ gives the distinct constraints,

$$\tilde{\epsilon}_{13}\Big|_A = \tilde{\epsilon}_{13}^{DI}\Big|_A \qquad \tilde{\epsilon}_{13}\Big|_C = \tilde{\epsilon}_{13}^{DI}\Big|_C$$

$$\tilde{\epsilon}_{23}\Big|_D = \tilde{\epsilon}_{23}^{DI}\Big|_D \qquad \tilde{\epsilon}_{23}\Big|_B = \tilde{\epsilon}_{23}^{DI}\Big|_B \tag{3.6}$$

Hence the complete element stiffness matrix is calculated using the functional:

$$\Pi^* = \frac{1}{2}\int_V \tilde{\tau}^{ij}\,\tilde{\epsilon}_{ij}\,dV - W^{\phi} \tag{3.7}$$

with stress and strain components in convected coordinates and

- Eqs. (3.1) and (3.2) to evaluate the "in-surface" strain components $\tilde{\epsilon}_{11}$, $\tilde{\epsilon}_{22}$, $\tilde{\epsilon}_{33}$;

- Eqs. (3.3) to evaluate the strain component $\tilde{\epsilon}_{13}$, $\tilde{\epsilon}_{23}$; and
- Eqs. (3.6) to express the variables $\tilde{\epsilon}^{A}_{13}, \tilde{\epsilon}^{C}_{13}$, $\tilde{\epsilon}^{D}_{23}$ and $\tilde{\epsilon}^{B}_{23}$ in terms of the nodal point displacements and section rotations of Eq. (3.2).

Considering the representation that we have chosen for the transverse shear strains, we can make the following three important observations:

1) The element is able to represent the six rigid body modes. The element contains the rigid body modes because zero strains are calculated in the formulation when the element nodal point displacements and rotations correspond to an element rigid body displacement. This can be verified by using Eqs. (3.1) to (3.6) to evaluate the strains, but more easily we can use the fact that the 4-node shell element of Refs. [62, 63] satisfies the rigid body mode criterion. Hence, for a rigid body mode displacement the $\tilde{\epsilon}^{DI}_{13}$ and $\tilde{\epsilon}^{DI}_{23}$ are zero, from which it follows that also the shear strains in Eqs. (3.3) are zero, and the rigid body mode criterion is satisfied.

2) The element can approximate the Kirchhoff-Love hypothesis of negligible shear deformation effects and therefore can be used for thin shells.

Various demonstrative solutions are given in Chapter 5.

3) The element does not contain any spurious zero energy modes, using "full" numerical integration; (see Appendix 3).

Considering the practical use of the element, the interpolation employed for the transverse shear strains shows that $\tilde{\epsilon}_{13}$ is constant

with r_1 and in general discontinuous at $r_1 = \pm 1$ (between elements), and similarly $\tilde{\epsilon}_{23}$ is constant with r_2 and in general discontinuous at $r_2 = \pm 1$. As a consequence, the accuracy with which transverse shear stresses are predicted depends to a significant degree on the mesh used and the geometric distortions of the elements. However, our experience is that the bending and membrane stress predictions are relatively little affected by element distortions (see Chapter 5).

To employ Eq. (3.7), we also need to use the appropriate constitutive relations:

$$\tilde{\tau}^{ij} = \tilde{C}^{ijkl} \tilde{\epsilon}_{kl} \tag{3.8}$$

where $\tilde{C}^{ijkl}$ is the fourth-order contravariant constitutive tensor in the convected coordinates r_i. The constitutive relation is known in the local Cartesian system of orthonormal base vectors $\hat{e}_i$, i = 1, 2, 3, with the general shell condition $\hat{\tau}^{33} = 0$ (see Fig. 2.2) [29, 62, 63]. Denoting this constitutive tensor by $\hat{C}^{mnop}$, the constitutive tensor for Eq. (3.8) is obtained using the transformation [2-5],

$$\tilde{C}^{ijkl} = (\underline{g}^i \cdot \underline{\hat{e}}_m)(\underline{g}^j \cdot \underline{\hat{e}}_n)(\underline{g}^k \cdot \underline{\hat{e}}_o)(\underline{g}^l \cdot \underline{\hat{e}}_p)\, \hat{C}^{mnop} \tag{3.9}$$

where the $\underline{g}^i$ are the contravariant base vectors of the convected coordinates r_i. These vectors are calculated using the covariant base

vectors $\underline{g}_i$, where

$$\underline{g}_i = \frac{\partial {}^{\circ}\underline{x}}{\partial r_i} \tag{3.10}$$

with ${}^{\circ}\underline{x}$ from Eq. (3.1) and the following relations [2, 4],

$$g_{ij} = \underline{g}_i \cdot \underline{g}_j \tag{3.11-a}$$

and

$$\underline{g}^i = g^{ij} \cdot \underline{g}_j \tag{3.11-b}$$

$$g^{ij} = \frac{D^{ij}}{|\underline{J}|^2} \tag{3.12}$$

where D^{ij} is the cofactor of the term g_{ij} in the matrix of the metric tensor and $|\underline{J}|$ is the determinant of the Jacobian matrix at the point considered.

Now that the distinct features of the element have been presented, we will focus our attention onto a general nonlinear formulation (although limited to small strains as stated above); the linear case will then be obtained as a subset of the more general nonlinear one.

3.2 Total Lagrangian formulation

The large displacement/rotation formulation of the shell element is based on the derivation given in Refs. [29, 62, 63], and the concepts and interpolations presented in the previous section.

Equations (2.1), (2.2) and (2.3) are used, as in the Bathe-Bolourchi element to describe the geometry of the element at any time t, the displacements at t and the incremental displacements from t. Therefore, this new element also introduces the kinematic assumptions of straight director vectors after deformations and constant thickness measured along the director vectors, after deformation. Hence the limitation of small strains is still in the new element.

The geometric and material nonlinear response is analyzed using an incremental fromulation [29], in which the configuration is sought for time (load step) $t+\Delta t$ when the configuration for time t is known. The basis of this incremental formulation is the use of the virtual work principle applied to the configuration at time $t+\Delta t$. In essence, two approaches can be employed leading to the updated Lagrangian (U.L.) and total Lagrangian (T.L.) formulations. These approaches are, from a continuum mechanics point of view, equivalent, and in the following we develop the governing finite element relations for the T.L. formulation.

The principle of virtual work applied to the configuration at time $t+\Delta t$ is [29],

$$\int_{{}^0V} {}_0^{t+\Delta t}\tilde{S}^{ij}\,\delta\,{}_0^{t+\Delta t}\tilde{\varepsilon}_{ij}\,{}^0dV = {}^{t+\Delta t}R \qquad (3.13)$$

where the ${}^{t+\Delta t}_{0}\tilde{S}^{ij}$ are the contravariant components of the second Piola-Kirchhoff stress tensor at time $t+\Delta t$ and referred to the configuration at time 0 [1, 2, 5, 29], and the ${}^{t+\Delta t}_{0}\tilde{\epsilon}_{ij}$ are the covariant components of the Green-Lagrange strain tensor at time $t+\Delta t$ and referred to the configuration at time 0 [1-5, 29].

Both sets of tensor components are measured in the convected coordinate system r_i ; $i = 1, 2, 3$. The external virtual work is given by ${}^{t+\Delta t}R_0$ and includes the work due to the applied surface tractions and body forces.

For the incremental solution, the stresses and strains are decomposed [29] into the known quantities, ${}^{t}_{0}\tilde{S}^{ij}$ and ${}^{t}_{0}\tilde{\epsilon}_{ij}$, and unknown increments, ${}_{0}\tilde{S}^{ij}$ and ${}_{0}\tilde{\epsilon}_{ij}$, so that

$$ {}^{t+\Delta t}_{0}\tilde{S}^{ij} = {}^{t}_{0}\tilde{S}^{ij} + {}_{0}\tilde{S}^{ij} \tag{3.14} $$

$$ {}^{t+\Delta t}_{0}\tilde{\epsilon}_{ij} = {}^{t}_{0}\tilde{\epsilon}_{ij} + {}_{0}\tilde{\epsilon}_{ij} \tag{3.15} $$

In addition, the strain increment can be also decomposed into a linear part, ${}_{0}\tilde{e}_{ij}$, and a nonlinear part, ${}_{0}\tilde{\eta}_{ij}$, hence

$$ {}_{0}\tilde{\epsilon}_{ij} = {}_{0}\tilde{e}_{ij} + {}_{0}\tilde{\eta}_{ij} \tag{3.16} $$

Substituting from Eqs. (3.14) to (3.16) into Eq. (3.13) and linearizing the step by using

$$ {}_0\tilde{S}^{ij} = {}_0\tilde{C}^{ijkl}\, {}_0\tilde{e}_{kl} \tag{3.17} $$

and

$$ \delta_0\tilde{\varepsilon}_{ij} = \delta_0\tilde{e}_{ij} \tag{3.18} $$

we obtain the linearized equation of motion

$$ \int_{{}^0V} {}_0\tilde{C}^{ijkl}\, {}_0\tilde{e}_{kl}\, \delta_0\tilde{e}_{ij}\, {}^0dV + \int_{{}^0V} {}_0^t\tilde{S}^{ij}\, \delta_0\tilde{\eta}_{ij}\, {}^0dV $$

$$ = {}^{t+\Delta t}R - \int_{{}^0V} {}_0^t\tilde{S}^{ij}\, \delta_0\tilde{e}_{ij}\, {}^0dV \tag{3.19} $$

This equation is the basic equilibrium relation employed to develop the governing finite element matrices. For the actual solution of problems it is frequently important to use equilibrium iterations [29, Chapter 8]. The finite element matrices and vectors used in these iterations can be derived directly from the matrices obtained using Eq. (3.19). Note that

the incremental constitutive fourth-order tensor ${}_0\tilde{C}^{ijkl}$ is now obtained using in Eq. (3.9) ${}_0\hat{C}^{mnop}$, based on the condition that ${}^t_0\hat{S}^{33} = 0$, which implies the natural shell condition ${}^t\hat{\tau}^{33} = 0$ only in the small strain case [29, 109].

The basic problem of the finite element discretization of Eq. (3.19) lies in expressing the strain terms by the finite element interpolations. Using the definition of the Green-Lagrange strain components:

$$ {}^t_0\tilde{E}_{ij} = \frac{1}{2}\left({}^t\underline{g}_i \cdot {}^t\underline{g}_j - {}^0\underline{g}_i \cdot {}^0\underline{g}_j \right) \tag{3.20} $$

and the relations in Eqs. (2.1), (2.2), and (2.3) we obtain

$$ {}_0\tilde{e}_{ii} = h_{k,i}\, {}^t\underline{g}_i \cdot \underline{u}_k + \frac{r_3}{2} \partial_k h_{k,i} \left(-\alpha_k\, {}^t\underline{g}_i \cdot {}^t\underline{V}_2^k + \beta_k\, {}^t\underline{g}_i \cdot {}^t\underline{V}_1^k \right) \tag{3.21-a} $$

$$ {}_0\tilde{\gamma}_{ii} = \frac{1}{2} h_{k,i}\, h_{p,i}\, \underline{u}_k \cdot \underline{u}_p + \frac{r_3}{2} h_{k,i}\, h_{p,i}\, \partial_p \left(-\alpha_p\, {}^t\underline{V}_2^p \cdot \underline{u}_k + \beta_p\, {}^t\underline{V}_1^p \cdot \underline{u}_k \right) $$

$$ + \frac{(r_3)^2}{8} h_{k,i}\, h_{p,i}\, \partial_k \partial_p \left(-\alpha_k\, {}^t\underline{V}_2^k + \beta_k\, {}^t\underline{V}_1^k \right) \cdot \left(-\alpha_p\, {}^t\underline{V}_2^p + \beta_p\, {}^t\underline{V}_1^p \right) \tag{3.21-b} $$

$$ (i = 1,2) $$

with the notation $h_{k,i} = \dfrac{\partial h_k}{\partial r_i}$, $\underline{u}_k^T = [\, u_1^k \;\; u_2^k \;\; u_3^k \,]$, and

$$
{}_0\tilde{e}_{12} = \frac{1}{2}\Big[h_{k,2}\,{}^t\underline{g}_1\cdot\underline{u}_k + h_{k,1}\,{}^t\underline{g}_2\cdot\underline{u}_k
+ \frac{r_3}{2}h_{k,2}\,\partial_k\left(-\alpha_k\,{}^t\underline{v}_2^k\cdot{}^t\underline{g}_1 + \beta_k\,{}^t\underline{v}_1^k\cdot{}^t\underline{g}_1\right)
+ \frac{r_3}{2}h_{k,1}\,\partial_k\left(-\alpha_k\,{}^t\underline{v}_2^k\cdot{}^t\underline{g}_2 + \beta_k\,{}^t\underline{v}_1^k\cdot{}^t\underline{g}_2\right)\Big] \qquad (3.22\text{-a})
$$

$$
{}_0\tilde{\varepsilon}_{12} = \frac{1}{2}\Big[h_{k,1}h_{p,2}\,\underline{u}_k\cdot\underline{u}_p
+ \frac{r_3}{2}h_{k,1}h_{p,2}\,\partial_p\left(-\alpha_p\,{}^t\underline{v}_2^p\cdot\underline{u}_k + \beta_p\,{}^t\underline{v}_1^p\cdot\underline{u}_k\right)
+ \frac{r_3}{2}h_{k,1}h_{p,2}\,\partial_k\left(-\alpha_k\,{}^t\underline{v}_2^k\cdot\underline{u}_p + \beta_k\,{}^t\underline{v}_1^k\cdot\underline{u}_p\right)
+ \frac{(r_3)^2}{4}h_{k,1}h_{p,2}\,\partial_k\partial_p\left(-\alpha_k\,{}^t\underline{v}_2^k + \beta_k\,{}^t\underline{v}_1^k\right)\cdot\left(-\alpha_p\,{}^t\underline{v}_2^p + \beta_p\,{}^t\underline{v}_1^p\right)\Big] \qquad (3.22\text{-b})
$$

Further, we obtain for the transverse shear strains, using Eqs. (3.3) and (3.6),

$$
{}_0\tilde{e}_{13} = \frac{1}{8}(1+r_2)\Big[{}^tg^A_{3i}\left(u^1_i - u^2_i\right) + \frac{1}{2}\,{}^tg^A_{1i}\left(-\alpha_1\partial_1\,{}^tv^1_{2i} + \beta_1\partial_1\,{}^tv^1_{1i} - \alpha_2\partial_2\,{}^tv^2_{2i} + \beta_2\partial_2\,{}^tv^2_{1i}\right)\Big]
+ \frac{1}{8}(1-r_2)\Big[{}^tg^C_{3i}\left(u^4_i - u^3_i\right) + \frac{1}{2}\,{}^tg^C_{1i}\left(-\alpha_4\partial_4\,{}^tv^4_{2i} + \beta_4\partial_4\,{}^tv^4_{1i} - \alpha_3\partial_3\,{}^tv^3_{2i} + \beta_3\partial_3\,{}^tv^3_{1i}\right)\Big] \qquad (3.23\text{-a})
$$

$$\circ \tilde{\eta}_{13} = \frac{1}{32}(1+\Gamma_2)\Big[(-\alpha_1 a_1 {}^t V_{2i}^1 + \beta_1 a_1 {}^t V_{1i}^1 - \alpha_2 a_2 {}^t V_{2i}^2 + \beta_2 a_2 {}^t V_{1i}^2)(U_i^1 - U_i^2)\Big] + \frac{1}{32}(1-\Gamma_2)\Big[(-\alpha_4 a_4 {}^t V_{2i}^4 + \beta_4 a_4 {}^t V_{1i}^4 - \alpha_3 a_3 {}^t V_{2i}^3 + \beta_3 a_3 {}^t V_{1i}^3)(U_i^4 - U_i^3)\Big] \qquad (3.23\text{-b})$$

and,

$$\circ \tilde{e}_{23} = \frac{1}{8}(1+\Gamma_1)\Big[{}^t g_{3i}^D (U_i^1 - U_i^4) + \frac{1}{2} {}^t g_{2i}^D (-\alpha_1 a_1 {}^t V_{2i}^1 + \beta_1 a_1 {}^t V_{1i}^1 - \alpha_4 a_4 {}^t V_{2i}^4 + \beta_4 a_4 {}^t V_{1i}^4)\Big] + \frac{1}{8}(1-\Gamma_1)\Big[{}^t g_{3i}^B (U_i^2 - U_i^3) + \frac{1}{2} {}^t g_{2i}^B (-\alpha_2 a_2 {}^t V_{2i}^2 + \beta_2 a_2 {}^t V_{1i}^2 - \alpha_3 a_3 {}^t V_{2i}^3 + \beta_3 a_3 {}^t V_{1i}^3)\Big] \qquad (3.24\text{-a})$$

$$\circ \tilde{\eta}_{23} = \frac{1}{32}(1+\Gamma_1)\Big[(-\alpha_1 a_1 {}^t V_{2i}^1 + \beta_1 a_1 {}^t V_{1i}^1 - \alpha_4 a_4 {}^t V_{2i}^4 + \beta_4 a_4 {}^t V_{1i}^4)(U_i^1 - U_i^4)\Big] + \frac{1}{32}(1-\Gamma_1)\Big[(-\alpha_2 a_2 {}^t V_{2i}^2 + \beta_2 a_2 {}^t V_{1i}^2 - \alpha_3 a_3 {}^t V_{2i}^3 + \beta_3 a_3 {}^t V_{1i}^3)(U_i^2 - U_i^3)\Big] \qquad (3.24\text{-b})$$

Note that, since we assume the thickness of the shell to remain constant during the deformations, the strain ${}^{t}_{0}\tilde{\varepsilon}_{33}$ through the element thickness is zero.

The expressions in Eqs. (3.21) to (3.24) are substituted into Eq. (3.19) which in the standard manner yields the linear strain incremental stiffness matrix ${}^{t}_{0}\underline{K}_{L}$, the nonlinear strain (or geometric) incremental stiffness matrix ${}^{t}_{0}\underline{K}_{NL}$ and the nodal point force vector ${}^{t}_{0}\underline{F}$ in the finite element incremental equilibrium relations [29],

$$({}^{t}_{0}\underline{K}_{L} + {}^{t}_{0}\underline{K}_{NL})\,\underline{U} = {}^{t+\Delta t}\underline{R} - {}^{t}_{0}\underline{F} \tag{3.25}$$

where,

$${}^{t}_{0}\underline{K}_{L} = \int_{{}^{0}V} {}^{t}_{0}\tilde{\underline{B}}_{L}^{T}\; {}_{0}\tilde{\underline{C}}\; {}^{t}_{0}\tilde{\underline{B}}_{L}\; {}^{0}dV \tag{3.26}$$

and

$${}^{t}_{0}\underline{K}_{NL} = \int_{{}^{0}V} {}^{t}_{0}\tilde{\underline{B}}_{NL}^{T}\; {}^{t}_{0}\tilde{\underline{S}}\; {}^{t}_{0}\tilde{\underline{B}}_{NL}\; {}^{0}dV \tag{3.27}$$

For the definition of ${}^{t}_{0}\tilde{\underline{B}}_{L}$, ${}^{t}_{0}\tilde{\underline{B}}_{NL}$ and ${}^{t}_{0}\tilde{\underline{S}}$ see Appendix 4.

The element matrices in Eq. (3.25) correspond to 5 degrees of

freedom per node (see Fig. 2.1), but as we have already stated above, in some applications it is convenient to use instead of α_k and β_k three rotations about the global coordinate axes. In this case, we simply transform the matrices of Eq. (3.25) in the standard manner [29].

In order to evaluate the element behavior we have considered three different material models:

(i) The linear elastic material model, with a linear relation between the second Piola-Kirchhoff stress components and the Green-Lagrange strain components,

$$ {}^{t}_{0}\tilde{S}^{ij} = {}^{t}_{0}\tilde{C}^{ijkl} \, {}^{t}_{0}\tilde{\epsilon}_{kl} \tag{3.28} $$

where ${}^{t}_{0}\tilde{C}^{ijkl}$ is constant with t.

(ii) The elastic-plastic material model, using the von Mises yield condition and isotropic hardening [104, 105]. It has been implemented as described in Ref. [62].

(iii) The thermoelastic material model, in which

$$ {}^{t}_{0}\tilde{S}^{ij} = {}^{t}_{0}\tilde{C}^{ijkl} \left({}^{t}_{0}\tilde{\epsilon}_{kl} - {}^{t}g_{kl} \, {}^{t}\alpha \, {}^{t}\theta \right) \tag{3.29} $$

where the ${}^{t}g_{kl}$ are the covariant components of the metric tensor at time t in the convected system, ${}^{t}\alpha$ is the thermal expansion coefficient and ${}^{t}\theta$ is the temperature at time t. This material model considers temperature-

dependent mechanical constants $E = E(\theta)$, $\nu = \nu(\theta)$, $\alpha = \alpha(\theta)$, and has been implemented as described in Ref. [88].

3.3 Some remarks on the presented element

Since the strains $\tilde{\varepsilon}_{13}$ and $\tilde{\varepsilon}_{23}$ do not satisfy the displacement-strain relations (kinematic relations), the element contains incompatible modes. Therefore, it is necessary that the patch-test [35, 36] be passed. In Chapter 5 we begin our numerical investigation of the element by:

a) verifying that under various conditions of distortion, the element does not contain spurious rigid body modes, as was stated earlier;

b) verifying that the patch test is passed.

Much effort has been directed in the last decades towards the development of a simple and efficient plate element (geometric linear analysis). Although our general 4-node shell element can, of course, be used to analyze plates, and is used as such in some of the examples of Chapter 5, the formulation can be much more effective if specialized for a plate element. In Appendix 5, we present such a specialization. The plate element obtained is very similar to the modified QUAD4 element reported in Ref. [82-b]; the difference lies in that we interpolate covariant tensor components measured in the convected coordinate system for the transverse shear strains and MacNeal, using the same interpolation, interpolates physical components. Our formulation allows the development of non-flat and nonlinear elements, as shown above.

4. SOLUTION OF NONLINEAR FINITE ELEMENT EQUATIONS

In this chapter we develop first an algorithm for tracing the static nonlinear equilibrium path, in the load-displacements space, of a general finite element structural model. Then also an algorithm for calculating linearized buckling loads is given [90].

Both algorithms were implemented in the general purpose nonlinear finite element computer program ADINA [111], and in the last section of this chapter some small demonstrative examples are presented. In Chapter 5, we use the algorithms for solving shell structural models.

4.1 Incremental solution algorithm

We assume that an appropriate finite element representation to idealize the physical problem has been selected and that now we are only concerned with the solution of the governing equations. Using the notation of Ref. [29], these equations are

$$ {}^{t+\Delta t}\underline{R} - {}^{t+\Delta t}\underline{F} = \underline{0} \tag{4.1} $$

where ${}^{t+\Delta t}\underline{R}$ is a vector of externally applied nodal point loads, and ${}^{t+\Delta t}\underline{F}$ is a vector of nodal point forces equivalent (in the virtual work sense) to the internal element stresses, both being evaluated at time $t+\Delta t$.

We consider only static response of structures and time independent constitutive relations. Hence, the time veriable is merely denoting

a load level.

The usual incremental solution of Eq. (4.1) results in the following iterative scheme [29, Chapter 8],

$$ {}^{\tau}\underline{K}^{(i-1)}\,\Delta\underline{U}^{(i)} = {}^{t+\Delta t}\underline{R} - {}^{t+\Delta t}\underline{F}^{(i-1)} \tag{4.2} $$

where ${}^{\tau}\underline{K}^{(i-1)}$ is a coefficient matrix and $\Delta\underline{U}^{(i)}$ is an increment to the current displacement vector,

$$ {}^{t+\Delta t}\underline{U}^{(i)} = {}^{t+\Delta t}\underline{U}^{(i-1)} + \Delta\underline{U}^{(i)} \tag{4.3} $$

The coefficient matrix ${}^{\tau}\underline{K}^{(i-1)}$ is different in the various procedures used. In the full Newton-Raphson technique and the BFGS method [29], the matrix is updated in every iteration, whereas in a modified Newton iteration, the matrix is only updated at certain times. Line searches can also be effective using each of these methods [29, 96], and it is clearly possible to combine Newton and quasi-Newton iterations and line searches in one step-by-step solution scheme.

An early study of the advantages and disadvantages of various solution procedures was reported in [89].

However, in that reference two major assumptions were made. First, it was assumed that the analyst prescribes the various load levels for which the equilibrium configurations are to be calculated; this is

not possible without an a-priori knowledge of the load carrying capacity of the structure. Second, it was assumed that only the response up to the collapse of the structure was sought; i.e. the post-collapse response was not required. However, in some analyses the response after the (or a) critical point has been reached is of interest. By a critical point we mean a bifurcation point or limit (collapse) point [14, 15].

In this section we describe an algorithm that we have developed and implemented to automatically choose appropriate load steps and calculate the pre- and post-collapse response of a structure.

4.1.1 Incremental solution algorithm using modified Newton iterations

In what follows we assume that the structure is subjected to a proportionally varying load. In this case, the basic equations to be solved are, based on Eq. (4.2),

$$ {}^{\tau}\underline{K}\,\Delta\underline{U}^{(i)} = {}^{t+\Delta t}\lambda\underline{R} - {}^{t+\Delta t}\underline{F}^{(i-1)} \tag{4.4} $$

where ${}^{t+\Delta t}\lambda$ is the load factor that describes the intensity of the reference load vector $\underline{R}$ to be applied at time $t+\Delta t$. The difficulty lies in defining the load factor for each load step Δt, $2\Delta t$, ... prior to the incremental analysis.

4.1.1.1 Load constraints

The essence of the automatic algorithm that we have studied lies in the automatic selection of the incremental load levels, and the

iteration with the load level and the displacements. The basic idea of iterating in the load-displacement space was researched earlier by a number of investigators (see Refs. [91-101]).

When the iteration is performed in the load-displacement space, Eq. (4.4) is used in the form

$$ {}^{\tau}\underline{K}\,\Delta\underline{U}^{(i)} = ({}^{t+\Delta t}\lambda^{(i-1)} + \Delta\lambda^{(i)})\,\underline{R} - {}^{t+\Delta t}\underline{F}^{(i-1)} \qquad (4.5) $$

and an additional equation is employed to constrain the length of the load step:

$$ f(\Delta\lambda^{(i)}, \Delta\underline{U}^{(i)}) = 0 \qquad (4.6) $$

Several constraint equations of this form have been proposed, such as the tangent constant arc-length [91], and the spherical constant arc-length techniques [93, 95].

In our research, we found that for an automatic algorithm it is effective to use two different constraints depending on the response and load level considered; namely, the spherical constant arc-length and the constant increment of external work.

We use the spherical constant arc-length in the response regions far from the critical points, and in this case Eq. (4.6) is

$$\left[\left({}^{t+\Delta t}\lambda^{(i-1)} - {}^{t}\lambda\right) + \Delta\lambda^{(i)}\right]^2 + \frac{\underline{U}_D^{(i)T}\,\underline{U}_D^{(i)}}{\underline{U}_D^{T\,\Delta t}\,\underline{U}_D} + \underline{U}_R^{(i)T}\,\underline{U}_R^{(i)} = \Delta\ell^2 \qquad (4.7\text{-a})$$

where

$$\underline{U}^{(i)} = {}^{t+\Delta t}\underline{U}^{(i)} - {}^{t}\underline{U} \qquad (4.7\text{-b})$$

and $\underline{U}^T = [\,\underline{U}_D^T \;\; \underline{U}_R^T\,]$; where $\underline{U}_D$ corresponds to the translational degrees of freedom and $\underline{U}_R$ to the rotational ones; $\Delta\ell$ (dimensionless) is the arc-length.

The scheme of constant increment of external work is used "near" the critical points. In this case, Eq. (4.6) is for the first iteration,

$$\left({}^{t}\lambda + \frac{1}{2}\Delta\lambda^{(1)}\right)\underline{R}^T\,\Delta\underline{U}^{(1)} = W \qquad (4.8\text{-a})$$

and for the next iterations,

$$\left({}^{t+\Delta t}\lambda^{(i-1)} + \frac{1}{2}\Delta\lambda^{(1)}\right)\underline{R}^T\,\Delta\underline{U}^{(i)} = 0 \qquad (4.8\text{-b})$$

where W is the amount of external work in the step (and is positive or negative).

4.1.1.2 Iterations within a load step

Prior to the start of the incremental solution, the analyst specifies three items.

(1) The user inputs the reference load distribution, which corresponds to the vector $\underline{R}$ in Eq. (4.5). This load is varied proportionally during the analysis ($^{t}\lambda\,\underline{R}$), and can be due to distributed and concentrated loads.

(2) The user specifies the displacement at a node corresponding to the first load level (i.e. corresponding to $^{\Delta t}\lambda$). We denote this displacement as $^{\Delta t}U_k^*$. Here we consider that to start the incremental solution it is easier to specify the displacement at a node, that the user selects, than the intensity ($^{\Delta t}\lambda$) of the loads.

(3) The displacements corresponding to time Δt determined by the specified displacement $^{\Delta t}U_k^*$ also limit the size of any subsequent load change per step, because the user specifies a constant α and the algorithm assures that

$$\| \underline{U} \| \leq \alpha \, \| {}^{\Delta t}\underline{U} \| \tag{4.9}$$

where $\| \underline{U} \|$ denotes the Euclidian norm of the vector $\underline{U}$, which is the displacement increment in any load step and $^{\Delta t}\underline{U}$ are the displacements corresponding to time Δt.

a) Solution for the equilibrium configuration at time Δt with prescribed displacement $^{\Delta t}U_k^*$

For this first load step, Eq. (4.5) reduces to

$$ {}^{0}\underline{K}\,\Delta\underline{U}^{(i)} = ({}^{\Delta t}\lambda^{(i-1)} + \Delta\lambda^{(i)})\,\underline{R} - {}^{\Delta t}\underline{F}^{(i-1)} \tag{4.10} $$

with the initial conditions

$$ {}^{\Delta t}\lambda^{(0)} = 0 \tag{4.11-a} $$

$$ {}^{\Delta t}\underline{F}^{(0)} = \underline{0} \tag{4.11-b} $$

The solution is obtained using the scheme discussed in [94].

For i=1, we use

$$ {}^{0}\underline{K}\,\Delta\underline{U}^{(1)} = \underline{R} \tag{4.12} $$

$$ {}^{\Delta t}\lambda^{(1)} = \frac{{}^{\Delta t}U_k^{*}}{\Delta U_k^{(1)}} \tag{4.13-a} $$

$$ {}^{\Delta t}\underline{U}^{(1)} = {}^{\Delta t}\lambda^{(1)}\,\Delta\underline{U}^{(1)} \tag{4.13-b} $$

Then for i=2, 3, ... we use two equations instead of Eq. (4.10),

$$ {}^{0}\underline{K}\,\Delta\bar{\underline{U}}^{(i)} = {}^{\Delta t}\lambda^{(i-1)}\,\underline{R} - {}^{\Delta t}\underline{F}^{(i-1)} \tag{4.14} $$

$$ {}^{\circ}\underline{K}\,\Delta\bar{\underline{U}}^{(i)} = \Delta\lambda^{(i)}\,\underline{R} \tag{4.15} $$

where we note that $\Delta\bar{\underline{U}}^{(i)} = \Delta\lambda^{(i)}\,\Delta\underline{U}^{(1)}$. Since the displacement at the degree of freedom k is imposed, we have the condition

$$ \Delta\lambda^{(i)} = -\frac{\Delta\bar{U}_k^{(i)}}{\Delta U_k^{(1)}} \tag{4.16} $$

and then,

$$ {}^{\Delta t}\lambda^{(i)} = {}^{\Delta t}\lambda^{(i-1)} + \Delta\lambda^{(i)} \tag{4.17} $$

$$ {}^{\Delta t}\underline{U}^{(i)} = {}^{\Delta t}\underline{U}^{(i-1)} + \Delta\underline{U}^{(i)} \tag{4.18-a} $$

$$ \Delta\underline{U}^{(i)} = \Delta\bar{\underline{U}}^{(i)} + \Delta\lambda^{(i)}\,\Delta\underline{U}^{(1)} \tag{4.18-b} $$

Convergence of the iteration is reached when [29, 89]

$$ \frac{\Delta\underline{U}^{(i)T}\left({}^{\Delta t}\lambda^{(i-1)}\,\underline{R} - {}^{\Delta t}\underline{F}^{(i-1)}\right)}{\Delta\underline{U}^{(1)T}\left({}^{\Delta t}\lambda^{(1)}\,\underline{R}\right)} \leq ETOL \tag{4.19-a} $$

where $ETOL$ is an energy convergence tolerance.

An additional convergence criterion that can be used is

$$\| {}^{\Delta t}\lambda^{(i)} \underline{R}_F - {}^{\Delta t}\underline{F}_F^{(i)} \| \leq RNORM \qquad (4.19\text{-b})$$

$$\| {}^{\Delta t}\lambda^{(i)} \underline{R}_M - {}^{\Delta t}\underline{F}_M^{(i)} \| \leq AMNORM \qquad (4.19\text{-c})$$

In (4.19-b), the generalized forces corresponding to translational degrees of freedom are considered (unbalanced force), and in (4.19-c), the ones corresponding to rotational degrees of freedom (unbalanced moment) are considered. To decide whether Eqs. (4.19-b) and (4.19-c) are going to be used, and in the selection of ETOL , RNORM and AMNORM , some insight on the part of the analyst is required.

b) Solutions for the equilibrium configurations at times $2\Delta t$, $3\Delta t$, $4\Delta t$, ... using the spherical constant arc-length algorithm

At the beginning of each such solution we calculate the load-step length Δl,

$$\Delta l = \beta \sqrt{({}^{t}\lambda - {}^{t-\Delta t}\lambda)^2 + \frac{\underline{U}_D^T \underline{U}_D}{{}^{\Delta t}\underline{U}_D^T \, {}^{\Delta t}\underline{U}_D} + \underline{U}_R^T \underline{U}_R} \qquad (4.20)$$

where $\underline{U} = {}^{t}\underline{U} - {}^{t-\Delta t}\underline{U}$; and the constant β scales the previous load step length to an appropriate current load step length as discussed in Eqs. (4.30) and (4.31).

Using Eq. (4.5) we now obtain for iteration i=1,

$$ {}^{\tau}\underline{K}\ \Delta\bar{\underline{U}}^{(1)} = {}^{t}\lambda\ \underline{R} - {}^{t}\underline{F} \tag{4.21} $$

$$ {}^{\tau}\underline{K}\ \Delta\bar{\bar{\underline{U}}}^{(1)} = \underline{R} \tag{4.22} $$

and

$$ \Delta\underline{U}^{(1)} = \Delta\bar{\underline{U}}^{(1)} + \Delta\lambda^{(1)}\ \Delta\bar{\bar{\underline{U}}}^{(1)} \tag{4.23-a} $$

$$ {}^{t+\Delta t}\underline{U}^{(1)} = {}^{t}\underline{U} + \Delta\underline{U}^{(1)} \tag{4.23-b} $$

$$ {}^{t+\Delta t}\lambda^{(1)} = {}^{t}\lambda + \Delta\lambda^{(1)} \tag{4.23-c} $$

where the load increment $\Delta\lambda^{(1)}$ is determined from the current load step length, i.e. Eq. (4.7-a)

$$ \frac{\Delta\underline{U}_D^{(1)T}\ \Delta\underline{U}_D^{(1)}}{{}^{\Delta t}\underline{U}_D^{T}\ {}^{\Delta t}\underline{U}_D} + \Delta\underline{U}_R^{(1)T}\ \Delta\underline{U}_R^{(1)} + (\Delta\lambda^{(1)})^2 = \Delta l^2 \tag{4.24} $$

For iterations i=2, 3, ... we use the solution of Eq. (4.22), and

in addition we solve

$$ {}^{\tau}\underline{K}\,\Delta\underline{\bar{U}}^{(i)} = {}^{t+\Delta t}\lambda^{(i-1)}\underline{R} - {}^{t+\Delta t}F^{(i-1)} \qquad (4.25) $$

so that

$$ {}^{t+\Delta t}\underline{U}^{(i)} = {}^{t+\Delta t}\underline{U}^{(i-1)} + \Delta\underline{\bar{U}}^{(i)} + \Delta\lambda^{(i)}\Delta\underline{\bar{U}}^{(1)} \qquad (4.26) $$

Equation (4.7-a) now yields $\Delta\lambda^{(i)}$, and we then have

$$ {}^{t+\Delta t}\lambda^{(i)} = {}^{t+\Delta t}\lambda^{(i-1)} + \Delta\lambda^{(i)} \qquad (4.27) $$

Convergence in the iteration is again measured with the energy criterion plus (optionally) the unbalanced force/moment criterion.

$$ \frac{\Delta\underline{U}^{(i)T}\left({}^{t+\Delta t}\lambda^{(i-1)}\underline{R} - {}^{t+\Delta t}\underline{F}^{(i-1)}\right)}{\Delta\underline{U}^{(1)T}\left(\Delta\lambda^{(1)}\underline{R}\right)} \leq ETOL \qquad (4.28\text{-a}) $$

$$ \left\| {}^{t+\Delta t}\lambda^{(i)}\underline{R}_F - {}^{t+\Delta t}\underline{F}_F \right\| \leq RNORM \qquad (4.28\text{-b}) $$

$$ \left\| {}^{t+\Delta t}\lambda^{(i)}\underline{R}_M - {}^{t+\Delta t}\underline{F}_M \right\| \leq AMNORM \qquad (4.28\text{-c}) $$

We note that $\Delta\lambda^{(i)}$ is obtained from a quadratic equation, so that different situations can arise.

(i) We do not obtain any real roots. In this case we restart from the last established equilibrium position using the constant increment of external work algorithm (see -c-).

(ii) We obtain two real roots. To select between both roots, we use a criterion based on the one discussed in [96]. First we define for each root (j=1, 2)

$$\gamma_j = \underline{U}^{(i-1)T} \underline{U}_j^{(i)} \tag{4.29}$$

If $\text{sgn}\ \gamma_1 \neq \text{sgn}\ \gamma_2$, we select the root for which γ_j is positive; if $\text{sgn}\ \gamma_1 = \text{sgn}\ \gamma_2$, we select the root that gives a solution closest to the one that would provide a tangent arc-length algorithm.

Once a new equilibrium configuration has been determined, we check whether the condition in Eq. (4.9) is satisfied. If it is not satisfied, we restart from the previous equilibrium configuration using

$$\Delta\ell\big|_{new} = \Delta\ell\big|_{old} \frac{\| \underline{U} \|_{allowable}}{\| \underline{U} \|_{actual}} \tag{4.30}$$

If Eq. (4.9) is satisfied, we proceed with the solution for the next load increment using

$$\Delta l\big|_{new} = \Delta l\big|_{old} \sqrt{\frac{N_1}{N_2}} \quad \frac{\|\underline{U}\|_{allowable}}{\|\underline{U}\|_{actual}} \tag{4.31}$$

where N_1 is the optimum number of iterations (input to the program), and N_2 is the number of iterations that were used in the previous load step increment.

The decision of whether or not to reform ${}^{\tau}\underline{K}$ is also made based on the comparison of N_2 vs. N_1.

In our numerical experimentation we found the above scheme to be effective as long as the solution is not too close to a critical point, at which time it is more efficient to use the scheme of constant increment of external work. The measure used to decide whether to switch from the constant arc-length to the constant increment of external work scheme is the value of ${}^{t}W/{}^{t-\Delta t}W$. When this value is close to unity, i.e. when $1-\delta \leq |{}^{t}W/{}^{t-\Delta t}W| \leq 1+\delta$ where δ is small (e.g. 0.15), the algorithm uses the constant increment of external work scheme.

c) <u>Solutions for the equilibrium configurations at times $2\Delta t$, $3\Delta t$, $4\Delta t$, ..., using the constant increment of external work algorithm</u>

At the beginning of each step we calculate

$${}^{t+\Delta t}W = \beta' \, {}^{t}W \tag{4.32}$$

where ${}^{t}W$ corresponds to Eq. (4.8-a) and β' is a constant which we set

equal to ${}^{t}\lambda / {}^{t-\Delta t}\lambda$.

The iteration is now performed as for the scheme using the spherical constant arc-length (see -b-), but with Eqs. (4.8-a) and (4.8-b), to determine the increment $\Delta\lambda^{(i)}$.

For the first iteration we use Eqs. (4.21) to (4.23) and Eq. (4.8-a).

For iterations i=2, 3, 4, ... we use Eqs. (4.22), (4.25) to (4.27), and (4.8-b), and convergence is measured in the same way as in the spherical constant arc-length scheme.

In these iterations we always obtain two real roots for $\Delta\lambda^{(i)}$ when i=2, 3, ...; and the same holds for $\Delta\lambda^{(1)}$ provided ${}^{t+\Delta t}W$ is "small enough" and equilibrium was sufficiently well satisfied at the end of the previous load step.

For the definition of a "small enough ${}^{t+\Delta t}W$ " consider a one degree of freedom case, see Fig. 4.1

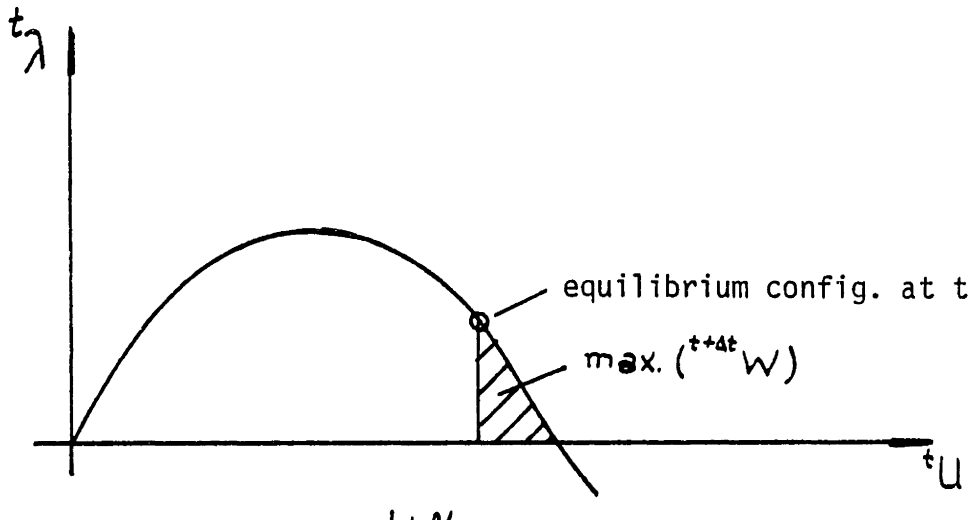


Figure 4.1 Maximum ${}^{t+\Delta t}W$ to be used in a step

4.1.1.3 Some general remarks

Considering the iterative schemes described in the previous sections we note that the coefficient matrix is not necessarily positive definite. If the matrix is not positive definite, a critical point has been passed, but the triangular factorization can be completed, provided there is no multiplier growth [29]. In practice, the triangular factorization only fails if it is attempted at, or very close to, a critical point - a situation that is hardly observed.

We also note that a number of constants have to be selected and initialized for the algorithm; namely, α , δ and N_1 . Reasonable values for δ and N_1 are 0.15 and 6, respectively; effective values for α are problem-dependent. If the prescribed displacement is small, a large value of α may be appropriate.

The proper choice of these constants, the definition of β' in (4.32) and Eqs. (4.30) and (4.31) does affect the performance of the solution algorithm, but more experience need be gained before more specific recommendations can be made.

4.1.2 Incremental solution algorithm using full Newton iterations

The same solution algorithm described in Section 1.1 was implemented using a full Newton iteration strategy. Although the stiffness matrix has to be reformed for every iteration, implying very costly numerical integrations, and Eqs. (4.12) or (4.22) have to be solved for every iteration, in some cases (e.g. snap-back characteristic), the use of this strategy results in a more efficient solution.

4.2 Linearized buckling analysis

The automatic solution procedures presented in Section 4.1 calculate incrementally the complete equilibrium path, including the post-collapse response. The analysis of the complete nonlinear response can be quite expensive and in some cases, in which the pre-buckling displacements are negligible, a linearized buckling analysis can be of value for the designer. In the case of shell structural analyses, due to the imperfection sensitivity [13, 14, 16, 17, 19, 20, 23] of some of these structures, great care must be taken when using a linearized buckling load for design purposes and use should be made of the historical data available on the shell considered in codes and other references (knock-down factors) [24].

Let τ decide the load level at which buckling would occur in an incremental analysis, then we have

$$\det ({}^{\tau}\underline{K}) = 0 \tag{4.33}$$

In the linearized buckling analysis we assume that

$${}^{\tau}\underline{K} = {}^{t-\Delta t}\underline{K} + \lambda \left({}^{t}\underline{K} - {}^{t-\Delta t}\underline{K} \right) \tag{4.34}$$

where ${}^{t-\Delta t}\underline{R} + \lambda \left({}^{t}\underline{R} - {}^{t-\Delta t}\underline{R} \right)$ is the linear approximation to the buckling load. The relation in Eq. (4.34) can be applied at any time

Δt, $2\Delta t$, $3\Delta t$, ..., but clearly assumes that from time $t-\Delta t$ onwards the linear strain and nonlinear strain stiffness matrices change proportionally with additional load increments. Obviously, this is a severe assumption and may lead to greatly overestimating the buckling load [29, 102] in problems with a softening characteristic.

Considering Eqs. (4.33) and (4.34) we obtain the eigenproblem

$$ {}^{t-\Delta t}\underline{K}\,\underline{\phi} = \lambda\,\Delta\underline{K}\,\underline{\phi} \tag{4.35} $$

where $\Delta\underline{K} = {}^{t-\Delta t}\underline{K} - {}^{t}\underline{K}$ (in general indefinite). Hence, in general the problem in Eq. (4.35) has negative and positive eigenvalues [113, 114].

Another eigenproblem for calculating the buckling load is reached by writing Eq. (4.35) in the form

$$ \Delta\underline{K}\,\underline{\phi} = \alpha\,{}^{t-\Delta t}\underline{K}\,\underline{\phi} \tag{4.36} $$

where $\alpha = 1/\lambda$ and—assuming that we require the smallest positive eigenvalue of Eq. (4.35), which we call λ_1 — we now want to calculate the largest positive eigenvalue of Eq. (4.36).

Hence we can impose a shift $\mu = 1.0$ onto the problem in Eq. (4.36) and consider the eigenproblem

$$ {}^{t}\underline{K}\,\underline{\phi} = \gamma\,{}^{t-\Delta t}\underline{K}\,\underline{\phi} \tag{4.37} $$

where now all eigenvalues γ_i are positive and we seek the smallest positive eigenvalue γ_1 . The critical load factor is given by

$$\lambda_1 = \frac{1}{1 - \gamma_1} \tag{4.38}$$

Considering Eqs. (4.35) and (4.37) it appears that Eq. (4.37) is employed most effectively, because $\Delta \underline{K}$ does not need to be formed and all eigenvalues are positive. The subspace iteration method [29, 115] is used to solve the eigenproblem.

If λ_1 is large, γ_1 is close to 1.0, then all the eigenvalues of (4.37) are closely spaced between γ_1 and 1.0, making the eigensolution quite difficult [29]. Also, if we calculate

$$\frac{d\lambda_1}{d\gamma_1} = \frac{1}{(1-\gamma_1)^2} \tag{4.39}$$

we see that the error in the determination of γ_1 is magnified when calculating λ_1 , if γ_1 is close to unity.

In this case, to enlarge the relative spacing (ratio) between eigenvalues and improve the solution convergence [29], an additional shift $\rho < 1.0$ is to be imposed, in the form

$$({}^{t}\underline{K} - \rho\, {}^{t-\Delta t}\underline{K})\,\underline{\phi} = (\gamma - \rho)\, {}^{t-\Delta t}\underline{K}\,\underline{\phi} \tag{4.40}$$

In our numerical experimentation we obtained good results with the following strategy:

(i) After the second of the subspace iterations in which q trial vectors [29] are used we calculate

$$r = \bar{\lambda}_q \; / \; \bar{\lambda}_1 \tag{4.41}$$

where $\bar{\lambda}_j$ is the current approximation to the j-th eigenvalue of (4.40). If $r \geq 1.01$ no initial shifting is applied, but if $r < 1.01$

$$s_{initial} = (101 - 100\, r)\, \bar{\lambda}_1 \tag{4.42}$$

In case the above results in $s_{initial} < 0.5$, no initial shifting is applied.

(ii) Additional shifts $s' = 0.8\, \bar{\lambda}_1$ are imposed if prior to reaching a tolerance [29] of 10^{-2} for the first eigenvalue, the expected number of additional iterations for convergence (t) calculated as in [115], is larger than the available number of iterations (t_{av}),

$$t = \frac{\log(toli)}{\log(d)} \tag{4.43}$$

where $toli$ is the increase in accuracy still to be gained for the first

eigenvalue in the subspace iterations, and d is the current approximation to the convergence rate. Also,

$$t_{av} = t_{max} - t_c \tag{4.44}$$

where t_{max} is defined by the analyst (maximum number of iterations per eigenvalue being sought) and t_c is the number of iterations that have already been performed after the latest shift.

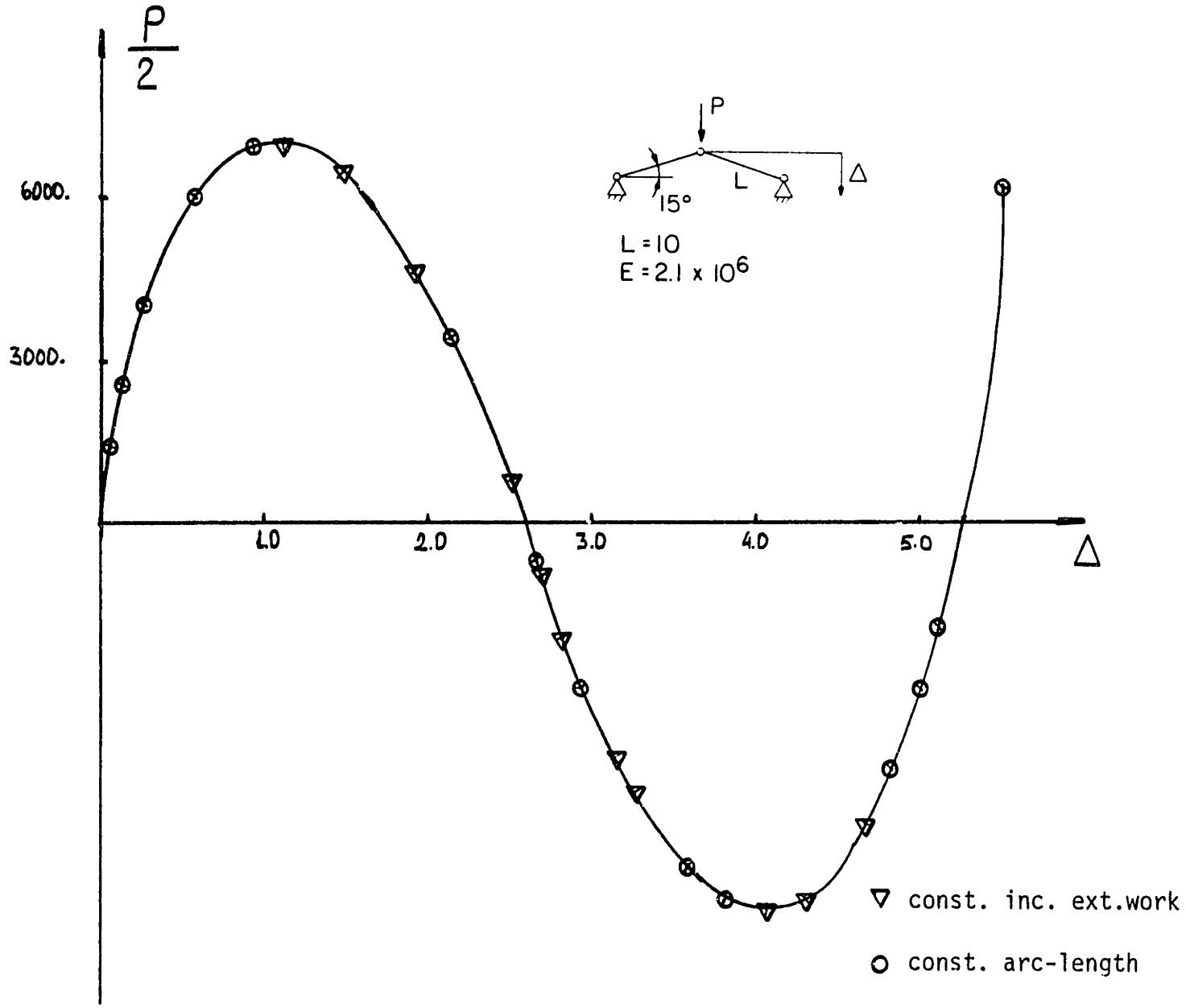
4.3 Some sample solutions

In this section we present some experiences using the algorithms described above.

In the analyses described below we deal with somewhat simple structures whose responses, however, contain the important different features of complex analyses.

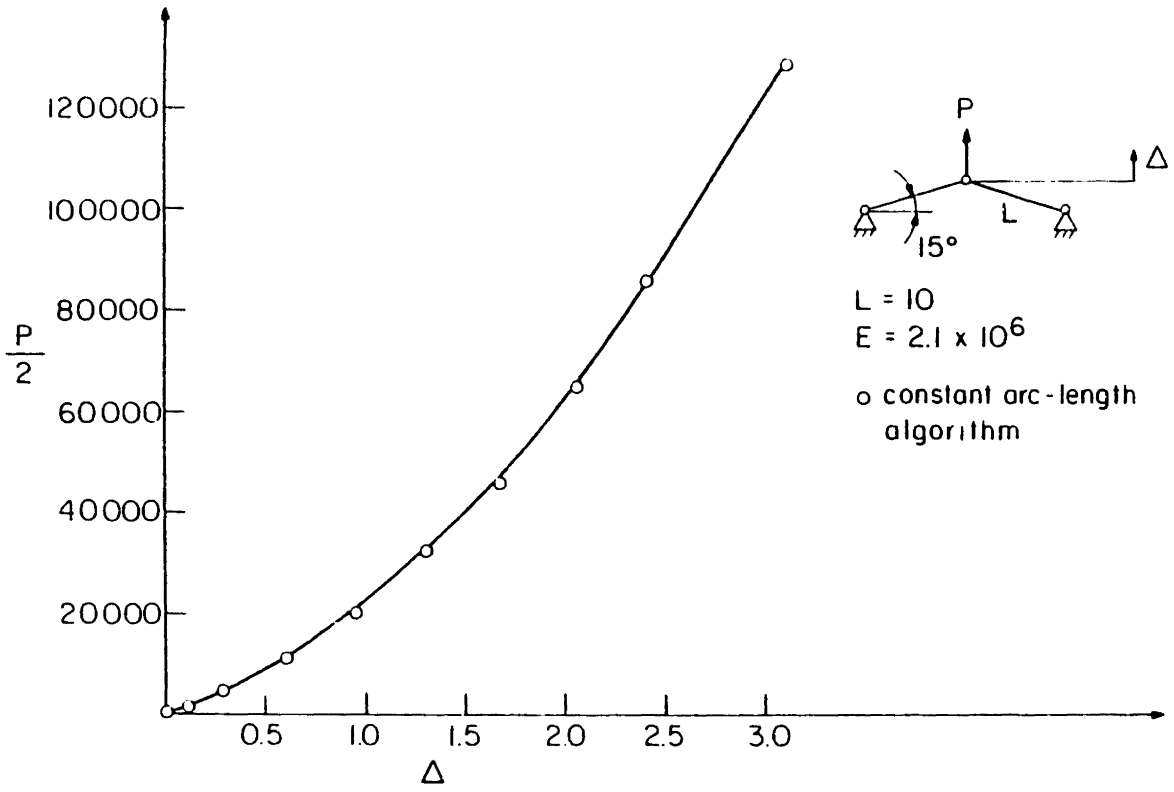
4.3.1 Structure with snap-through characteristic

Figure 4.2.a shows a two bar structure considered subjected to a compressive load. The equilibrium path obtained using the automatic algorithm is coincident with the one determined analytically in [29]. The performance of the automatic load stepping algorithm is interesting. We note that it switched near the critical points automatically from the constant arc-length criterion to the constant external work criterion, and vice versa. For this case, the algorithm that uses the full Newton iteration strategy is slightly more efficient than the one that uses the modified Newton strategy.



a) Snap-through problem

Figure 4.2 Analysis of a simple arch structure using updated Lagrangian formulation



b) Stiffening problem

Figure 4.2 continued

4.3.2 Structures with stiffening characteristic

Figures 4.2.b and 4.3 present the results obtained for problems with stiffening behavior (using the modified Newton iteration).

4.3.3 Structure with snap-back characteristic

The simple elastic truss structure shown in Fig. 4.4 was analyzed in [99] using a displacement controlled method. Due to the snap-back characteristic, the displacement at node 1 could not be used as the controlling displacement.

To use the automatic algorithm, an initial displacement was imposed at node 1 and from there on, the response was automatically traced.

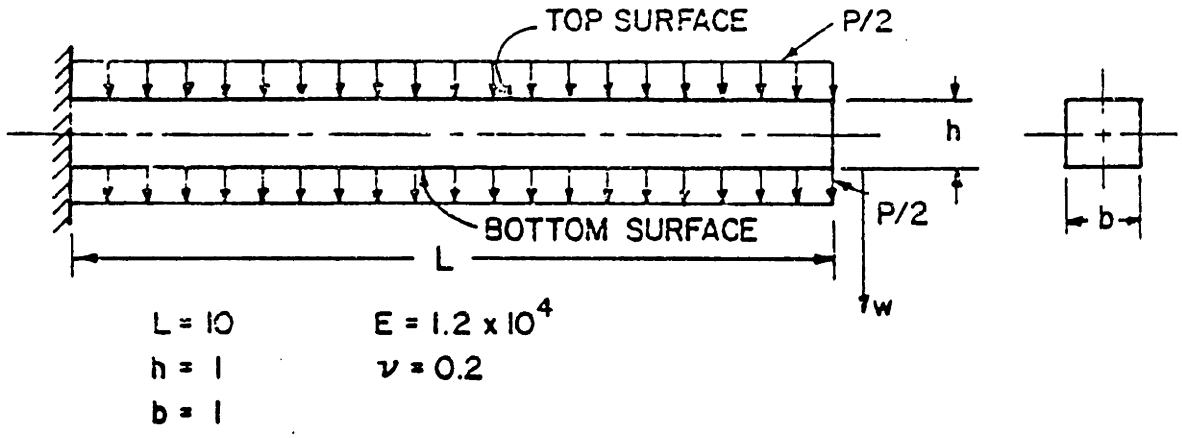
The solution results are given in Fig. 4.4 and are coincident with the solution obtained in [99].

For tracing the equilibrium path shown in the figure, the automatic algorithm using full Newton iterations needs 39 steps; in the same number of steps, the algorithm using modified Newton iterations only proceeds up to point A. In this case, the use of full Newton iterations results in a more effective solution.

4.3.4 Structures with collapse characteristics

Figure 4.5 shows the model considered for the analysis of an elastic-perfectly-plastic thick-walled cylinder. The response calculated with the automatic load stepping algorithm is also shown in the same figure, and compared with the solution reported in [106].

The difficulty of calculating the collapse load with prescribed load levels lies in that very small load increments near the ultimate load



$L = 10$ $\quad E = 1.2 \times 10^4$

$h = 1$ $\quad \nu = 0.2$

$b = 1$

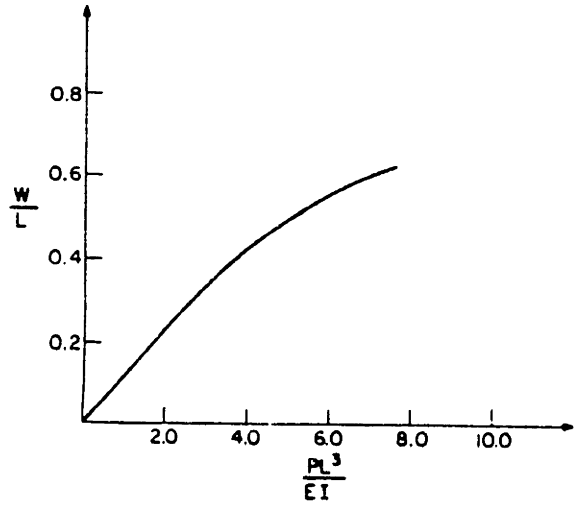
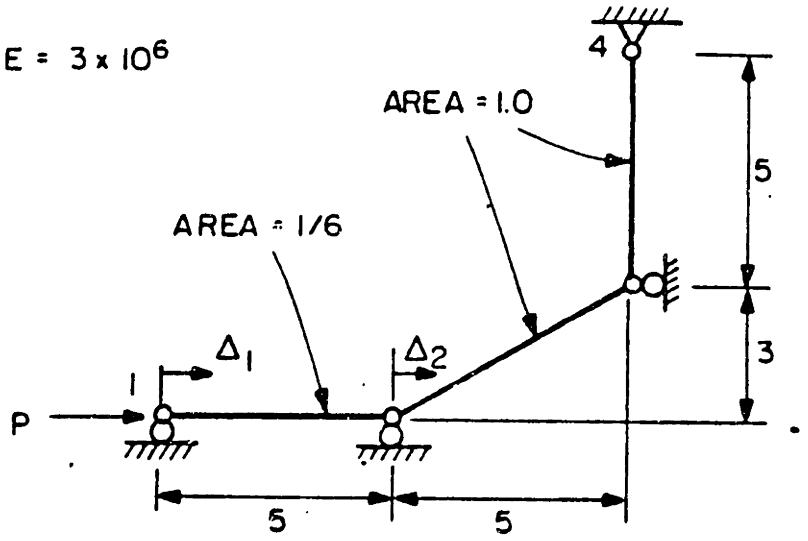


Figure 4.3 Large displacement analysis of a cantilever using total Lagrangian formulation



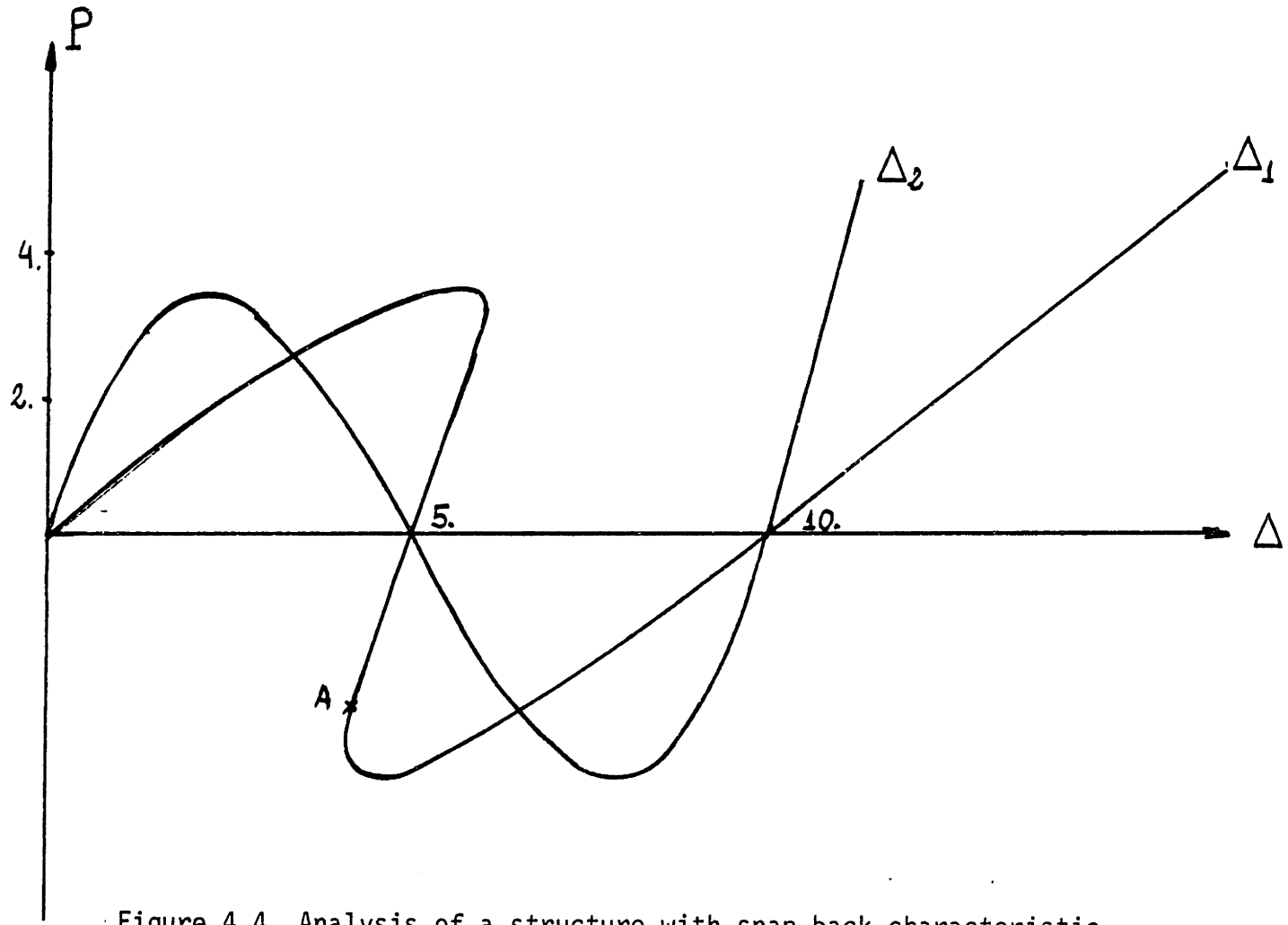


Figure 4.4 Analysis of a structure with snap-back characteristic using updated Lagrangian formulation

must be chosen—which for a complex structure in practice is not known—whereas the automatic load stepping algorithm computes the complete load-displacement response fully automatically.

In Figs. 4.6 and 4.7 the collapse response of two elastic-perfectly-plastic truss structures is calculated. In both cases geometric nonlinearities have to be included in order to be able to trace the complete equilibrium path, for a complete discussion of this two cases see Ref. [90].

4.3.5 Linearized buckling analysis of a circular ring

The circular ring shown in Fig. 4.8 was modeled using sixty 3-node isoparametric beam elements [29]. The ring is subjected to external pressure, which is assumed not to change direction.

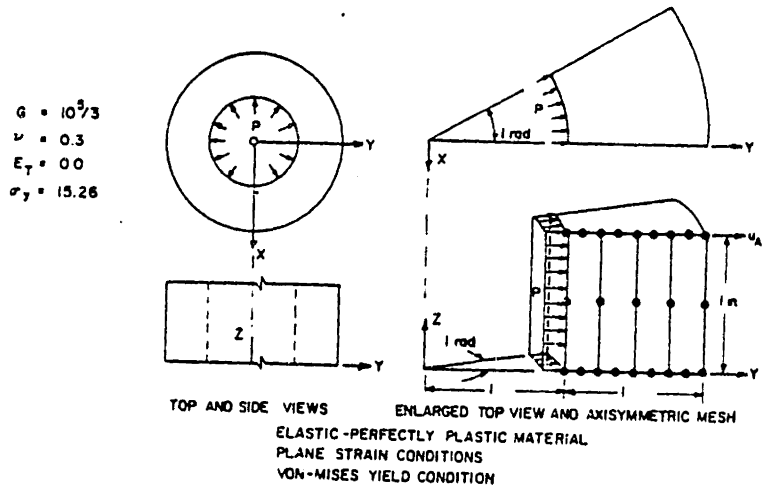
The analytical buckling pressure for the ring is given in [107].

We used Eqs. (4.35) and (4.37) to calculate the value of p_{cr} for the finite element model. Using 2 point Gauss integration along the element axes we obtained the exact value, whereas with 3 point integration the calculated buckling load was 8.3% too high.

4.3.6 Thermal buckling of rectangular plate

The simply supported plate subjected to increasing temperature was analyzed, as shown in Fig. 4.9, using 9-node shell elements [88].

The linearized buckling analysis was carried out using Eq. (4.37), and the calculated critical temperature, compared with the analytical one [103], has an error of 0.12%. Complete numerical integration was used in the evaluation of the shell element matrices.



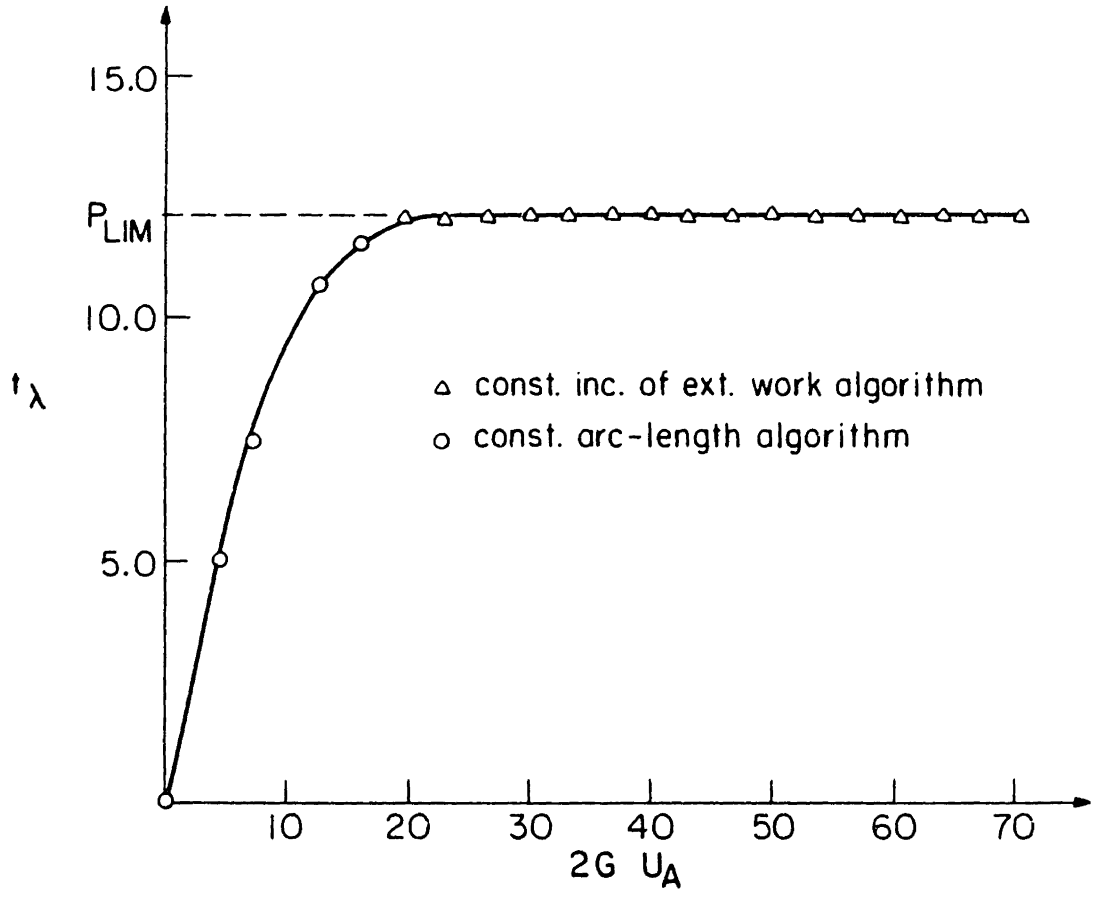
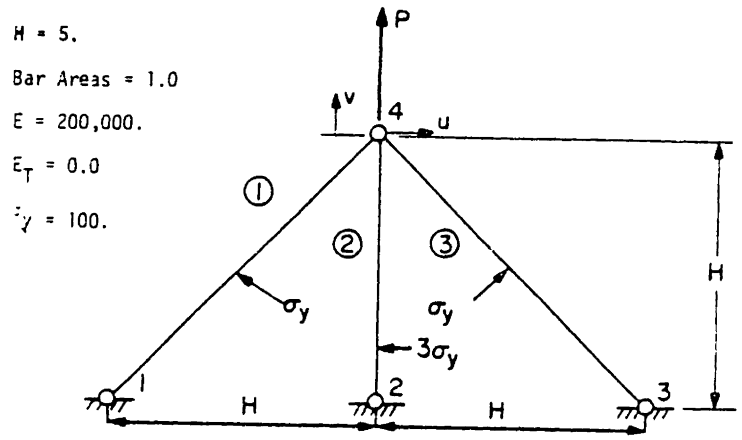


Figure 4.5 Analysis of a thick-walled elastic perfectly plastic cylinder using materially-nonlinear-only or updated Lagrangian formulation



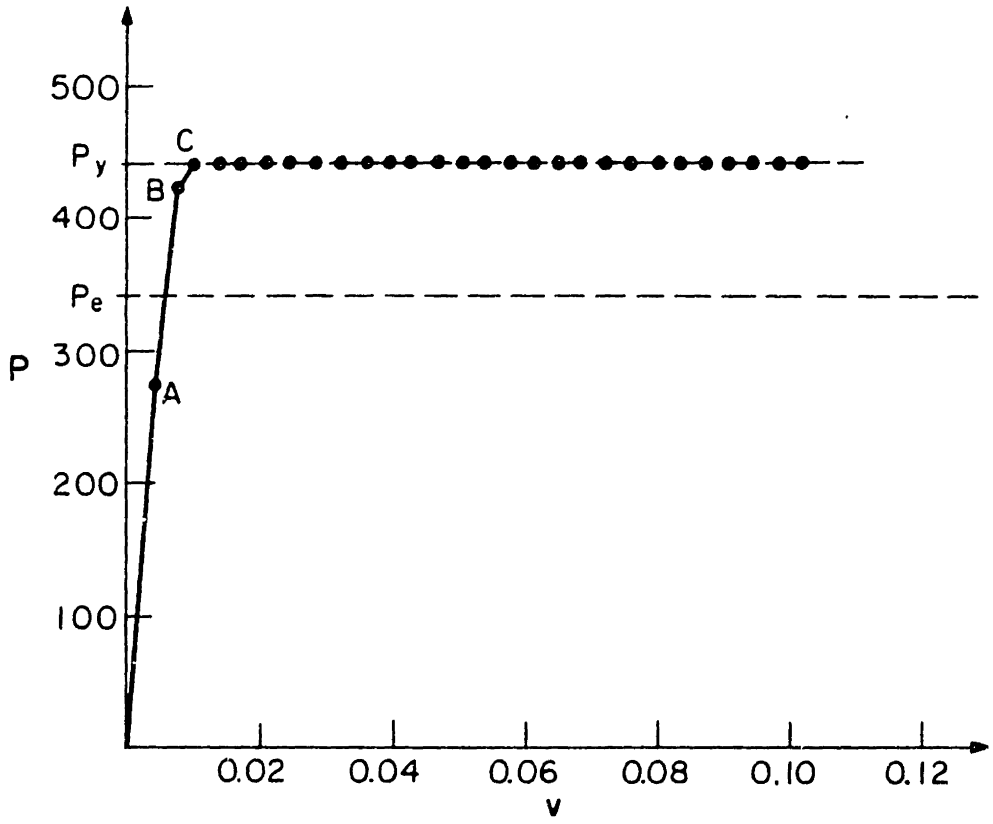
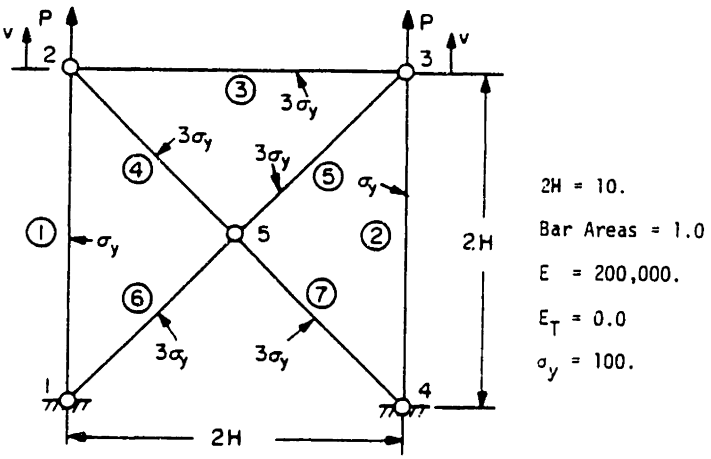


Figure 4.6 Analysis of a triangular truss structure using updated Lagrangian formulation



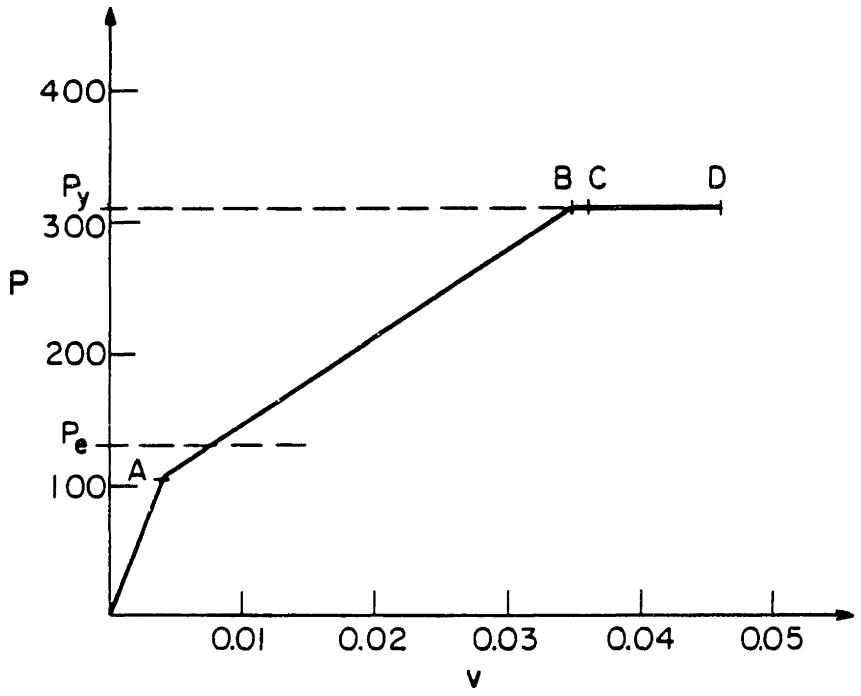


Figure 4.7 Analysis of a 7-bar truss using updated Lagrangian formulation

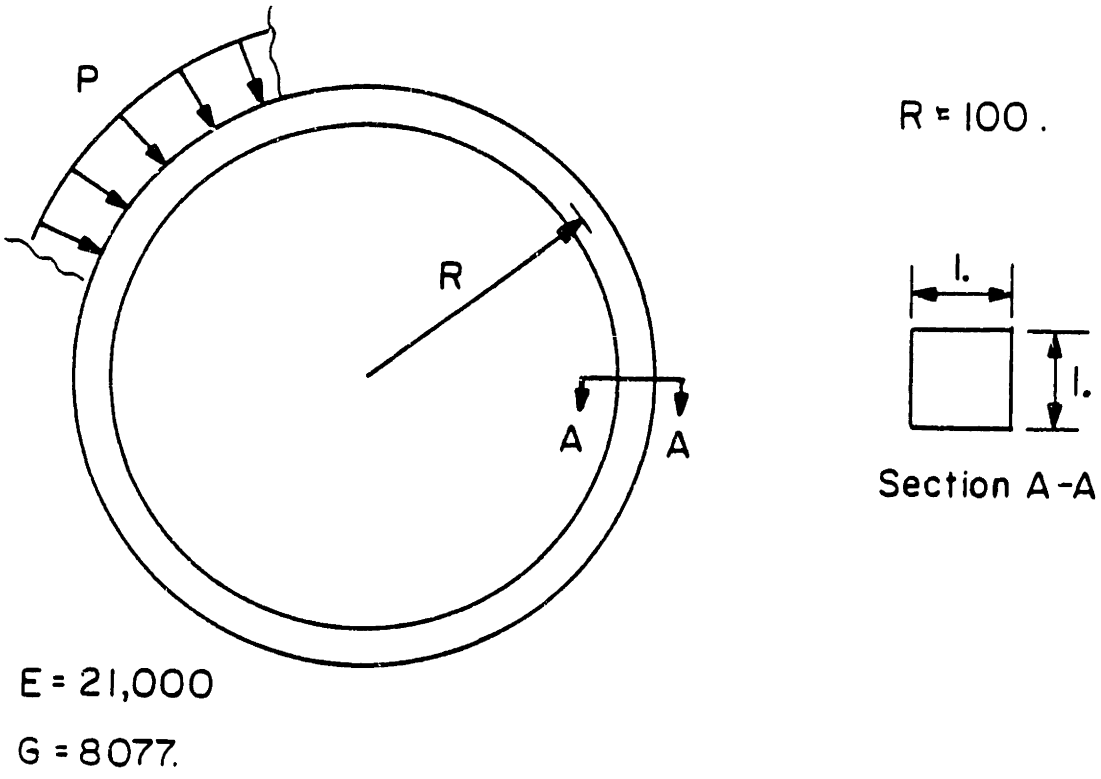
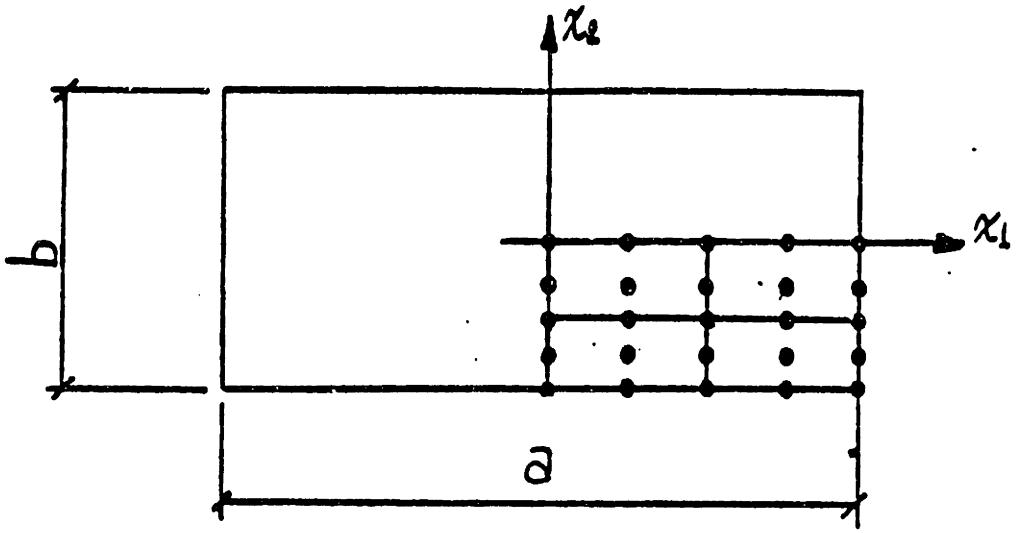


Figure 4.8 Analysis of a circular ring under constant pressure



a = 100
b = 50
thickness = 2.5

E = 2,100,000
ν = 0.3
α = 2×10^{-5}

Figure 4.9 Thermal buckling of a rectangular plate

5. NUMERICAL TESTS AND PROBLEM SOLUTIONS

In Chapter 3 we have presented the formulation of a new, non-flat, 4-node nonlinear shell element and stated that we implemented it in the computer program ADINA [111].

A study of the numerical behavior of the element must next be done. Our purpose, in the present chapter, is to report upon numerical experimentation in an organized way such that the following objectives are achieved:

(i) We show that the new element converges, implying by this [31] that it is stable and consistent.

(ii) We examine the solutions it provides for some elementary problems so that we can verify that the element behaves as we expected (e.g. ability to approximate the Kirchhoff-Love hypothesis for thin shells under different geometrical configurations), and at the same time gain more insight about the element performance.

(iii) For some benchmark linear problems we compare its rate of convergence with other existing shell elements.

(iv) We show via some simple problems that the element can be reliably used for general nonlinear analysis.

(v) We compare the solutions it provides in nonlinear analyses with experimental, analytical or numerical solutions obtained using other nonlinear shell elements. In this way we will be able to judge on the element performance (accuracy plus efficiency) in nonlinear analysis.

The numerical solutions are all obtained using 2x2 Gauss integration

in the $r_3 = 0$ surface of the element, and 2 and 4 point Gauss integration in the r_3 direction, for elastic and elasto-plastic analyses, respectively.

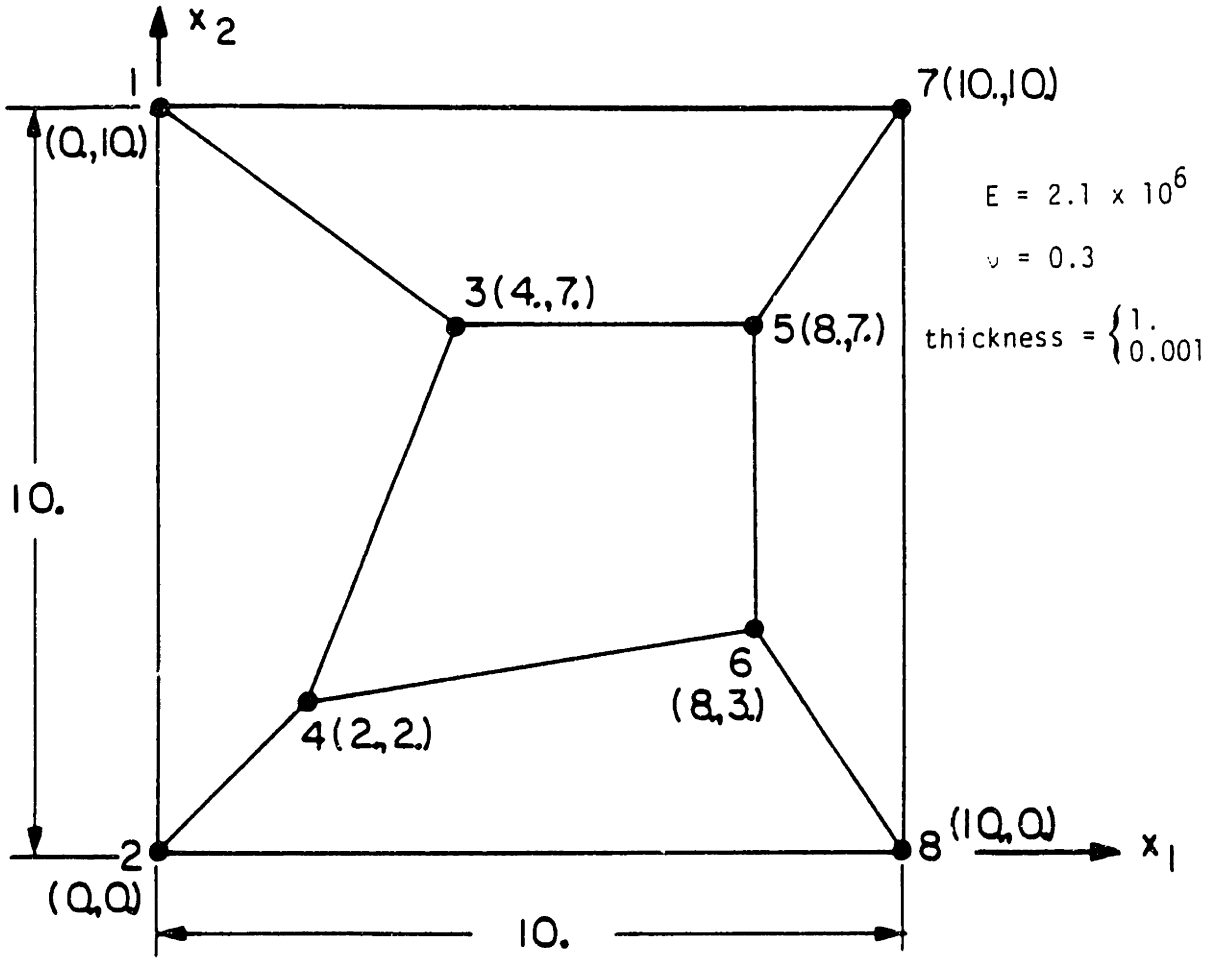
In some of the nonlinear problems the automatic load stepping algorithm of Chapter 4 is used.

5.1 Convergence check

First the stability issue will be discussed. In Appendix 3, we presented an argument towards showing that the formulated shell element does not present, under any geometrical configuration, spurious rigid body modes. As a first step to test the element, the eigenvalues of the stiffness matrices of undistorted and distorted elements were calculated. In all cases, as expected, the element displayed the six rigid body modes and no spurious zero energy modes.

In order to check for the consistency of the formulation, since the transverse shear stresses do not satisfy the strain-displacement relations (incompatibility), the patch test needs to be performed [35, 36]. For doing this, the mesh shown in Fig. 5.1 was used. In the first analysis, the mesh was loaded with the constant bending moment indicated and a constant curvature (linear distribution of rotations) was obtained for both plate thicknesses in the two plate directions. The transverse displacements predicted by the model were - as expected - those of Kirchhoff-Love plate theory at nodes 7 and 8.

In the second analysis, the rotational degrees of freedom were deleted and the mesh was subjected to shear forces. As expected, for



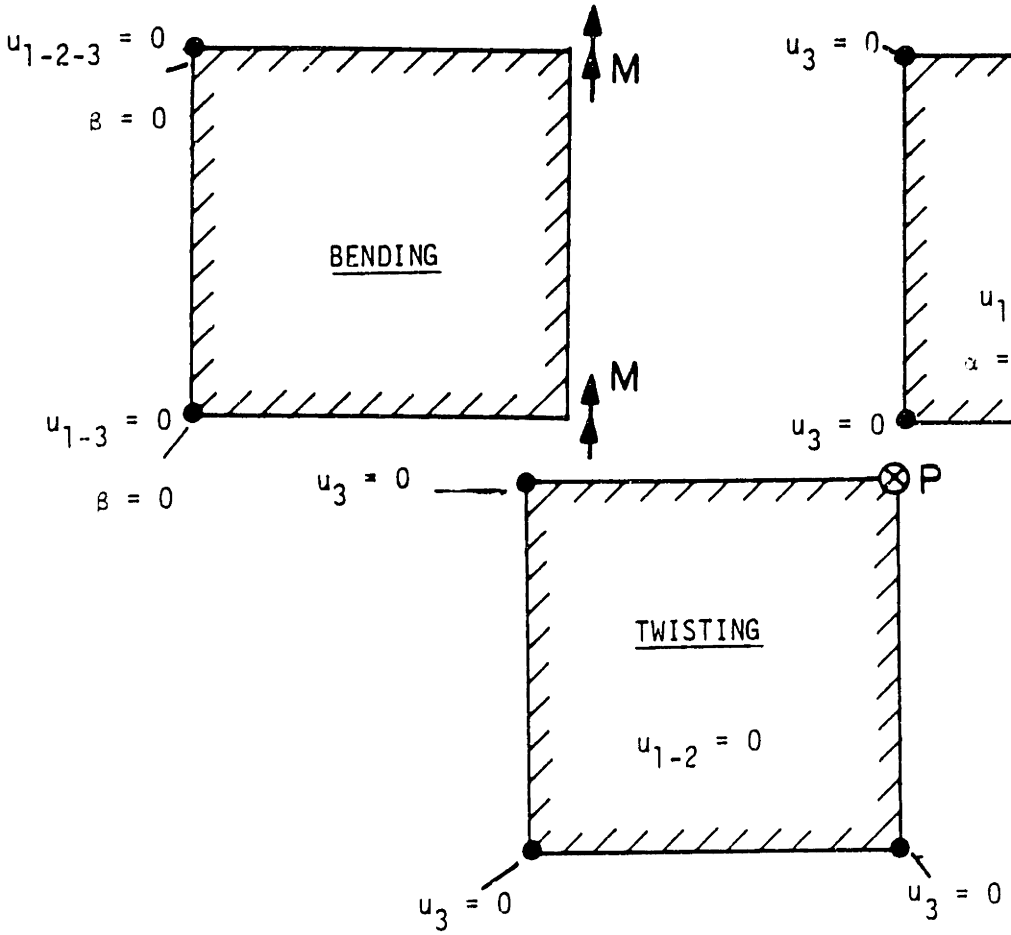


Figure 5.1 Patch tests

both plate thicknesses a linear distribution of transverse displacements was obtained.

In the third analysis, the mesh was subjected to an external twisting moment. In the thin plate analysis, constant curvatures were obtained in both plate directions and the transverse displacements agreed with the analytical thin plate theory solution. In the thick plate analysis, a slight nonsymmetry in the displacement response (the third digit) was obtained due to the nonsymmetric representation of the transverse shear deformations. This nonsymmetry is not observed, if the shear deformations are suppressed (which corresponds to thin plate theory) by choosing a large value for the shear correction factor k [29, p. 236] (or when using rectangular elements in the mesh).

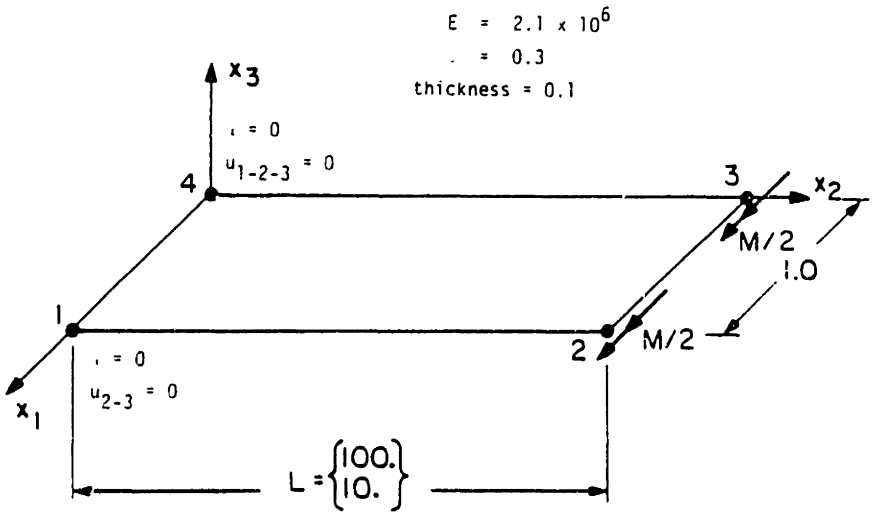
Finally, it should be noted that the patch test is of course passed for the three membrane stress states (τ_{11}, τ_{22} and τ_{12} constants).

5.2 Some simple problems in linear analysis

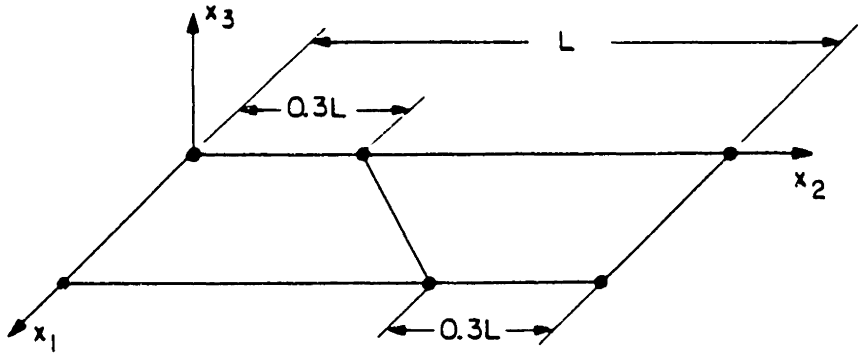
5.2.1 Cantilever linear analyses

A cantilever of unit width, thickness 0.1 and lengths 10 and 100 was subjected to a tip bending moment. The structure was modeled using one single element, two distorted elements and four triangular elements obtained each of them degenerating a quadrilateral element, as shown in Fig. 5.2. The results obtained in these analyses for the displacement and rotations at the cantilever tip and the stresses were coincident with those of Bernoulli beam theory.

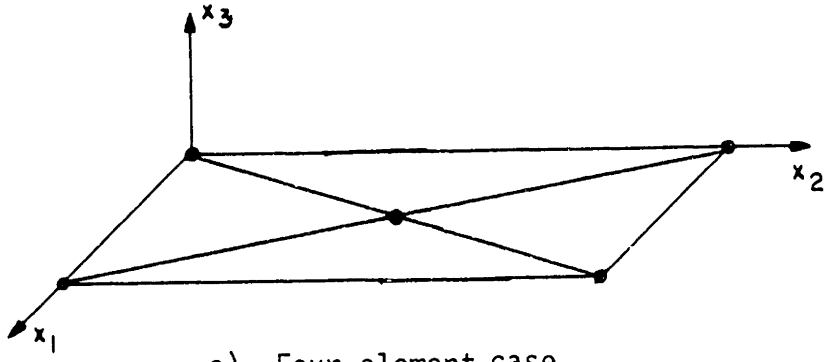
This shows, as expected, that



a) One element case

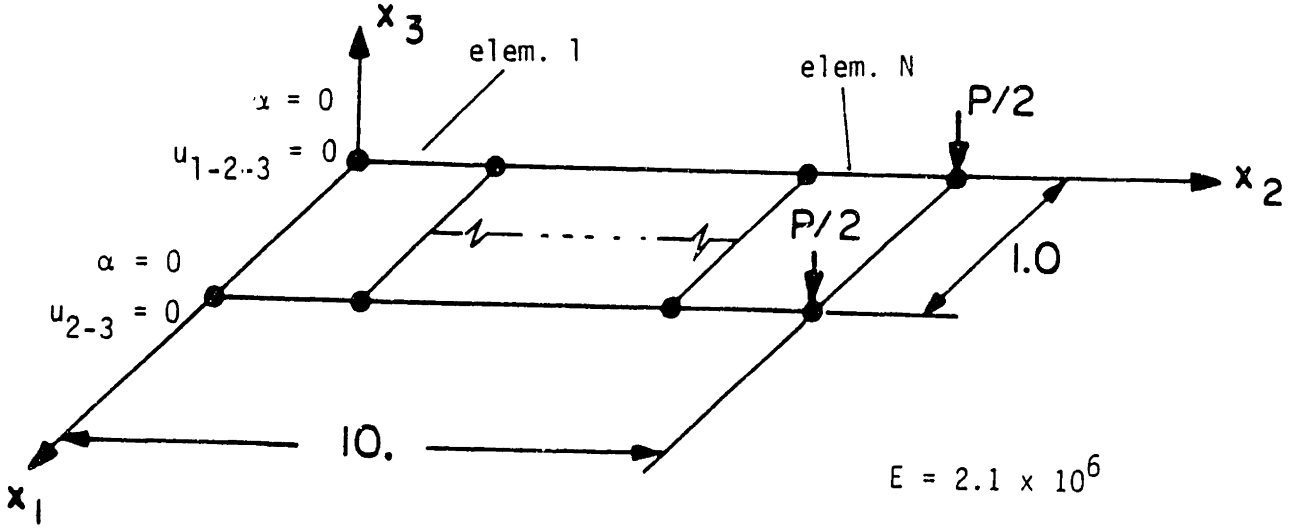


b) Two element case



c) Four element case

Figure 5.2 Cantilever subjected to tip bending moment



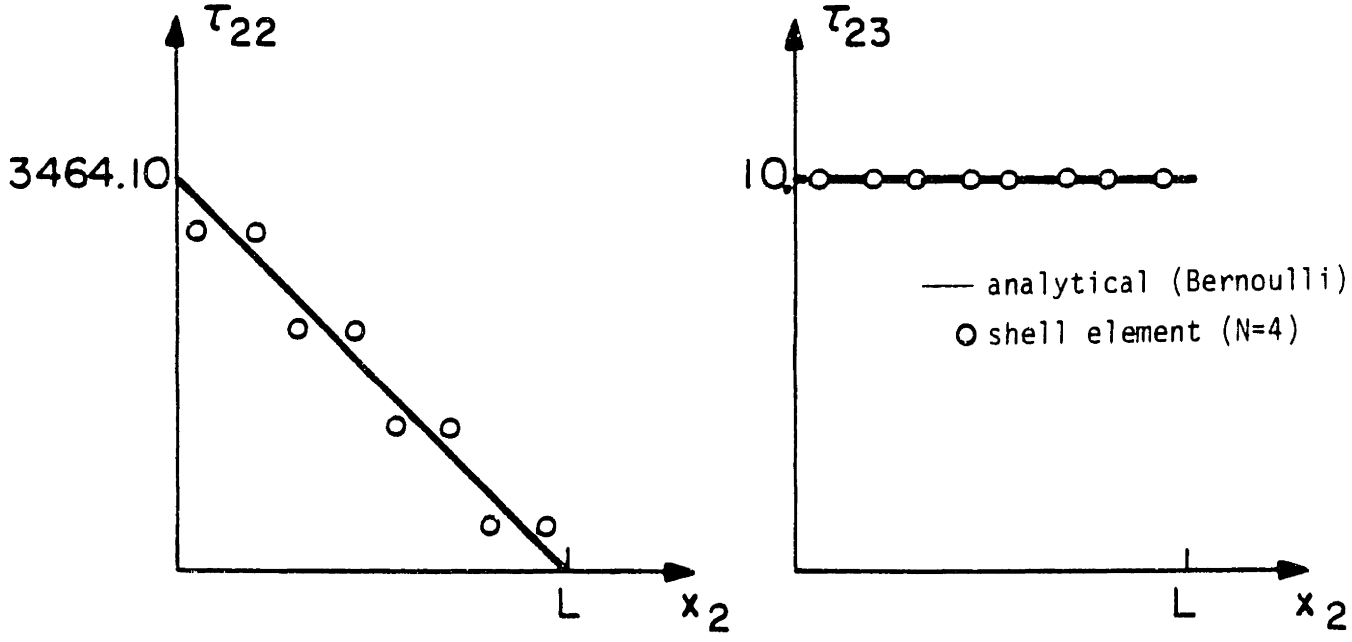
$E = 2.1 \times 10^6$

$\nu = 0.0$

thickness = 0.1

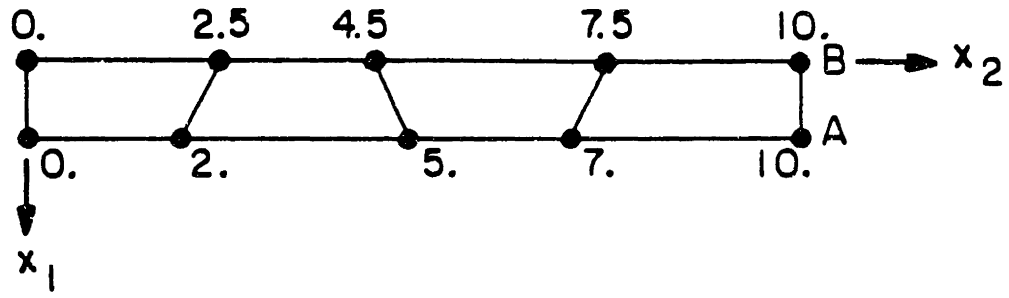
P = 1.0

N	$u_{3_{TIP}}^{FEM} / \left(\frac{PL^3}{3EI} + \frac{PL}{AG}\right)$
1	0.750
4	0.984



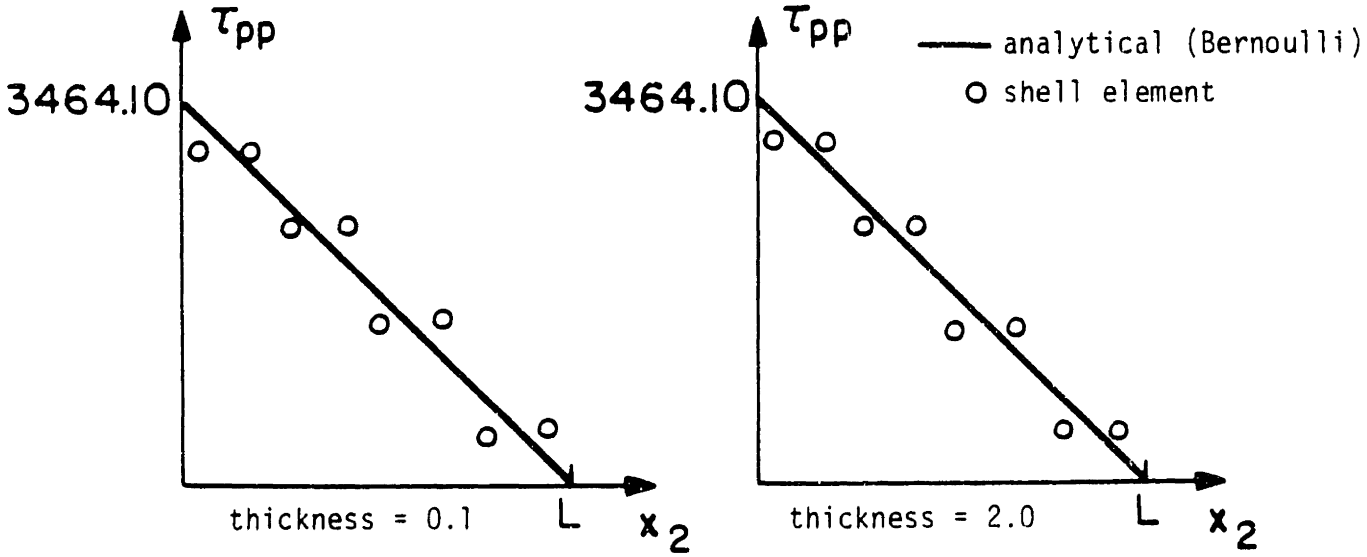
a) Solution using non-distorted elements

Figure 5.3 Response of a cantilever subjected to transverse tip load, stresses shown are those at the Gauss integration stations $r_3 = 0.57735$; τ_{pp}, is the principal stress in the distorted mesh, and its direction was always less than 11 degrees from the x_2 axis.



thickness	η|point B	η|point A
0.1	0.989	0.996
2.0	1.0013	0.9995

η = (u_3 distorted mesh)/(u_3 non-distorted mesh)



P = 1.0

P = 400.0

b) Solution using distorted elements

Figure 5.3 continued

(i) the element does not lock,

(ii) it can approximate the Kirchhoff-Love hypothesis.

Also it shows that (i) and (ii) are valid, regardless of the element distortions.

Next, the cantilever in Fig. 5.3.2 was analyzed for the transverse tip load shown. Using 4 equal size elements to idealize the cantilever, again good results were obtained when compared with beam theoretical results.

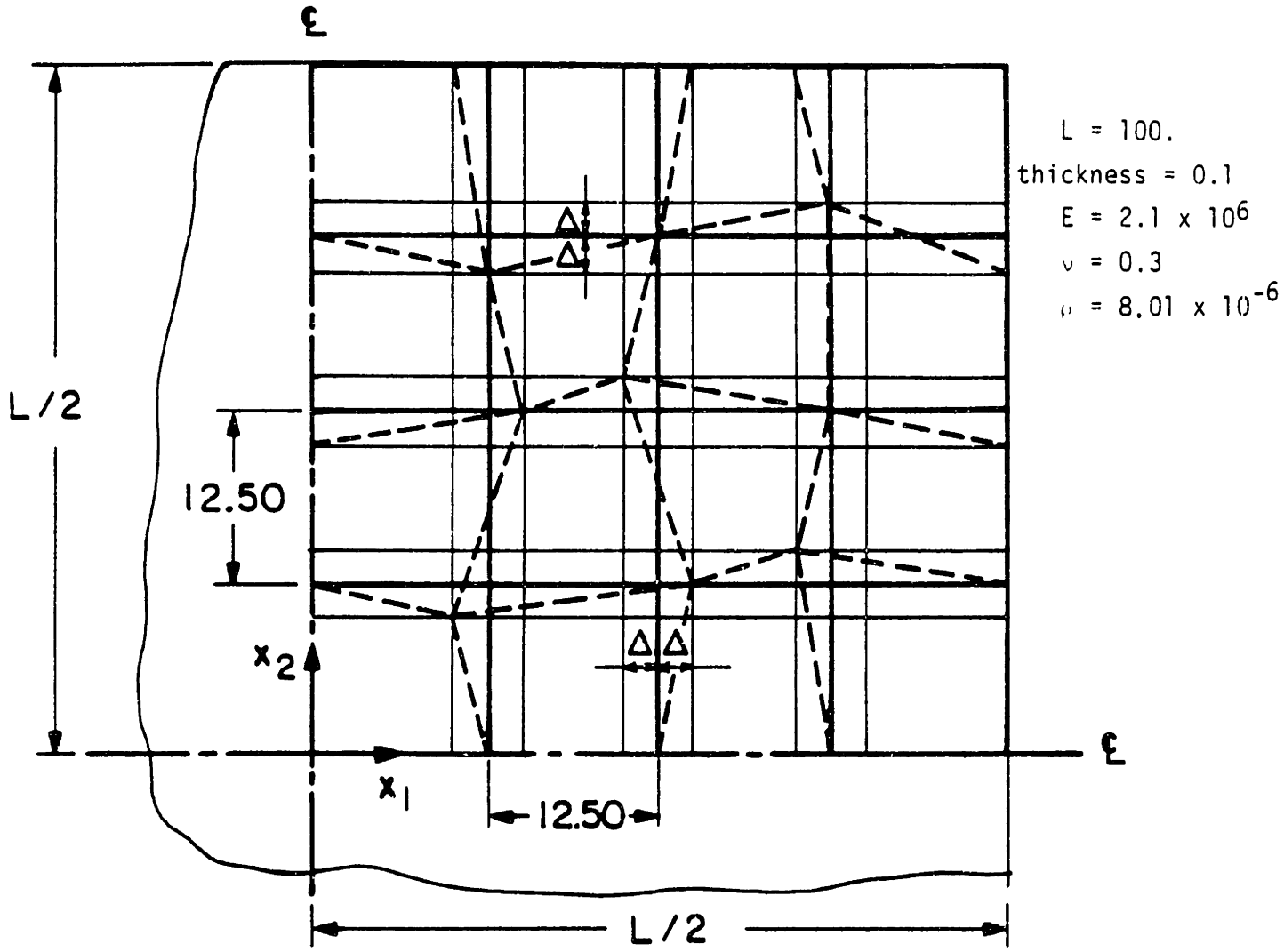
Finally, the elements modeling the cantilever were distorted as shown in Fig. 5.3.6. for a thin and a thick cantilever. The results show that the transverse displacements and normal bending stresses are almost insensitive to the element distortions. However, the calculated transverse shear stresses (not shown in the figure) are not accurate.

5.2.2 Linear analysis of simply supported plate

A simply supported plate was considered for a static and a frequency analysis using a consistent mass matrix. To model one quarter of the plate a 4x4 mesh of equal elements was used. Figure 5.4 gives a comparison of the numerically and analytically [6, 112] predicted results. The same plate was also analyzed for its static response using the distorted element mesh also shown in Fig. 5.4(a) and the results of Fig. 5.4(c) were obtained. Again, as in the previous example, we can see that the results are almost insensitive to the element distortions.

5.3 Linear analysis of a cylindrical (Scordelis-Lo) shell

The shell structure shown in Fig. 5.5 has frequently been used as



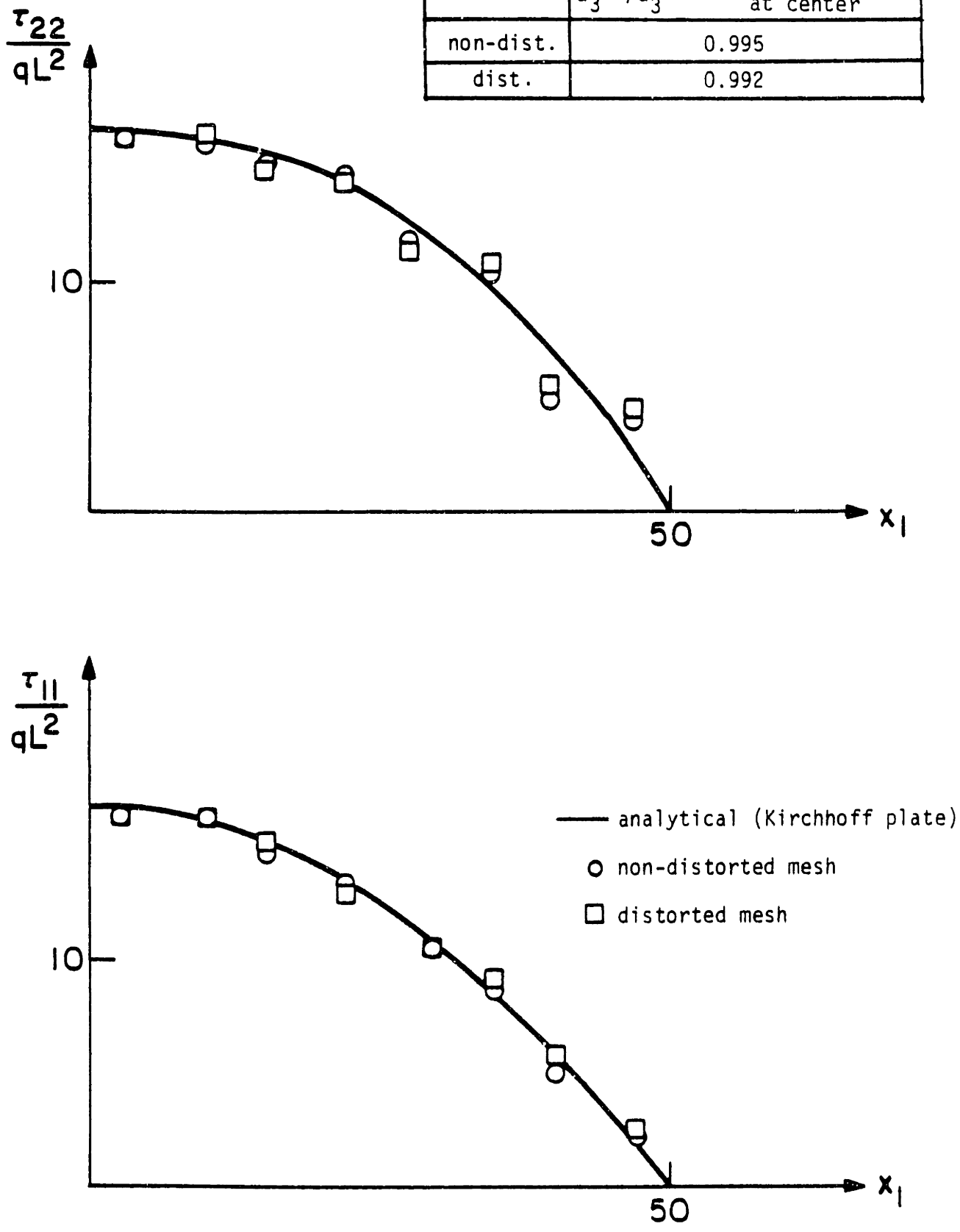
a) Finite element models

Mode shape	$f^{FEM} / f^{thin\ plate}$
1-1	1.02
1-3	1.18
3-3	1.17

b) Natural frequencies (cycles/sec) calculated using the non-distorted mesh

Figure 5.4 Linear analysis of a simply-supported square plate, the parameter of distortion, Δ, was equal to 2.50.

Model	$u_3^{FEM}/u_3^{thin\ plate}$ at center
non-dist.	0.995
dist.	0.992



c) Static response due to constant pressure loading, stresses are given along line $x_2 = 0$, $x_3 = 0.028868$.

Figure 5.4 continued

R = 300.

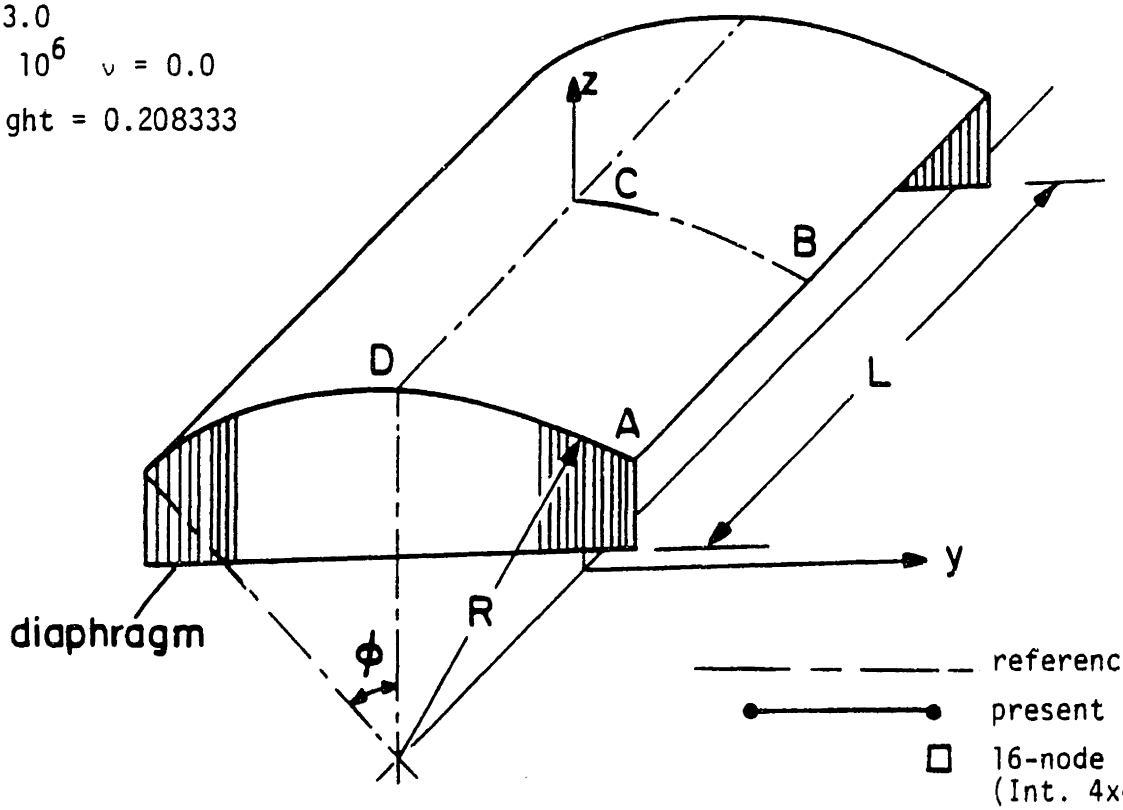
L = 600.

ϕ = 40°

thickness = 3.0

E = 3. x 10^6 ν = 0.0

specific weight = 0.208333



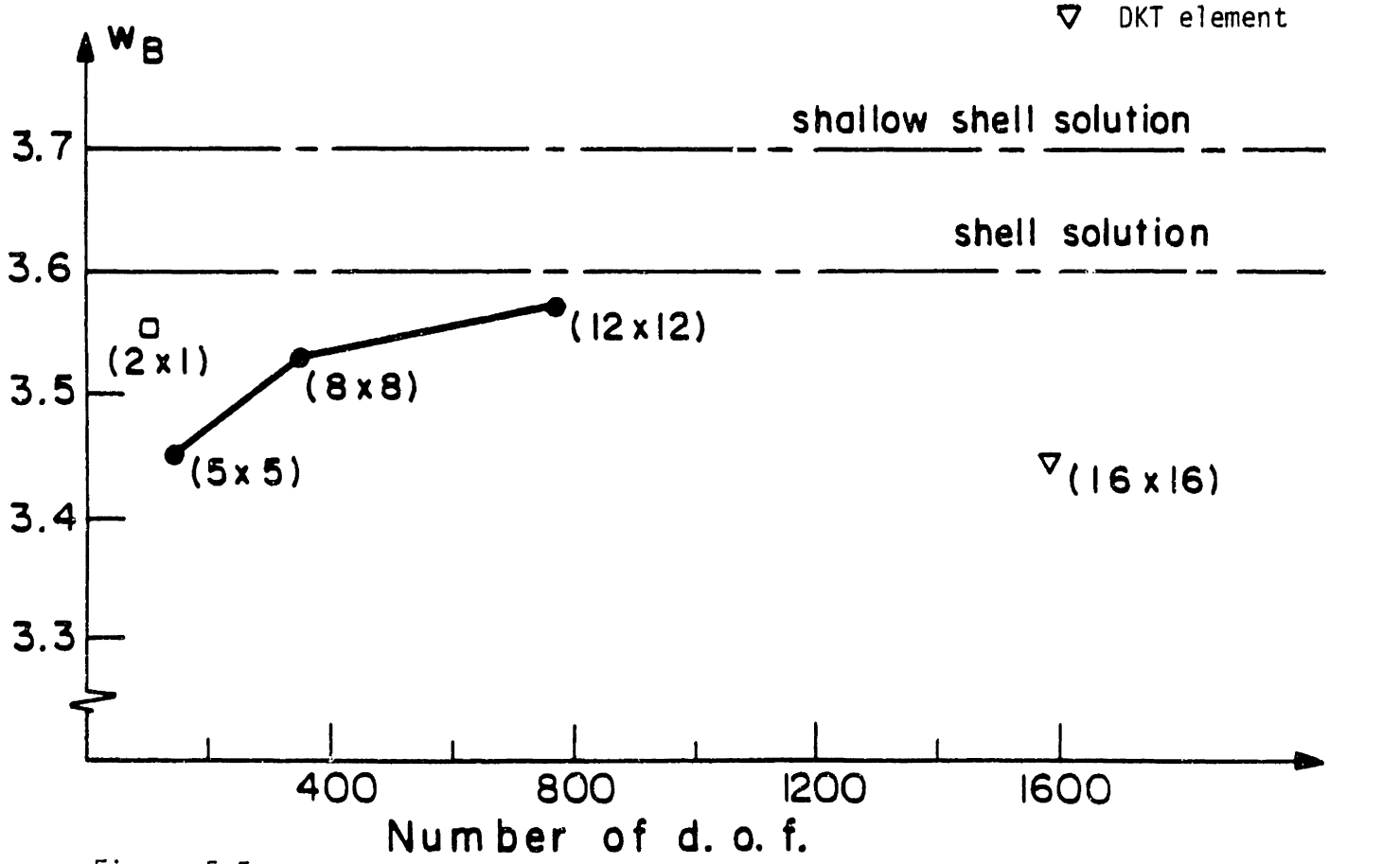


Figure 5.5 Linear analysis of a cylindrical shell subjected to dead weight. The 2x1 result refers to the solution obtained with two 16-node shell elements spanning from C to B. The 16x16 result refers to the use of 512 equal triangular DKT elements.

a benchmark problem to test shell elements [46, 87]. Figure 5.5 shows the solution obtained with our element. In each of the solutions uniform meshes with equal sized elements were employed over one quarter of the shell. Solutions obtained using the 3-node DKT triangular element [111] and the 16-node isoparamteric element [111] are also shown for comparison.

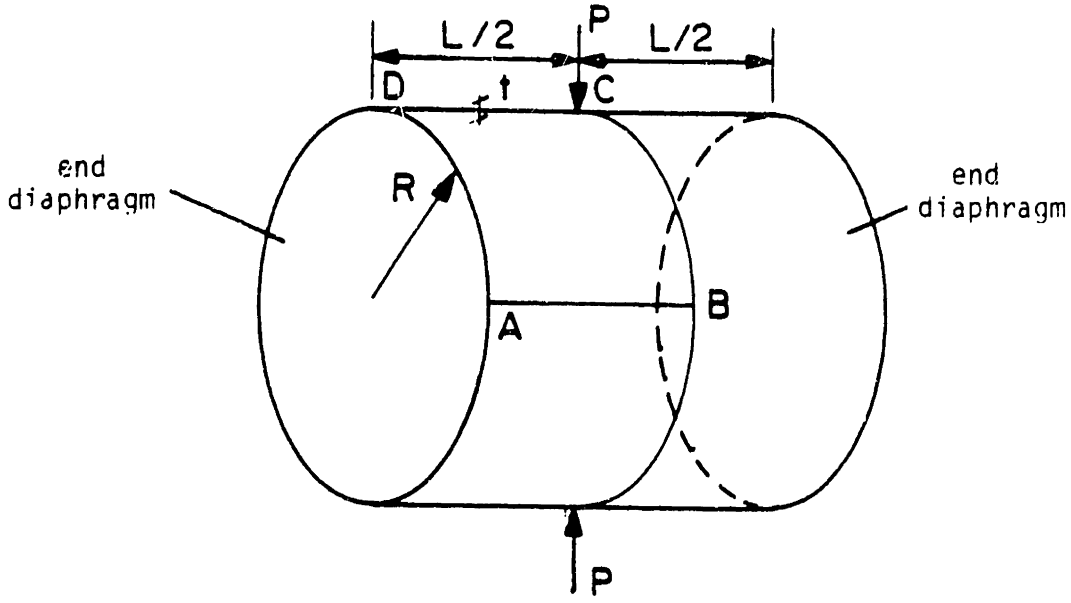
5.4 Linear analysis of a pinched cylinder

The pinched cylinder problem shown in Fig. 5.6 was also frequently analyzed to test shell elements. Figure 5.6 shows the convergence behavior obtained with our new element, when comparing the finite element solutions with the series given in Refs. [7, 51]. Note that using the 16-node isoparametric shell element of Refs. [62, 63], also a fairly large number of degrees of freedom are required to predict the response of the cylinder accurately.

5.5 Some simple problems of nonlinear analysis

5.5.1 Large deflection analysis of a cantilever

The cantilever shown in Fig. 5.7 was analyzed for its large displacement and large rotation response. This is a typical problem considered to test the geometric nonlinear behavior of beam and shell elements [60, 111]. Figure 5.7 shows also the models used in the analysis. The first two models are single element, cubic and parabolic isoparametric degenerated shell element models. Model I predicts the response of the cantilever very accurately, whereas model II yields an accurate response solution in linear analysis but locks once the element is curved in the nonlinear response solution. This observation is in accordance with



R/t = 100. $\hat{w}_C = \frac{W_C E t}{P}$ $\hat{w}_C$ series solution =-164.24

L/R = 2. by Lindberg et. al.

ν = 0.3

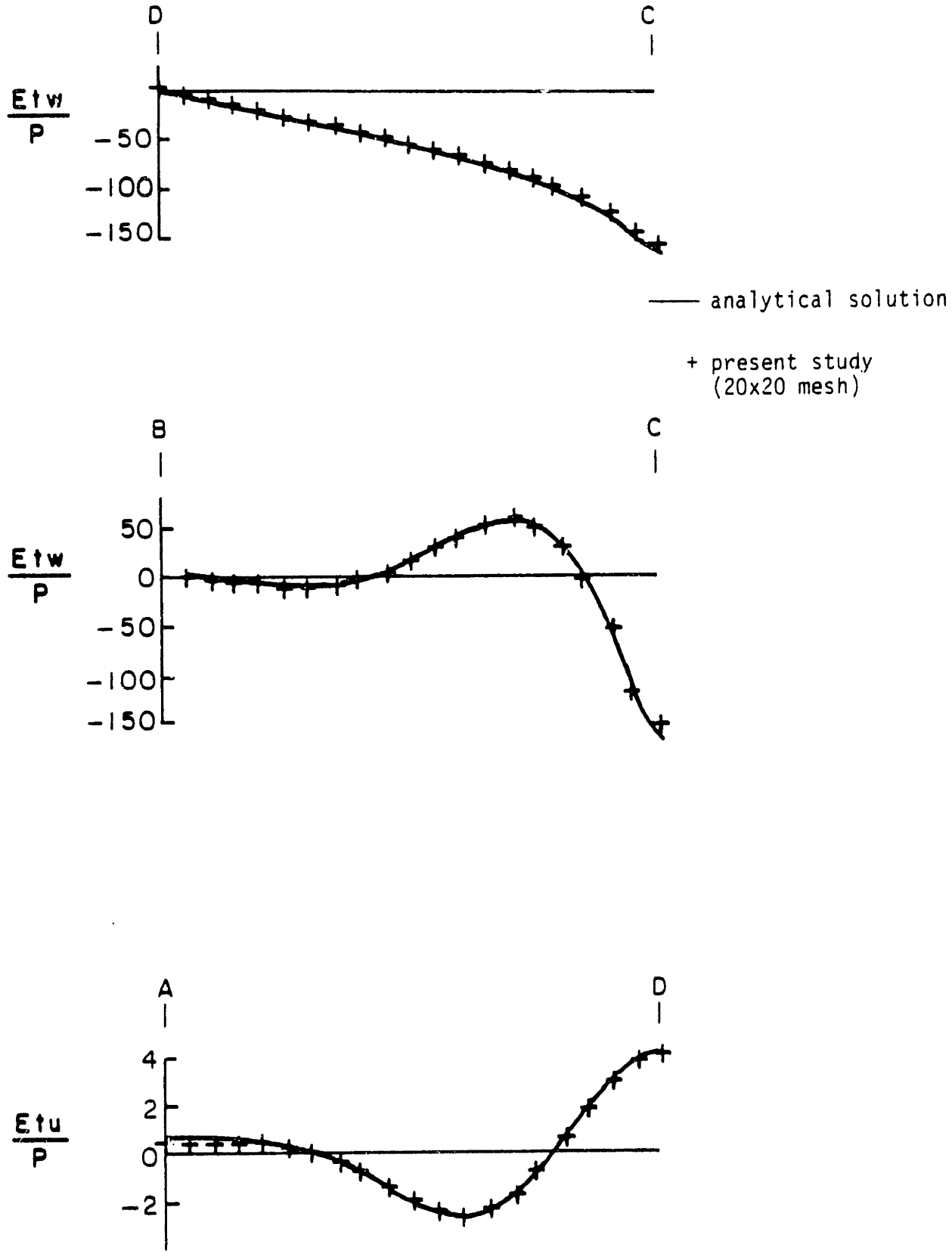
Mesh for $\frac{1}{8}$ th of shell	Number of d.o.f.	$\hat{w}_C^{FEM} / \hat{w}_C^{analyt.}$
5x5	130	0.51
10x10	510	0.83
20x20	2020	0.96

a) Convergence study for 4-node element

Element	Mesh for $\frac{1}{8}$th of shell	Number of d.o.f.	$\hat{w}_C^{FEM} / \hat{w}_C^{analyt.}$
4-node	20x20	2020	0.96
16-node	10x10	4530	0.98

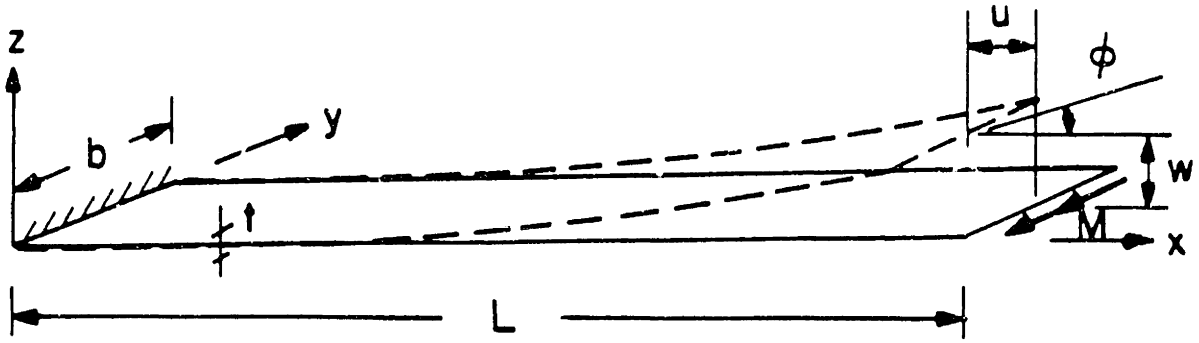
b) Comparison between 4-node and 16-node elements

Figure 5.6 Linear analysis of a pinched cylinder; u = axial displacement, w = radial displacement



c) Displacements

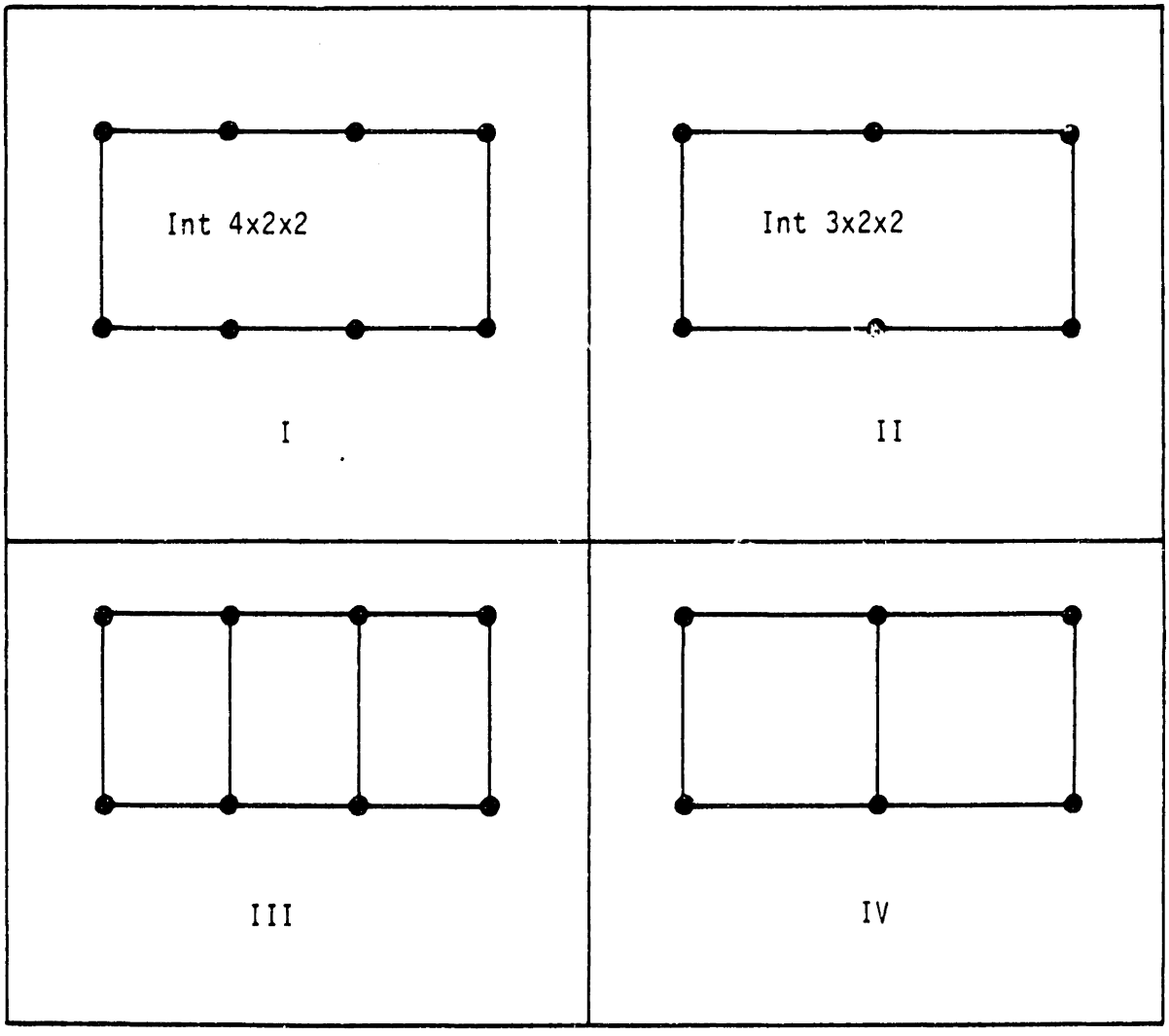
Figure 5.6 continued



b = 1.0 E = 1800.

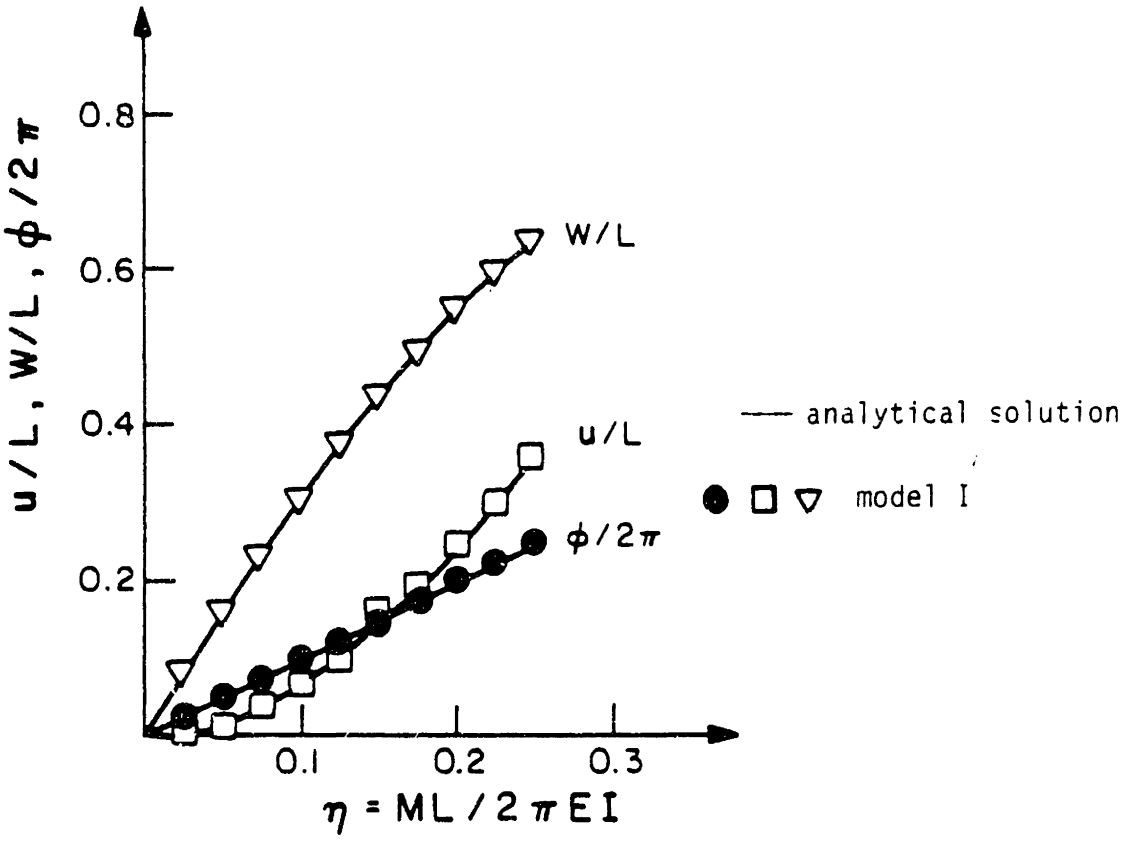
t = 1.0 ν = 0.0

L = 12.0

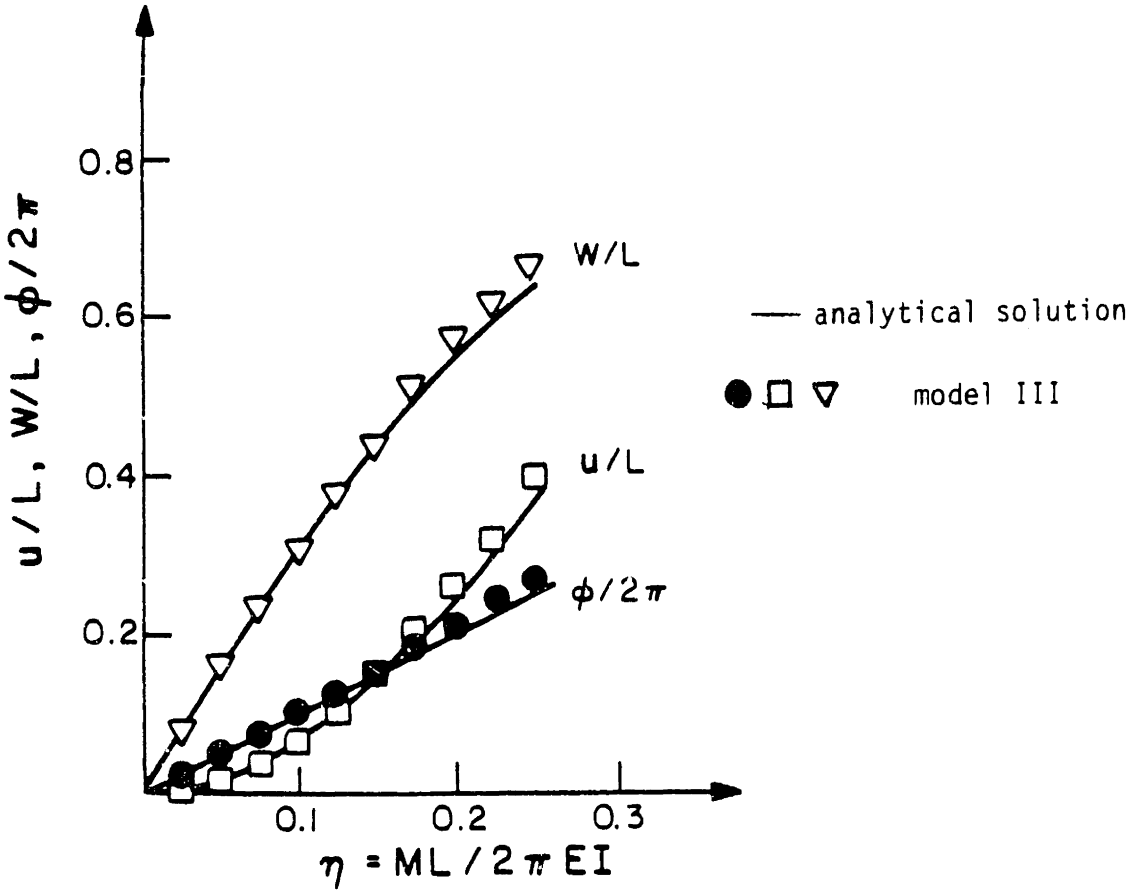


a) Finite element models

Figure 5.7 Large deflection analysis of a cantilever using non-distorted elements

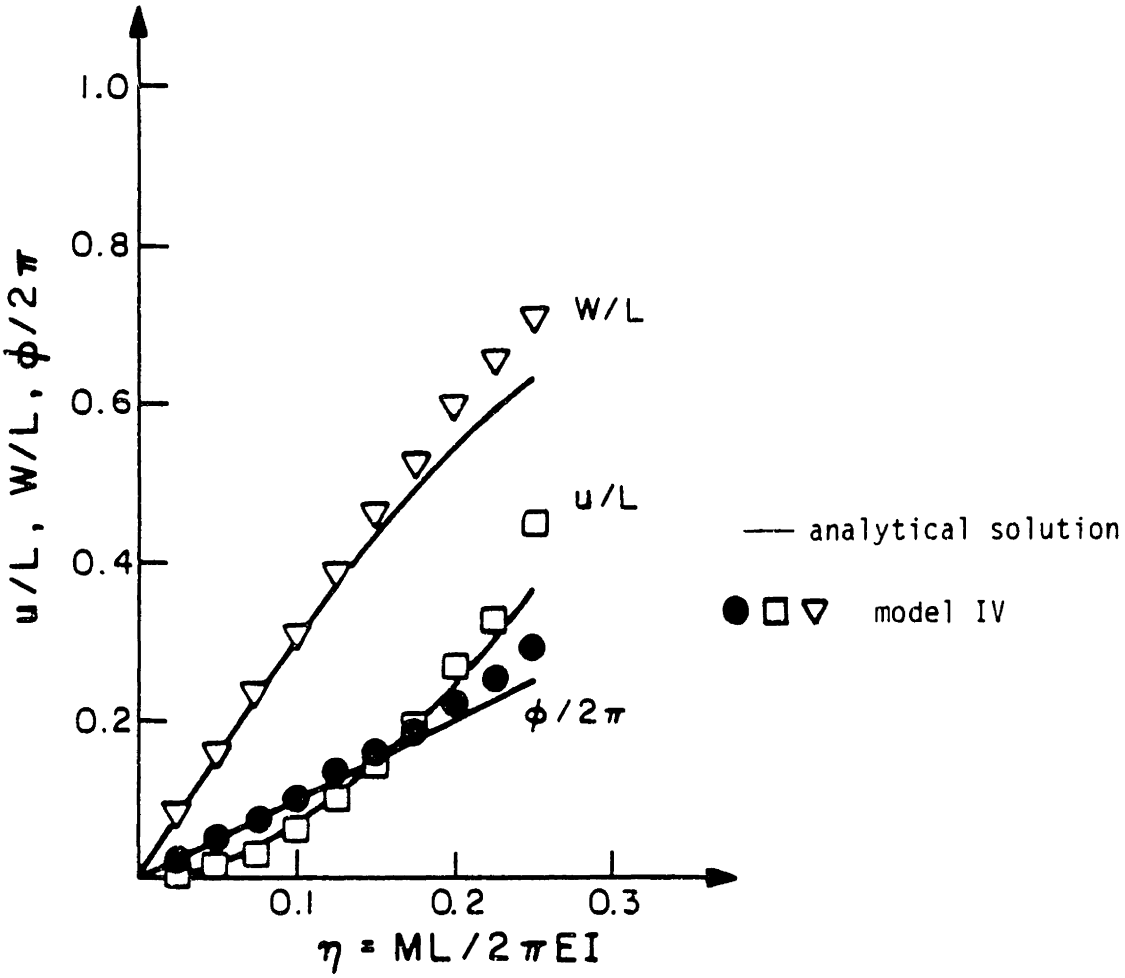


b) Response of model I



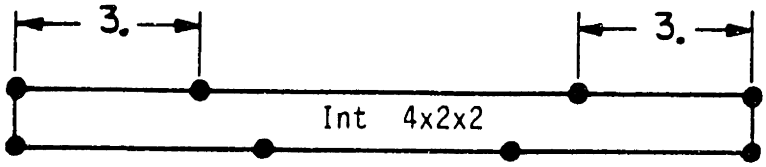
c) Response of model III

Figure 5.7 continued

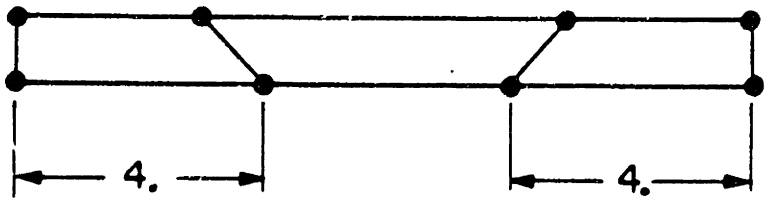


d) Response of model IV

Figure 5.7 continued



Model I - distorted



Model III - distorted

	Model I - distorted			Model III - distorted		
	step 2	step 5	step 8	step 2	step 5	step 8
$\phi^{FEM}/\phi^{ANALYT.}$	0.13	0.13	0.13	0.95	0.84	0.76
$u^{FEM}/u^{ANALYT.}$	0.01	0.01	0.01	0.89	0.68	0.56
$w^{FEM}/w^{ANALYT.}$	0.10	0.11	0.12	0.95	0.86	0.81
$\phi^{ANALYT.}$	18°	45°	72°	18°	45°	72°

Figure 5.8 Large deflection analysis of a cantilever using distorted elements

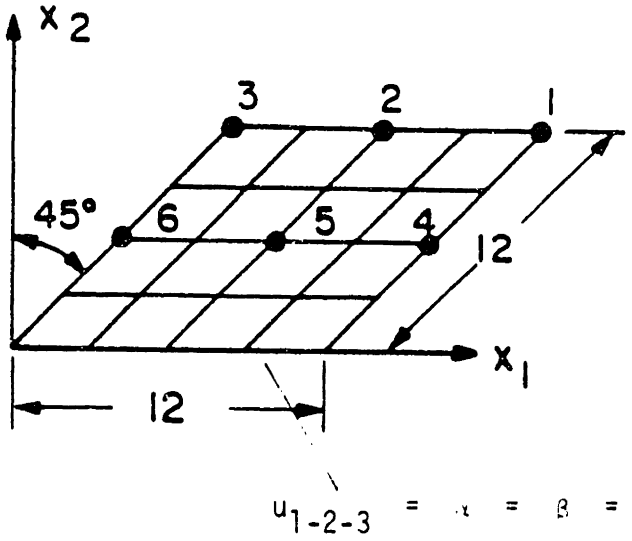
the results reported in Chapter 2 and in Ref. [66].

The same nodal point layouts were employed for models III and IV using our new 4-node shell element. Figure 5.7 gives also the results obtained with these models. It is seen that model III yields an accurate large displacement response prediction, and even model IV yields quite accurate results up to about 60 degrees of rotation. The computer time required in these analyses was only little different using models I, III and IV.

Another important result is shown in Fig. 5.8. As reported in Chapter 2 and Ref. [66], the cubic shell element is sensitive to "in-plane" distortions, and hence it is interesting to study the effect of using a distorted element mesh in the analysis of a cantilever. Figure 5.8 summarizes the results obtained using the one cubic element and three 4-node elements with a nodal layout that corresponds to distorting the elements. It is seen that the predictive capability of our new 4-node element is considerably less sensitive to the element distortions.

5.5.2 Analysis of a rhombic cantilever

The rhombic cantilever shown in Fig. 5.9, fixed at one side and subjected to constant pressure was analyzed using a 4x4 element mesh. The results for the transverse displacements at six locations are compared against the solutions obtained using the DKT triangular element of Ref. [64], using the 16-node isoparametric element (with 4x4x2 Gauss integration) and experimental measurements reported in Ref. [85]. In all cases a one step geometric nonlinear analysis with BFGS equilibrium



$q = 0.26066$

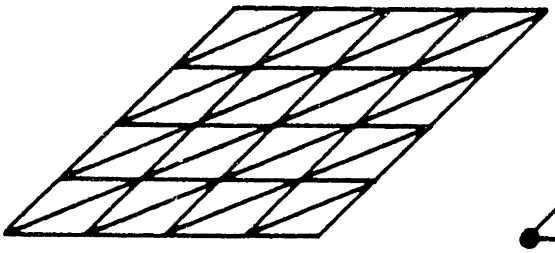
$E = 10.5 \times 10^6$

thickness = 0.125

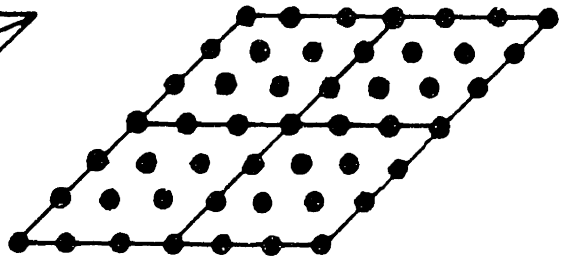
$\nu = 0.3$

$u_{1-2-3} = \alpha = \beta = 0$

4 x 4 mesh — 4-node elements



4 x 4 mesh — DKT elements



2 x 2 mesh — 16-node elements
(Int. 4x4x2)

Element	Mesh	CPU time / CPU time of DKT	Deflection at location					
			1	2	3	4	5	6
DKT	4x4	1.00	0.293	0.196	0.114	0.118	0.055	0.024
4-node	4x4	approx. 2	0.272	0.183	0.106	0.102	0.046	0.019
16-node	2x2	approx. $6\frac{1}{2}$	0.266	0.182	0.110	0.105	0.048	0.019
Experimental [1]			0.297	0.204	0.121	0.129	0.056	0.022

Figure 5.9 Response of rhombic cantilever subjected to constant pressure

iterations [29] was performed. Good correspondence between the experimental results and the solution obtained using our new 4-node element is observed.

5.6 Geometric nonlinear response of a shallow spherical shell

Figure 5.10 shows the spherical shell that was also analyzed in Ref. [63] with one cubic shell element, modeling one quarter of the shell. To test our new 4-node shell element, the same nodal point layout as in Ref. [63] was used, giving a mesh of nine elements. Figure 5.10 shows the response calculated, including the post-buckling response (not reported in Ref. [63]), with the automatic load stepping algorithm (modified Newton iterations) of Chapter 4 and Ref. [90]. Good correspondence with the analytical solution of Leicester [11] and the solution of Horrigmoe [86] was obtained. The solution with the 16-node element was almost twice as expensive as the 4-node element solution (using in both cases the same parameters for the automatic step-by-step solution algorithm).

5.7 Linear buckling analysis and large deflection response of a simply-supported stiffened plate

The stiffened plate shown in Fig. 5.11 was analyzed for its buckling response. Since we expect the buckling mode to be symmetric [12], only one quarter of the plate was modeled using symmetry boundary conditions. The model consists of nine 4-node shell elements and three 2-node isobeam elements. At the nodes where the shell element connects to a beam element, three rotational degrees of freedom aligned with the

$R_1 = R_2 = 2540.$

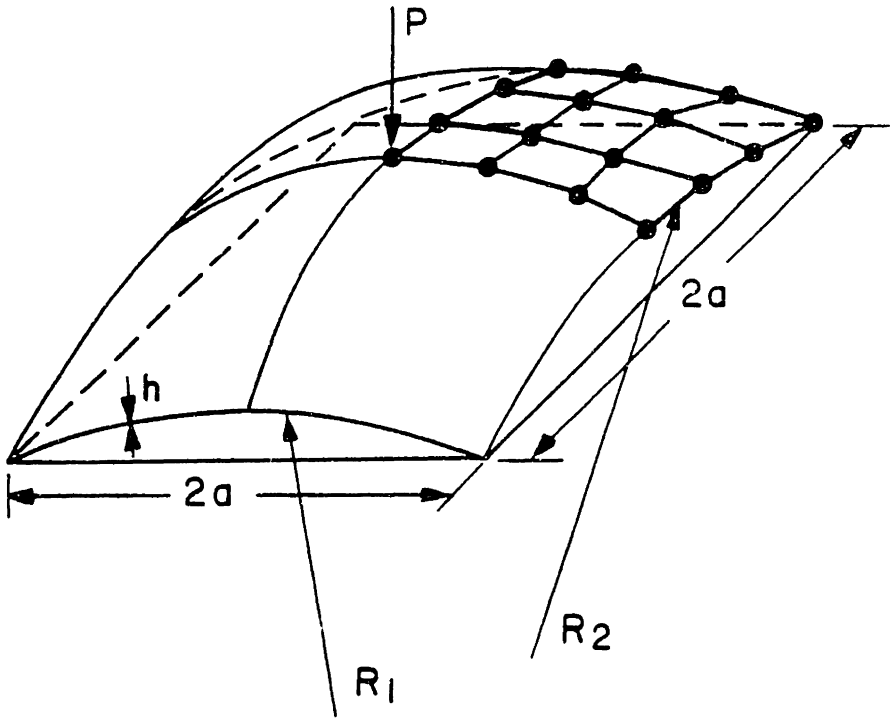
$a = 784.90$

$h = 99.45$

$E = 68.95$

$\nu = 0.3$

All edges are hinged and immovable.



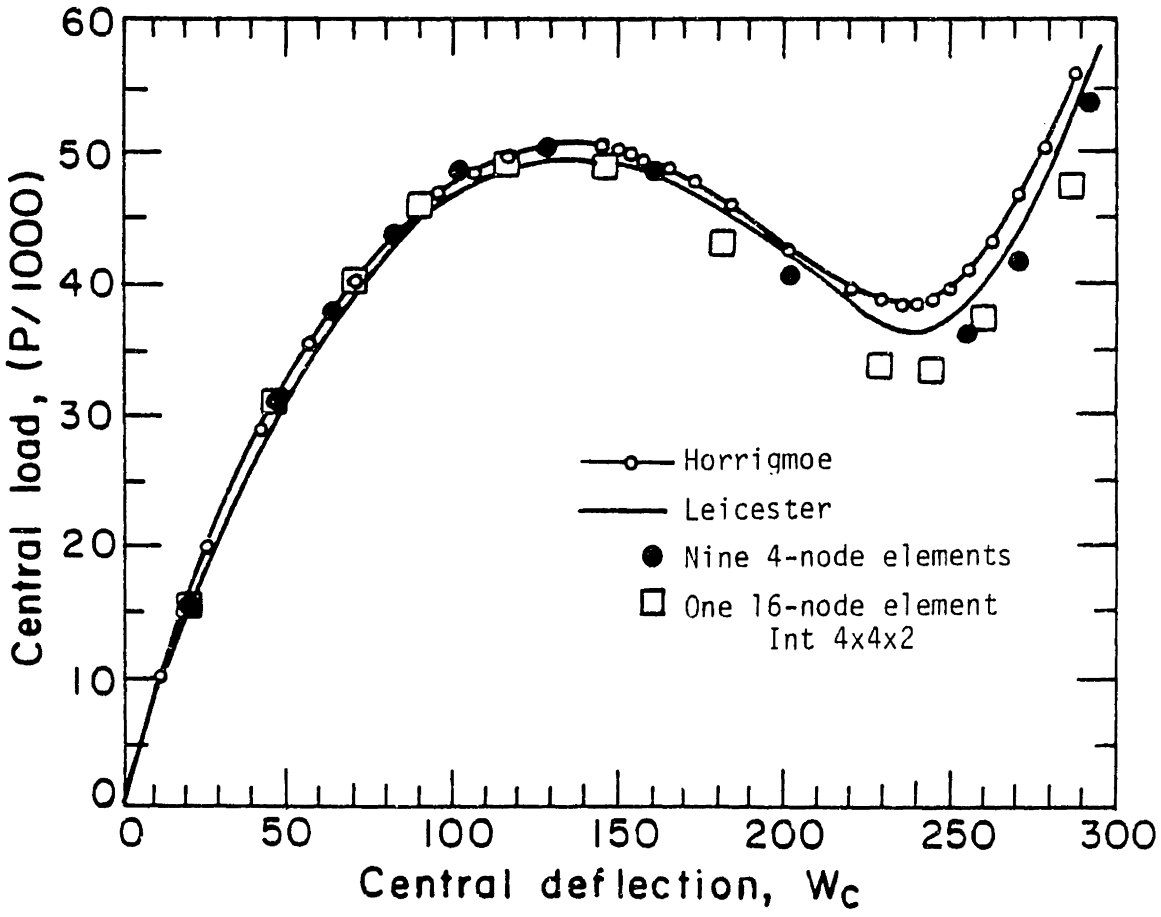


Figure 5.10 Geometric nonlinear response of a spherical shell

global axes are considered for the shell element. In order to avoid locking of the isoparametric beam elements, one point Gauss integration along the beam axes was used. This does not introduce spurious zero energy modes in the model, and it provides an isobeam formulation equivalent to the new shell formulation.

The linearized buckling problem was solved as described in Chapter 4, Eq. (4.37), and we obtained

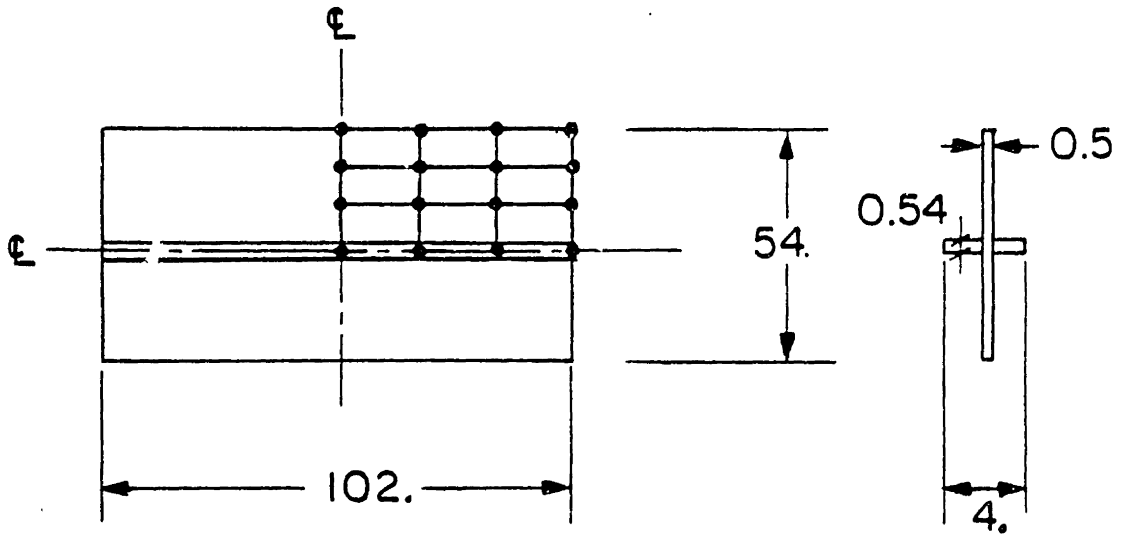
$$\frac{\sigma_{cr} \text{ (finite element solution)}}{\sigma_{cr} \text{ (analytical solution)}} = 1.02$$

Next, an initial imperfection with the shape of the first buckling mode and a maximum amplitude of 1/5th of the plate thickness was introduced. Figure 5.11 shows the large deflection response of this model as calculated using the automatic load stepping scheme of Chapter 4, with modified Newton iterations (Ref. [90]). A tight energy convergence tolerance was used to obtain the solution.

5.8 Analysis of elastic-plastic response of a circular plate

The thin circular plate shown in Fig. 5.12 was analyzed for its elastic-plastic response when subjected to a concentrated load at its center. The plate is simply-supported with its edges restrained from moving in its plane.

In a first solution, the plate model shown in Fig. 5.12(a) was used to analyze the plate assuming small displacements (material-nonlinear-only conditions). Figure 5.12 shows that the theoretical collapse



simply supported plate

$E = 2.1 \times 10^6$

$\nu = 0.3$

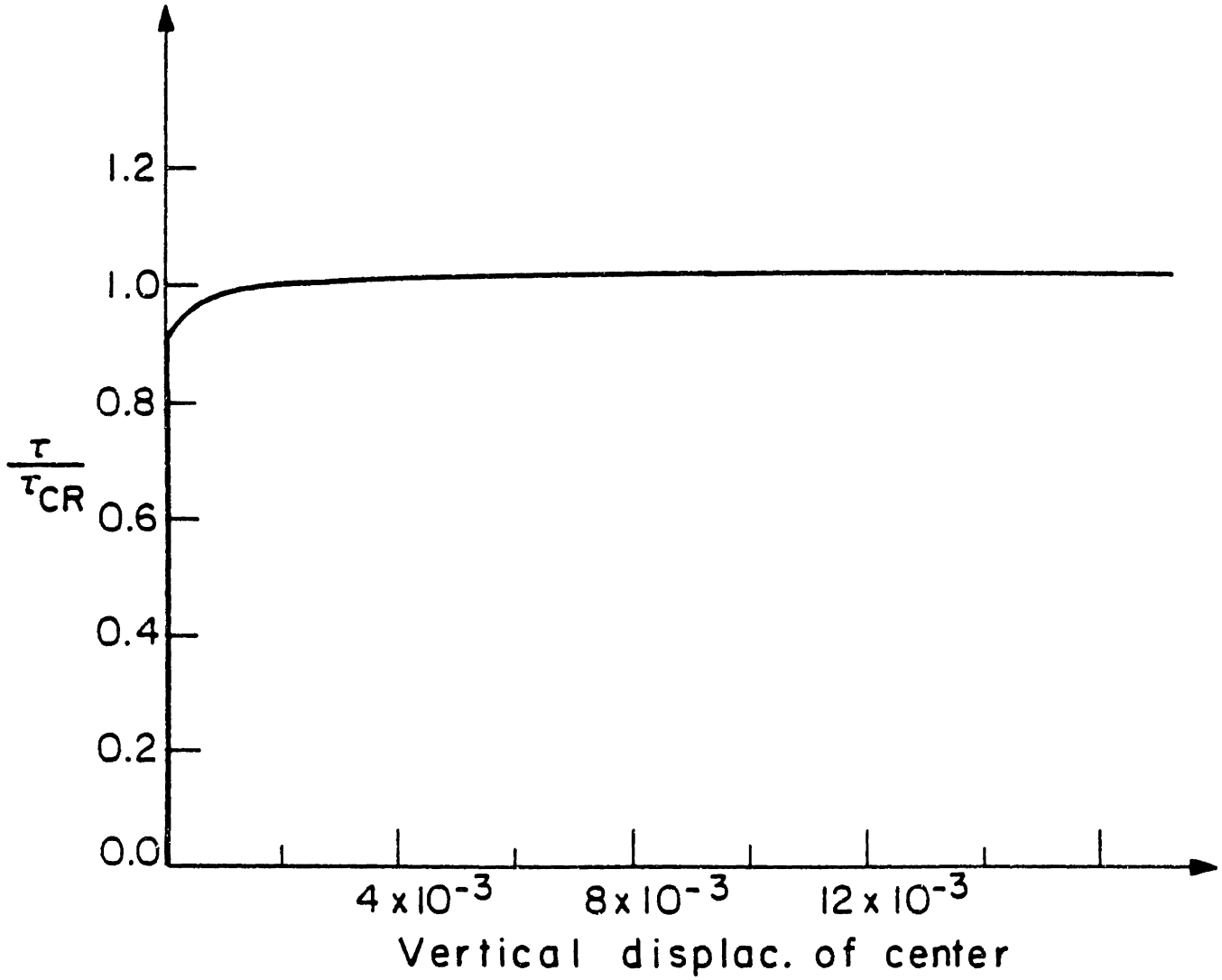


Figure 5.11 Nonlinear response of a stiffened plate

load [108] is overestimated, but for the coarse mesh used, the predicted response is quite reasonable.

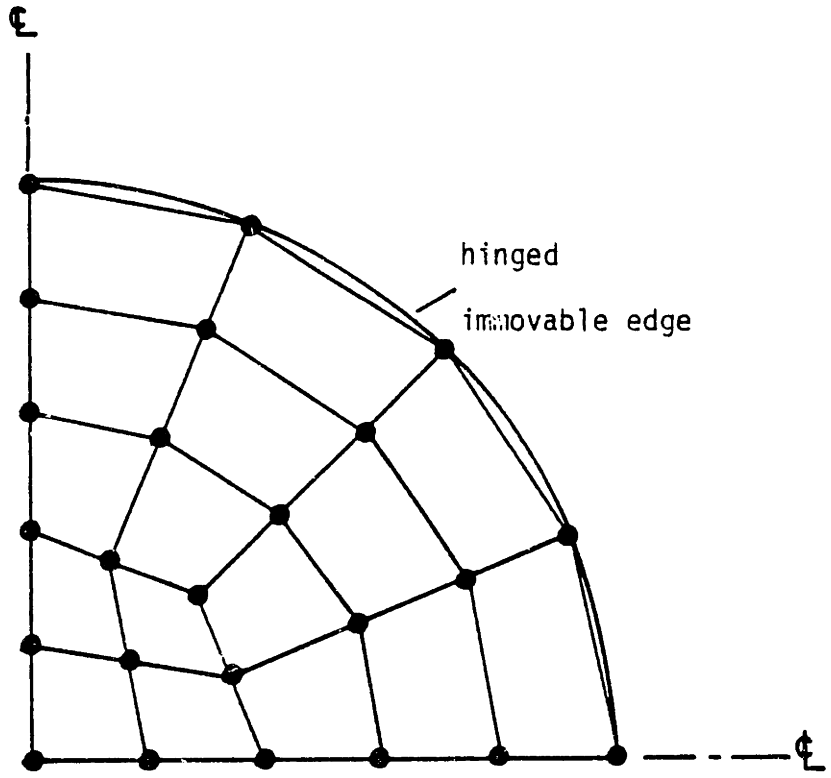
In a second solution, large displacements and elastic-plastic conditions were assumed and in this case the stiffening behavior of the plate shown in Fig. 5.12(b) was predicted. In order to have a comparison, also the model of five axisymmetric 8-node elements shown in Fig. 5.12(a) was solved. Figure 5.12 shows that both models predict in essence the same response; however, in this case relatively little plasticity was developed for the range of displacements considered.

5.9 Large deflection elastic-plastic analysis of cylindrical shell

Figure 5.13 shows a cylindrical shell, made of an elastic-perfectly-plastic material, subjected to a constant vertical pressure per unit of projected area on the horizontal plane. The shell is simply-supported at its ends on in-plane rigid diaphragms (they do not have stiffness in the axial direction of the shell).

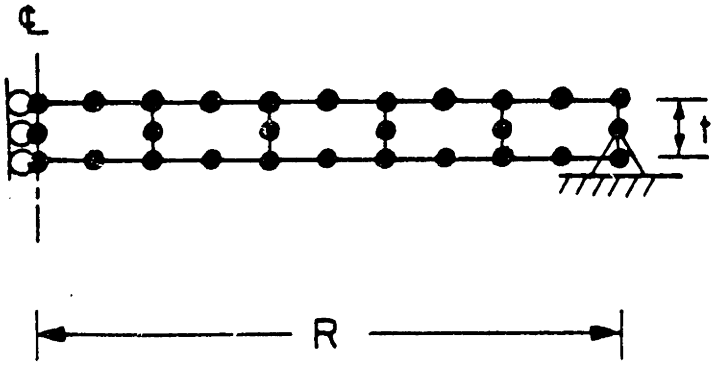
The problem was analyzed using a 9x9 mesh of our 4-node element and, using the same nodal layout, a 3x3 mesh of the 16-node isoparamteric shell element (with 4x4x4 Gauss integration). For both models a geometric and material nonlinear analysis (TLF) was performed using the modified Newton version of the automatic stepping algorithm [90].

The solutions obtained are shown in Fig. 5.13, and they are coincident with the solution reported in Ref. [59] (in that case, the solution was carried out only up to approximately $W_B = 125$).



R = 100
t = 1
E = 2.1 x 10^6 E_T = 0
ν = 0.3
σ_y = 1000

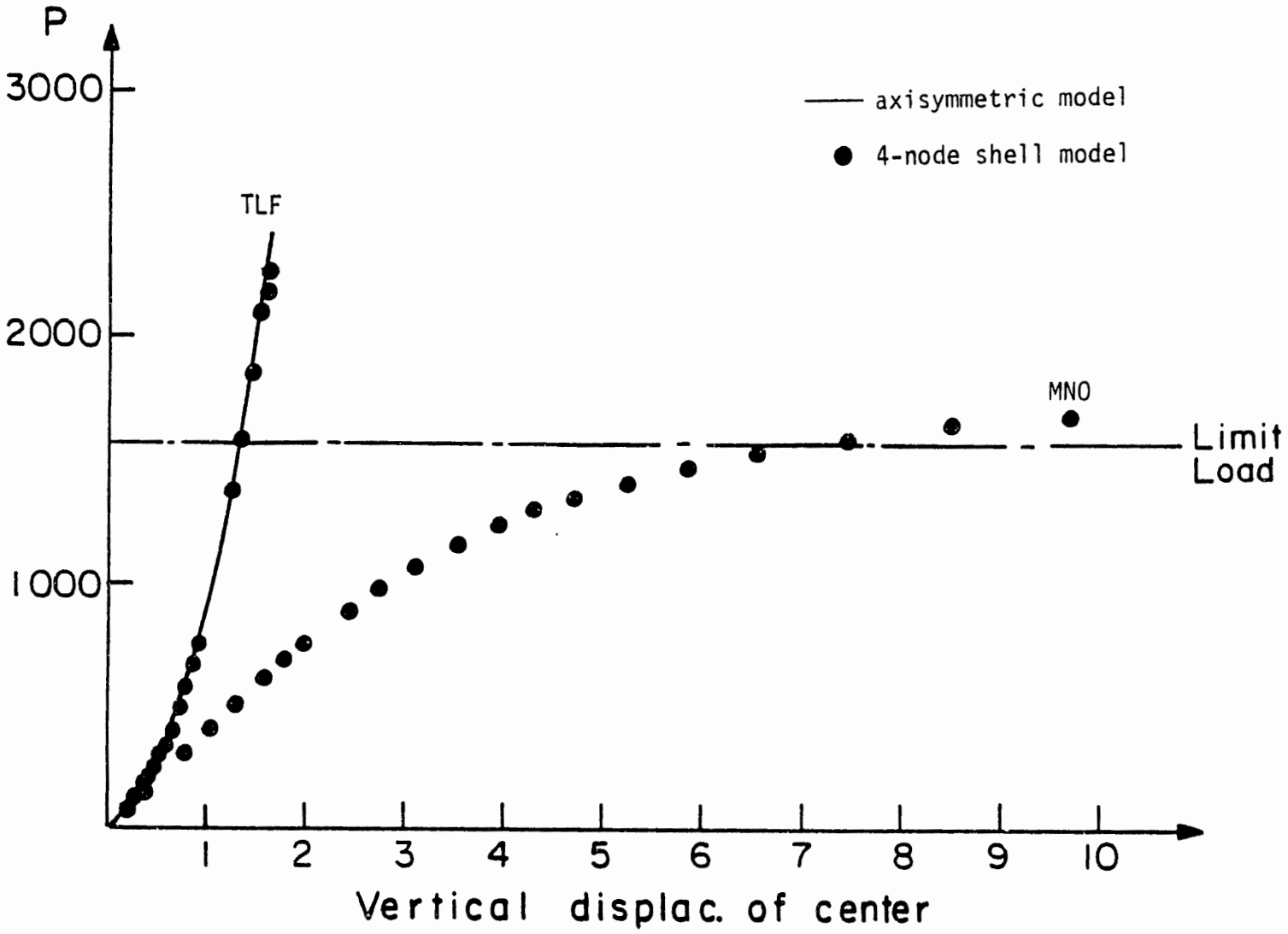
4-node shell model



axisymmetric model

a) Finite element models

Figure 5.12 Response of elastic-perfectly-plastic circular plate subjected to a concentrated load, P, at its center. TLF abbreviates use of total Lagrangian formulation and MNO abbreviates use of materially-nonlinear-only formulation.



b) Circular plate response

Figure 5.12 continued

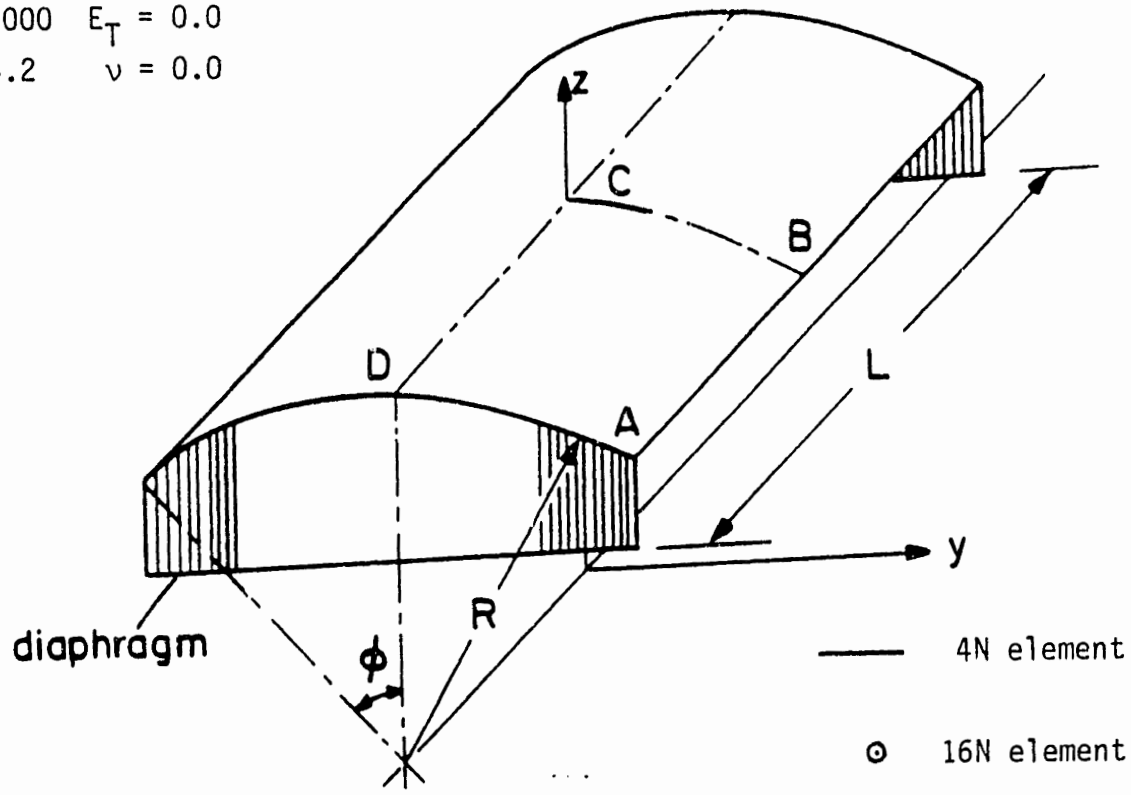
R = 7600 thickness = 76

Ø = 40°

L = 15200

E = 21000 E_T = 0.0

σ_y = 4.2 ν = 0.0



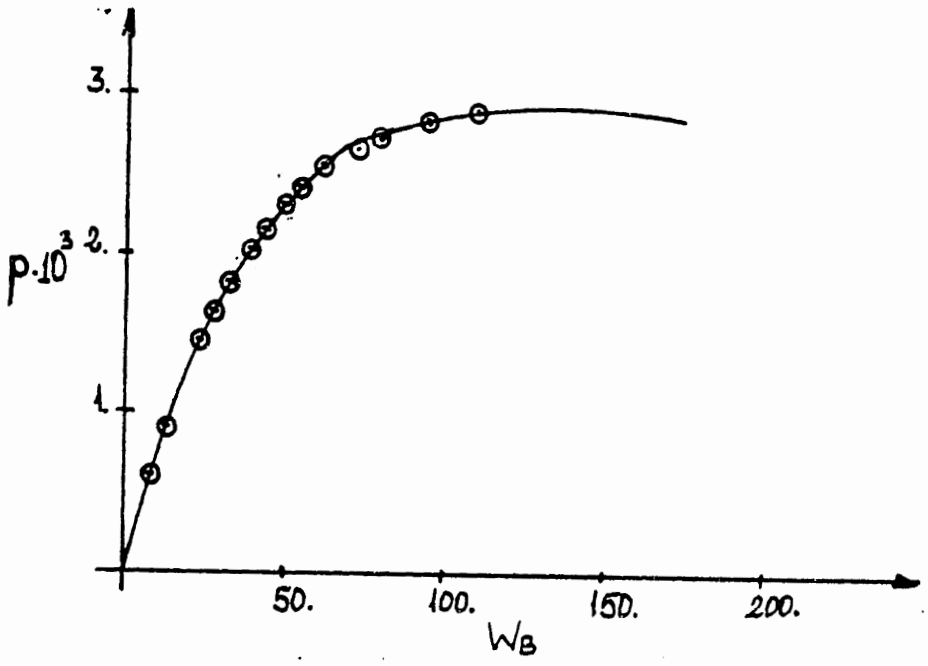


Figure 5.13 Large deflection elastic-plastic analysis of cylindrical shell

5.10 Dynamic analysis of a simply-supported elastic-plastic plate

The shell element presented in Chapter 3 can also be used for nonlinear dynamic analysis of shells using any time integration scheme.

The plate shown in Fig. 5.14(a) was modeled, as shown, using sixteen 4-node elements. The central difference method [29] was used in order to calculate its time history when subjected to a step uniform pressure, and therefore a lumped mass matrix was assembled, as shown in Ref. [62].

In performing the dynamic analysis we used a material-nonlinear-only formulation, and $\Delta t = 4.0 \times 10^{-6}$. The calculated time history of the vertical displacement at the center is compared with the solutions given in [110] and [62, 63] (using nine 8-node elements).

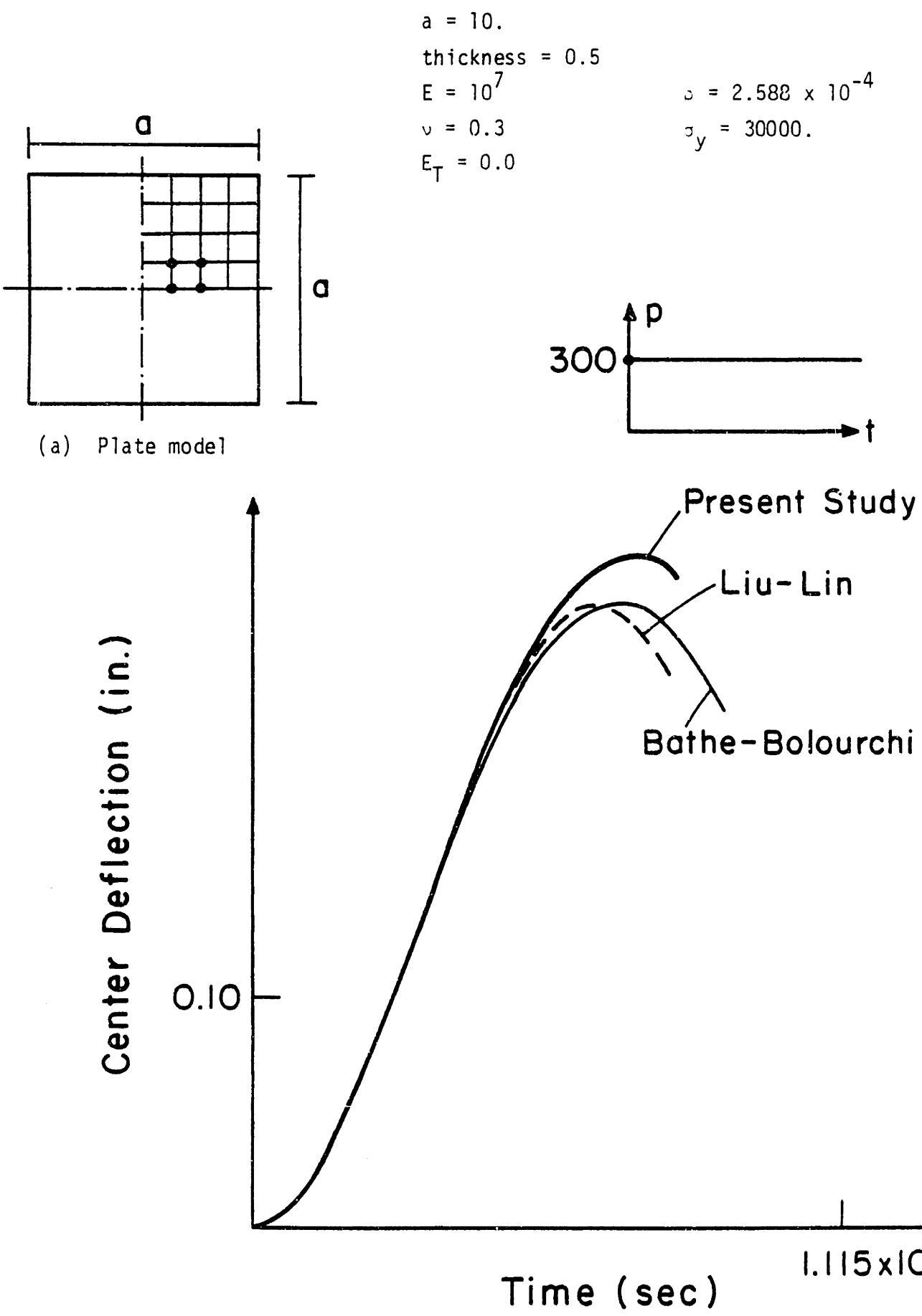
The peak response for this problem was reported to be, in a finite element model, dependent on the number of integration points through the elements thickness [84].

5.11 Circular plate with constant temperature gradient through the thickness

In order to test the element response, when using the thermo-elastic material model, a circular plate of R/h=10, simply supported along its edge, and subjected to constant temperature gradient through the thickness was considered, using a geometrically linear analysis.

The analytical solution is given in [103], and an important aspect of it is that $\tau_{ij}=0$ at every point inside the plate.

To perform the analysis, 8-node and 16-node isoparametric shell



(a) Plate model

b) Time history

Figure 5.14 Dynamic analysis of elastic-plastic plate

elements were used, with different numerical integration schemes [88], as well as our new 4-node shell element.

In Fig. 5.15 a resume of the results that were obtained is presented.

Two different measures of error are listed:

a) The error in the displacement at the center of the plate as compared with the displacement predicted in the analytical solution (ϵ_w).

b) The error in the stress prediction at the integration points is represented by

$$\epsilon_\tau = \max\left[\frac{|\tau_{pp}|}{|E\alpha\theta|} \right]$$

where τ_{pp} is the principal stress predicted at the integration point and θ its temperature.

The results show again the good predictive capability of our new 4-node shell element.

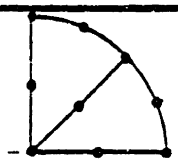
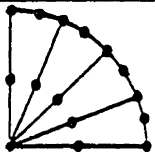
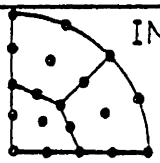
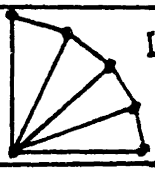
	F.E.M. MODEL	$\lvert\varepsilon_w\rvert = \frac{\lvert W_{FE} - W_{AN}\rvert}{\lvert W_{AN}\rvert}$	ε_τ
Bathe-Bolourchi element		-0.26	1.10
		-0.07	054
	 INT. 3×3×2	-0.008	0.62 Central elem. 0.22 Outer elems.
	SAME MODEL INT. 2×2×2	+0.014	0.02
	 IN T. 4×4×2	-0.003	0.26
	SAME MODEL INT. 3×3×2	+0.0001	0.04
New element	 INT. 2×2×2	0.0	0.0

Figure 5.15 Circular plate with constant temperature gradient through the thickness

6. CONCLUSIONS

A new four-node non-flat general nonlinear shell element, an algorithm for automatically tracing the nonlinear response of a finite element model in the load-displacement space and an algorithm for efficiently calculating linearized buckling loads have been developed.

The new shell element has the following important properties:

- The element is formulated using three-dimensional continuum mechanics theory; hence the use of the element is not restricted by application of a specific shell theory.
- The element is reliable and has good predictive capability in the analysis of moderately thick and thin shells (the element does not lock).
- The amount of computations required to calculate the element stiffness matrix are very closely those that are used in standard isoparametric formulations. The computer time used could be reduced considerably in elastic analysis by using analytical integration through the element thickness; in Appendix 5 we have presented this formulation for the specific case of linear plate elements.

In this thesis, we have presented the formulation and some applications of the element. The solution results obtained are most encouraging, but a formal mathematical convergence study of the element would be very valuable.

Finally, it should be noted that the element presented here provides a very attractive basic formulation that could be extended to large strain

analysis and analysis of composite shells. Also, the concepts applied here to formulate a 4-node element could equally well be employed in an effective manner to formulate higher-order shell elements.

Regarding the automatic stepping algorithm presented in Chapter 4, it has performed well in the solution of various problems using either modified or full Newton iterations (e.g. softening, stiffening, collapse, and post-buckling analyses). However, improvements in this solution procedure should still be pursued, in particular with regard to the use of the BFGS method and line searches in the solution strategy. Also, more experience with this algorithm will be valuable in order to confirm and possibly improve the use of the various tolerances and decision making processes employed in the solution procedure. An extension of the algorithm to solve problems with time dependent constitutive relations (creep) and deformation dependent loading could also be studied.

The linearized buckling analysis procedure is effective because the required matrices can be calculated very economically, and the solution is then performed using the subspace iteration method. However, improvements in the eigensolution method for the case of very closely-spaced eigenvalues would be valuable.

REFERENCES

[1] L.E. Malvern, Introduction to the Mechanics of a Continuous Medium, Prentice Hall, Englewood Cliffs, New Jersey, 1969.

[2] Y.C. Fung, Foundations of Solid Mechanics, Prentice-Hall, Englewood Cliffs, New Jersey, 1965.

[3] K. Washizu, Variational Methods in Elasticity and Plasticity, Pergamon Press, 1968.

[4] A.E. Green and W. Zerna, Theoretical Elasticity (2nd Edition), Oxford University Press, 1968.

[5] M.P. Cleary, Mechanics of Continuous Media, (notes for a course at the Department of Mechanical Engineering, M.I.T.), 1981.

[6] S.P. Timoshenko and S. Woinowsky-Krieger, Theory of Plates and Shells (2nd Edition), McGraw-Hill, 1959.

[7] W. Flügge, Stresses in Shells (2nd Edition), Springer-Verlag, 1973.

[8] H. Kraus, Thin Elastic Shells, John Wiley & Sons, 1967.

[9] R.D. Mindlin, "Influence of rotary inertia and Shear on Flexural Motion of Isotropic Elastic Plates", J. Appl. Mech., Vol. 18, pp. 31-38, 1951.

[10] E. Reissner, "On the Theory of Bending of Elastic Plates", J. Math. and Phys., Vol. 23, pp. 184-191, 1944.

[11] R.H. Leicester, "Finite Deformations of Shallow Shells", Proc. A.S.C.E., Vol. 94, EM6, pp. 1409-1423, 1968.

[12] S.P. Timoshenko and J.M. Gere, Theory of Elastic Stability (2nd Edition), McGraw-Hill, 1961.

[13] W.T. Koiter, On the Stability of Elastic Equilibrium, thesis in Delft University, 1945. English translation in NASA TT F-10, 833, 1967.

[14] D.O. Brush and B.O. Almroth, Buckling of Bars, Plates, and Shells, McGraw-Hill, 1975.

[15] S.J. Britvec, The Stability of Elastic Systems, Pergamon Press, New York, 1973.

[16] B. Budiansky (editor), Buckling of Structures, Springer-Verlag, 1976.

[17] Y.C. Fung and E.E. Sechler (editors), Thin Shell Structures, Prentice-Hall, Englewood Cliffs, New Jersey, 1974.

[18] E.E. Sechler, "The Historical Development of Shell Research and Design", published in [17].

[19] P. Seide, "A Reexamination of Koiter's Theory of Initial Post-buckling Behavior and Imperfection Sensitivity of Structures", published in [17].

[20] J. Arbocz and C.D. Babcock, Jr., "The Buckling Analysis of Imperfection Sensitive Shell Structures", NASA CR 3310, 1980.

[21] Y.C. Fung and E.E. Sechler, "Instability of Thin Elastic Shells", Structural Mechanics, (Edited by J.N. Goodier and N.J. Hoff), Pergamon Press, 1960.

[22] N.J. Hoff, "The Perplexing Behavior of Thin Circular Cylindrical Shells in Axial Compression", Israel Journal of Technology, Vol. 4, pp. 1-28, 1966.

[23] M. Esslinger and G. Geier, Postbuckling Behavior of Structures, CISM Courses and Lectures No. 236, Springer-Verlag, 1975.

[24] D. Bushnell, "Buckling of Shells — Pitfall for Designers", A.I.A.A. Journal, Vol. 19, No. 9, 1981.

[25] D. Bushnell, "Plastic Buckling of Various Shells", J. Pressure Vessel Technology, Vol. 104, pp. 51-72, May 1982.

[26] E. Ramm (editor), Buckling of Shells, Springer-Verlag, 1982.

[27] J.S. Przemieniecki, Theory of Matrix Structural Analysis, McGraw-Hill, 1968.

[28] O.C. Zienkiewizc, The Finite Element Method (3rd Edition), McGraw-Hill, 1977.

[29] K.J. Bathe, Finite Element Procedures in Engineering Analysis, Prentice-Hall, Englewood Cliffs, New Jersey, 1982.

[30] J.T. Oden, Finite Elements of Nonlinear Continua, McGraw-Hill, 1972.

[31] G. Strang and G.J. Fix, An Analysis of the Finite Element Method, Prentice-Hall, Englewood Cliffs, New Jersey, 1973.

[32] T.H.H. Pian and P. Tong, "Basis of Finite Element Methods for Solid Continua", Int. J. Numerical Meth. Eng., Vol. 1, pp. 3-28, 1969.

[33] T.H.H. Pian, "Variational and Finite Element Methods in Structural Analysis", RCA Review, Vol. 39, 1978.

[34] G. Wempner, "Finite Element Modeling of Solids Via the Hu-Washizu Functional", Computers in Mechanical Engineering, September 1983.

[35] B.M. Irons and A. Razzaque, "Experience with the Patch Test For Convergence of Finite Elements", The Mathematical Foundations of the Finite Element Method with Applications to Partial Differential Equations, (edited by A.K. Aziz), Academic Press, 1972.

[36] B. Irons and M. Loikkanen, "An Engineer's Defence of the Patch Test", Int. J. Numerical Meth. Eng., Vol. 19, pp. 1391-1401, 1983.

[37] K.J. Bathe, A. Chaudhary, E.N. Dvorkin, C.A. Almeida, L.W. Ho, and G. Larsson, "Some Advances in Finite Element Procedures for Non-linear Analysis", Numerical Methods for Nonlinear Problems - Proceedings, Barcelona, Spain, 1984.

[38] D.S. Malkus and T.J.R. Hughes, "Mixed Finite Elements - Reduced and Selective Integration Techniques: a Unification of Concepts", Comput. Meths. Appl. Mech. Eng., Vol. 15, pp. 63-81, 1978.

[39] O.C. Zienkiewicz, "Constrained Variational Principles and Penalty Function Methods in Finite Element Analysis", Conference on Numerical Solution of Differential Equations, (edited by G.A. Watson), Scotland, July 1973.

[40] G.F. Carey, A. Kabaila, and M. Utku, "On Penalty Methods for Inter-element Constraints", Comput. Meths. Appl. Mech. Eng., Vol. 30, pp. 151-171, 1982.

[41] M. Bercovier, Y. Hasbani, Y. Gilon, and K.J. Bathe, "On a Finite Element Procedure for Nonlinear Incompressible Elasticity", Hybrid and Mixed Finite Element Methods, (edited by S.M. Atluri et al), John Wiley & Sons, 1983.

[42] M. Bercovier, "Perturbation of Mixed Variational Problems. Application to Mixed Finite Element Methods", R.A.I.R.O. (Numerical Analysys), Vol. 12, No. 3, pp. 211-236, 1978.

[43] D.G. Ashwell and R.H. Gallagher (editors), Finite Elements for Thin Shells and Curved Members, John Wiley & Sons, 1976.

[44] R.H. Gallagher, "Problems and Progress in Thin Shell Finite Element Analysis", published in [43].

[45] R.H. Gallagher, "Finite Element Representations for Thin Shell Instability Analysis", published in [16].

[46] D.G. Ashwell, "Strain Elements with Applications to Arches, Rings and Cylindrical Shells", published in [43].

[47] S. Atluri and T.H.H. Pian, "Theoretical Formulation of Finite Element Methods in Linear-Elastic Analysis of General Shells", J. Struct. Mech., Vol. 1, pp. 1-41, 1972.

[48] C.A. Prato, "Shell Finite Element Method Via Reissner's Principle", Int. J. Solids Structures, Vol. 5, pp. 1119-1133, 1969.

[49] C.A. Prato, A Mixed Finite Element Method for Thin Shell Analysis, Research Report R68-33, Department of Civil Eng., M.I.T., 1968.

[50] K.P. Walker, "Vibration of Cambered Helicoidal Fan Blades", J. Sound and Vibration, Vol. 59, pp. 35-57, 1978.

[51] G.M. Lindberg, M.D. Olson, and G.R. Cowper, "New Developments in the Finite Element Analysis of Shells", Quarterly Bulletin of the Divisions of Mech. Eng. and the National Aeronautical Establishment, National Research Council of Canada, Vol. 4, 1969.

[52] G. Sander and S. Idelsohn, "A Family of Conforming Finite Elements for Deep Shell Analysis", Int. J. Numerical Meth. Eng., Vol. 18, pp. 363-380, 1982.

[53] S. Idelsohn, "On the Use of Deep, Shallow or Flat Shell Finite Elements for the Analysis of Thin Shell Structures", Comput. Meths. Appl. Mech. Eng., Vol. 26, pp. 321-330, 1981.

[54] G. Dupuis and J.J. Goël, "A Curved Finite Element for Thin Elastic Shells", Int. J. Solids Structures, Vol. 6, pp. 1413-1428, 1970.

[55] S. Ahmad, B.M. Irons, and O.C. Zienkiewicz, "Analysis of Thick and Thin Shell Structures by Curved Finite Elements", Int. J. Numerical Meth. Eng., Vol. 2, pp. 419-451, 1970.

[56] O.C. Zienkiewicz, R.L. Taylor, and J.M. Too, "Reduced Integration Technique in General Analysis of Plates and Shells", Int. J. Numerical Meth. Eng., Vol. 3, pp. 275-290, 1971.

[57] O.C. Zienkiewicz and E. Hinton, "Reduced Integration, Function Smoothing and Non-Conformity in Finite Element Analysis", J. Franklin Inst., 302, July-December 1976.

[58] O.C. Zienkiewicz, J. Bauer, K. Morgan, and E. Onate, "A Simple and Efficient Element for Axisymmetric Shells", Int. J. Numerical Meth. Eng., Vol. 11, pp. 1545-1558, 1977.

[59] B. Kråkeland, "Nonlinear Analysis of Shells Using Degenerate Isoparametric Elements", Finite Elements in Nonlinear Mechanics, Vol. 1, (edited by P.G. Bergan et al), Tapir Publishers, (Norwegian Inst. of Tech. Trondheim, Norway), 1978.

[60] E. Ramm, "A Plate/Shell Element for Large Deflections and Rotations", Formulations and Computational Algorithms in Finite Element Analysis, (edited by K.J. Bathe et al), M.I.T. Press, 1977.

[61] E. Ramm and J.M. Sattele, "Elasto-Plastic Large Deformation Shell Analysis Using Degenerated Elements", Nonlinear Finite Element Analysis of Plates and Shells, (edited by T.J.R. Hughes), A.S.M.E., AMD - Vol. 48, 1981.

[62] S. Bolourchi, On Finite Element Nonlinear Analysis of General Shell Structures, Ph.D. Thesis, Department of Mechanical Engineering, M.I.T., 1979.

[63] K.J. Bathe and S. Bolourchi, "A Geometric and Material Nonlinear Plate and Shell Element", J. Computers and Structures, Vol. 11, pp. 23-48, 1979.

[64] K.J. Bathe and L.W. Ho, "A Simple and Effective Element for Analysis of General Shell Structures", J. Computers and Structures, Vol. 13, pp. 673-682, 1980.

[65] K.J. Bathe and L.W. Ho, "Some Results in the Analysis of Thin Shell Structures", Nonlinear Finite Element Analysis in Structural Mechanics, (edited by W. Wunderlich et al), Springer-Verlag, Berlin, 1981.

[66] K.J. Bathe, E.N. Dvorkin, and L.W. Ho, "Our Discrete-Kirchhoff and Isoparametric Shell Elements for Nonlinear Analysis — An Assessment", J. Computers and Structures, Vol. 16, pp. 89-98, 1983.

[67] E.N. Dvorkin and K.J. Bathe, "A Continuum Mechanics Based Four-Node Shell Element for General Nonlinear Analysis", J. Engineering Computations, Vol. 1, 1984 (in press).

[68] E. Ramm and H. Stegmüller, "The Displacement Finite Element Method in Nonlinear Buckling Analysis of Shells", published in [26].

[69] J.L. Batoz, K.J. Bathe, and L.W. Ho, "A Study of Three-Node Triangular Plate Bending Elements", Int. J. Numerical Meth. Eng., Vol. 15, pp. 1771-1812, 1980.

[70] J.L. Batoz and M. Ben Tahar, "Evaluation of a New Quadrilateral Plate Bending Element", Int. J. Numerical Meth. Eng., Vol. 18, pp. 1655-1677, 1982.

[71] G. Wempner, D. Talaslidis, and C.-M. Hwang, "A Simple and Efficient Approximation of Shells via Finite Quadrilateral Elements", J. Appl. Mechs., Vol. 49, pp. 115-120, 1982.

[72] H.A. Mang, "Derivation of General Algebraic Constraint Conditions for 'Weak' C^1 Continuity for Thin Shells", Int. J. Numerical Meth. Eng., Vol. 11, pp. 1593-1604, 1977.

[73] T.J.R. Hughes, M. Cohen, M. Haroun, "Reduced and Selective Integration Techniques in the Finite Element Analysis of Plates", J. Nuclear Eng. and Design, Vol. 46, pp. 203-222, 1978.

[74] T.J.R. Hughes, R.L. Taylor, and W. Kanoknukulchai, "A Simple and Efficient Finite Element for Plate Bending", Int. J. Numerical Meth. Eng., Vol. 11, pp. 1529-1543, 1977.

[75] T.J.R. Hughes and W.K. Liu, "Nonlinear Finite Element Analysis of Shells: Part I, Three-Dimensional Shells", J. Computer Meths. Appl. Mech. Eng., Vol. 26, pp. 331-362, 1981.

[76] A. Tessler and T.J.R. Hughes, "An Improved Treatment of Transverse Shear in the Mindlin-Type Four-Node Quadrilateral Element", J. Computer Meths. Appl. Mech. Eng., Vol. 39, pp. 311-335, 1983.

[77] I. Fried, "Shear in C^0 and C^1 Bending Finite Elements", Int. J. Solids and Structures, Vol. 9, pp. 449-460, 1973.

[78] I. Fried and S.K. Yang, "Triangular, Nine-Degrees-Of-Freedom, C^0 Plate Bending Element of Quadratic Accuracy", Q. Appl. Math., October 1973.

[79] I. Fried, "Residual Energy Balancing Technique in the Generation of Plate Bending Finite Elements", J. Computers and Structures, Vol. 4, pp. 771-778, 1974.

[80] A.K. Noor and J.M. Peters, "Mixed Models and Reduced/Selective Integration Displacement Models for Nonlinear Analysis of Curved Beams", Int. J. Numerical Meth. Eng., Vol. 17, pp. 615-631, 1981.

[81] A.K. Noor and C.M. Andersen, "Mixed Models and Reduced/Selective Integration Displacement Models for Nonlinear Shell Analysis", Int. J. Numerical Meth. Eng., Vol. 18, pp. 1429-1454, 1982.

[82-a] R.H. MacNeal, "A Simple Quadrilateral Shell Element", J. Computers and Structures, Vol. 8, pp. 175-183, 1978.

[82-b] R.H. MacNeal, "Derivation of Element Stiffness Matrices by Assumed Strain Distributions", J. Nuclear Eng. and Design, Vol. 70, pp. 3-12, 1982.

[83] R.L. Spilker and T. Belytschko, "Hybrid-Stress Elements for Thin and Moderately-Thick Plates", Hybrid and Mixed Finite Element Methods, (edited by S.M. Atluri et al), John Wiley & Sons, 1983.

[84] T. Belytschko and C.S. Tsay, "Explicit Algorithms for Nonlinear Dynamics of Shells", Nonlinear Finite Element Analysis of Plates and Shells, (edited by T.J.R. Hughes), A.S.M.E., AMD - Vol. 48, 1981.

[85] A. Adini, Analysis of Shell Structures by the Finite Element Method, Ph.D. Thesis, Department of Civil Engineering, University of California at Berkeley, California, 1961.

[86] G. Horrigmoe, Finite Element Instability Analysis of Free-Form Shells, Report 77-2, Division of Structural Mechanics, The Norwegian Institute of Technology. The University of Trondheim, Norway, 1977.

[87] K. Forsberg and R. Hartung, "An Evaluation of Finite Difference and Finite Element Techniques for Analysis of General Shells", Symposium on High Speed Computing of Elastic Structures, I.U.T.A.M., Liège, 1970.

[88] E.N. Dvorkin, Nonlinear Thermo-Elastic Analysis of Shells Using the Finite Element Method, S.M. Thesis, Department of Mechanical Engineering, M.I.T., 1982.

[89] K.J. Bathe and A.P. Cimento, "Some Practical Procedures for the Solution of Nonlinear Finite Element Equations", J. Computer Meths. Appl. Mech. Eng., Vol. 22, pp. 231-277, 1980.

[90] K.J. Bathe and E.N. Dvorkin, "On the Automatic Solution of Nonlinear Finite Element Equations", J. Computers and Structures, Vol. 17, pp. 871-879, 1983.

[91] E. Riks, "An Incremental Approach to the Solution of Snapping and Buckling Problems", Int. J. Solids Structures, Vol. 15, pp. 529-551, 1979.

[92] P.G. Bergan, G. Horrigmoe, B. Kråkeland, and T.H. Søreide, "Solution Techniques for Nonlinear Finite Element Programs", Int. J. Numerical Meth. Eng., Vol. 12, pp. 1677-1696, 1978.

[93] E. Ramm, "Strategies for Tracing Nonlinear Responses near Limit Points", in Nonlinear Finite Element Analysis in Structural Mechanics, (edited by Wunderlich et al), Springer Verlag, New York, 1981.

[94] J.L. Batoz and G. Dhatt, "Incremental Displacement Algorithms for Nonlinear Problems", Int. J. Numerical Meth. Eng., Vol. 14, pp. 1262-1267, 1979.

[95] M.A. Crisfield, "A Fast Incremental/Iterative Solution Procedure that Handles Snap-Through", J. Computers and Structures, Vol. 13, pp. 55-62, 1981.

[96] M.A. Crisfield, "Variable Step-Lengths for Nonlinear Structural Analysis", TRR. Lab., Report 1049, 1982.

[97] M.A. Crisfield, "Incremental/Iterative Solution Procedures for Non-Linear Structural Analysis", Numerical Methods for Nonlinear Problems, (edited by C. Taylor et al), Pineridge Press, Swansea, 1980.

[98] P.G. Bergan, "Automated Incremental-Iterative Solution Schemes", Numerical Methods for Nonlinear Problems, (edited by C. Taylor et al), Pineridge Press, Swansea, 1980.

[99] G. Powell and J. Simons, "Improved Iteration Strategy for Nonlinear Structures", Int. J. Numerical Meth. Eng., Vol. 17, pp. 1455-1467, 1981.

[100] H. Rothert, T. Dickel, and D. Renner, "Snap-Through Buckling of Reticulated Space Trusses", ASCE, J. Struct. Div., Vol. 107, pp. 129-143, 1981.

[101] J. Padovan and S. Tovichakchaikul, "On the Solution of Elastic-Plastic Static and Dynamic Post-Buckling Collapse of General Structure", J. Computers and Structures, Vol. 16, pp. 199-205, 1983.

[102] B. Brendel and E. Ramm, "Nichtlineare Stabilitätsuntersuchungen mit der Methode der Finiten Elemente", Ingenieur-Archiv., Vol. 51, pp. 337-362, 1982.

[103] B.A. Boley and J.H. Weiner, Theory of Thermal Stresses, John Wiley & Sons, 1960.

[104] L.M. Kachanov, Fundamentals of the Theory of Plasticity, MIR Publishers, Moscow, 1974.

[105] W. Johnson and P.B. Mellor, Engineering Plasticity, Von Nostrand Reinhold Co., London, 1973.

[106] W. Prager and P.G. Hodge, Theory of Perfectly Plastic Solids, Dover Publications, New York, 1968.

[107] G.A. Wempner and N.E. Kesti, "On the Buckling of Circular Arches and Rings", Proc. 4th U.S. Nat. Cong. Appl. Mech., Vol. 2, A.S.M.E., 1962.

[108] H.G. Hopkins and A.J. Wang, "Load Carrying Capacities for Circular Plates of Perfectly-Plastic Material with Arbitrary Yield Condition", J. Mechs. and Phys. Sol., Vol. 3, pp. 117-129, 1954.

[109] J.J.A. Rodal and E.A. Witmer, Finite-Strain Large Deflection Elastic-Viscoplastic Finite-Element Transient Response Analysis of Structures, NASA CR 159874, 1979.

[110] S.C. Liu and T.H. Lin, "Elastic-Plastic Dynamic Analysis of Structures Using Known Elastic Solutions", Int. J. Earthquake Eng. and Struct. Dynamics, Vol. 7, pp. 147-159, 1979.

[111] ADINA - System Verification Manual, Report AE 83-5, ADINA Eng. Co., 1983.

[112] R.D. Blevins, Formulas for Natural Frequency and Mode Shape, Von Nostrand Reinhold Co., 1979.

[113] S.H. Crandall, Engineering Analysis, McGraw-Hill, 1956.

[114] G. Strang, Linear Algebra and Its Applications (2nd edition), Academic Press, 1980.

[115] K.J. Bathe and S. Ramaswamy, "An Accelerated Subspace Iteration Method", J. Computer Meths. Appl. Mech. Eng., Vol. 23, pp. 313-331, 1980.

APPENDIX 1: On reduced numerical integration

Let us evaluate, using numerical integration, the elements of a stiffness matrix,

$$\underline{K} = \int_{-1}^{1} \int_{-1}^{1} |J| \underline{B}^T \underline{C} \underline{B} \, d\tau \, ds \qquad \text{(A1.1)}$$

assuming $\underline{C}$ constant over the element. Then for each element we have to evaluate an integral of the form

$$I = \int_{-1}^{1} \int_{-1}^{1} \left(\sqrt{|J(\tau,s)|}\, B_1(\tau,s)\right)\left(\sqrt{|J(\tau,s)|}\, B_2(\tau,s)\right) d\tau ds \qquad \text{(A1.2)}$$

Its approximation using (n x n) Gauss integration points is

$$I_n = \sum_{i=1}^{n} \sum_{j=1}^{n} \alpha_i \; \alpha_j \; (|J| B_1 B_2)_{\substack{\tau_i \\ s_j}} \qquad \text{(A1.3)}$$

Now we define

$$\overline{\left(\sqrt{|J|} B_1\right)} = \sum_{i=1}^{n} \sum_{j=1}^{n} \left(\sqrt{|J|} B_1\right)_{\substack{\tau_i \\ s_j}} l_i(\tau)\, l_j(s) \qquad \text{(A1.4-a)}$$

$$\overline{(\sqrt{|J|}\,B_2)} = \sum_{i=1}^{n}\sum_{j=1}^{n} (\sqrt{|J|}\,B_2)_{\substack{r_i \\ s_j}} l_i(r)\,l_j(s) \qquad \text{(A1.4-b)}$$

where $l_i(r)$ is a Lagrange interpolation polynomial [29] along the r coordinate, with $l(r_i) = 1$ and $l(r_j) = 0$, $j = 1, \cdots, n$ and $j \neq i$

We can also define the following integral:

$$I_E = \int_{-1}^{1}\int_{-1}^{1} (\overline{\sqrt{|J|}\,B_1})(\overline{\sqrt{|J|}\,B_2})\,dr\,ds \qquad \text{(A1.5)}$$

Substituting from Eqs. (A1.4-a) and (A1.4-b) into Eq. (A1.5), we obtain

$$I_E = \sum_{i=1}^{n}\sum_{j=1}^{n}\sum_{k=1}^{n}\sum_{l=1}^{n} (\sqrt{|J|}\,B_1)_{\substack{r_i \\ s_j}} (\sqrt{|J|}\,B_2)_{\substack{r_k \\ s_l}} \int_{-1}^{1} l_i(r)\,l_k(r)\,dr \int_{-1}^{1} l_j(s)\,l_l(s)\,ds \qquad \text{(A1.6)}$$

It can be shown that if (r_i, s_j) are the Gauss points

$$\int_{-1}^{1} l_i(r)\, l_j(r)\, dr = 0 \quad i \neq j \tag{A1.7-a}$$

$$\int_{-1}^{1} l_k(r)\, l_k(r)\, dr = \alpha_k \tag{A1.7-b}$$

where α_k is the weight factor corresponding to α_k in a Gauss integration.

Then,

$$I_E = \sum_{i=1}^{n} \sum_{j=1}^{n} \alpha_i \alpha_j \left(|J| B_1 B_2 \right)_{\substack{r_i \\ s_j}} \tag{A1.8}$$

Comparing with (A1.3), we conclude that

$$I_n \equiv I_E \tag{A1.9}$$

Therefore, we can define a new strain-displacement matrix $\hat{\underline{B}}$, such that

$$\sqrt{|J|}\, \hat{\underline{B}} = \left(\sqrt{|J|}\, \underline{B} \right)_{\substack{r_i \\ s_j}} l_i(r)\, l_j(s) \tag{A1.10}$$

hence,

$$\hat{\underline{B}} = \frac{\sum_{i}^{} \sum_{j}^{} (\sqrt{|J|}\, \underline{B})_{r_i s_j} l_i(r) l_j(s)}{\sqrt{|J(r,s)|}} \qquad \text{(A1.11)}$$

It is then possible to state that using numerical integration is equivalent to replacing the strain-displacement matrix $\underline{B}$ with a new one $\hat{\underline{B}}$, defined by (A1.11) and then calculating

$$\underline{K}_n = \int_{-1}^{1} \int_{-1}^{1} |J|\, \hat{\underline{B}}^T \underline{C}\, \hat{\underline{B}}\, dr\, ds \qquad \text{(A1.12)}$$

using exact integration.

Assuming that the exactly-integrated element is complete [29], we will prove that the numerically integrated element is also complete provided that the integration order is, at least, high enough to exactly calculate the element volume.

We can define a new strain interpolation

$$\hat{\underline{\epsilon}} = \hat{\underline{B}}\, \underline{u} = \frac{\sum_{i=1}^{n} \sum_{j=1}^{n} (\sqrt{|J|}\, \underline{B}\, \underline{u})_{r_i s_j} l_i(r) l_j(s)}{\sqrt{|J|}} \qquad \text{(A1.13)}$$

so,

$$\hat{\underline{\epsilon}} = \frac{\sum_{i=1}^{n}\sum_{j=1}^{n}(\sqrt{|J|}\,\underline{\epsilon})_{r_i s_j}\, l_i(r)\, l_j(s)}{\sqrt{|J|}} \tag{A1.14}$$

With the exactly-integrated element complete, it can represent a constant strain state,

$$\underline{\epsilon} = const = \underline{\epsilon}^* \tag{A1.15}$$

which in the numerically-integrated element has the representation

$$\hat{\underline{\epsilon}} = \underline{\epsilon}^* \frac{\sum_{i=1}^{n}\sum_{j=1}^{n}(\sqrt{|J|})_{r_i s_j}\, l_i(r) l_j(s)}{\sqrt{|J|}} \tag{A1.16}$$

In general (except at the Gauss points) $\hat{\underline{\epsilon}} \neq \underline{\epsilon}^*$ because, in general

$$\sqrt{|J|} \neq \sum_{i=1}^{n}\sum_{j=1}^{n}(\sqrt{|J|})_{r_i s_j}\, l_i(r)\, l_j(s) \tag{A1.17}$$

But if we calculate a quantity proportional to the strain energy,

$$\bar{U} = \int_{-1}^{1} \int_{-1}^{1} |J| \, \hat{\underline{\epsilon}}^T \, \hat{\underline{\epsilon}} \, dr \, ds \qquad \text{(A1.18-a)}$$

$$\bar{U} = \int_{-1}^{1} \int_{-1}^{1} \underline{\epsilon}^{*T} \, \underline{\epsilon}^{*} \left\{ \left[\sum_{i=1}^{n} \sum_{j=1}^{n} \left(\sqrt{|J|} \right)_{\substack{r_i \\ s_j}} l_i(r) \, l_j(s) \right] \right.$$

$$\left. \left[\sum_{p=1}^{n} \sum_{q=1}^{n} \left(\sqrt{|J|} \right)_{\substack{r_p \\ s_q}} l_p(r) \, l_q(s) \right] \right\} dr \, ds \qquad \text{(A1.18-b)}$$

Using Eqs. (A1.7), we get

$$\bar{U} = \underline{\epsilon}^{*T} \, \underline{\epsilon}^{*} \sum_{i=1}^{n} \sum_{j=1}^{n} \alpha_i \, \alpha_j \, |J|_{\substack{r_i \\ s_j}} \qquad \text{(A1.18-c)}$$

Since, as a condition, we have imposed that the integration order must be high enough for the exact calculation of the element volume, from (A1.18-c), we conclude that the numerically-integrated element stores the same amount of strain energy as the exactly-integrated one, when the latter is in a state of constant strain. Therefore, we can assert that the numerically-integrated element is complete (in the energy sense) if the

exactly-integrated element is so.

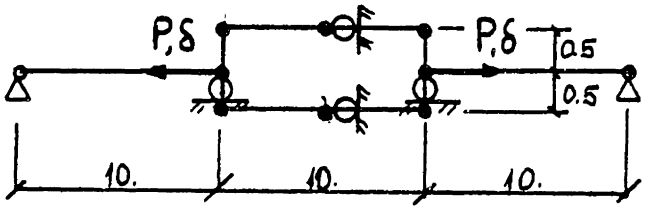
Since we cannot assure the existence of $\underline{\hat{H}}$, we cannot assure that the numerically-integrated element is compatible. But from what we show above, we can assure it passes the patch test if the original element does and if it does not contain zero energy modes free to manifest themselves.

APPENDIX 2: An example where the use of reduced integration in nonlinear analysis leads to incorrect results

It has widely been reported in the finite element literature, and in some examples presented in this thesis, that the use of reduced integration in linear analysis often improves the predictions of a finite element model.

In linear analysis the problem is relatively simple. If the assemblage of reduced-integrated elements presents a nonsingular stiffness matrix, then we frequently — but not necessarily — have an improvement over the results provided by "fully-integrated" elements (although we can not bound the solution any more [31]).

In nonlinear analysis the case is more involved, because at some instant during the analysis the restrained spurious rigid body modes could be made free. Let us consider the example of Fig. A2.1



2D element:
thickness = 1.0
$E = 2.0 \times 10^6$
$\nu = 0.3$

Truss elements:
Area = 1.0
$E = 2.0 \times 10^6$
$E_T = 0.0$
$\sigma_y = 1000$

Figure A2.1 Plane structure in nonlinear analysis

The results we obtain using a material-nonlinear-only formulation are presented in Fig. A2.2. When the two trusses reach the plastic state, the model in which the plane stress element is reduced-integrated, predicts a collapse; this is due to the fact that when Etruss=0.0, the spurious zero energy mode contained in the plane stress element is made free.

Similar results are obtained using a general nonlinear formulation.

This very simple example shows that when performing a nonlinear structural analysis, in principle, the results obtained when using reduced integration are less reliable than those obtained with "full integration".

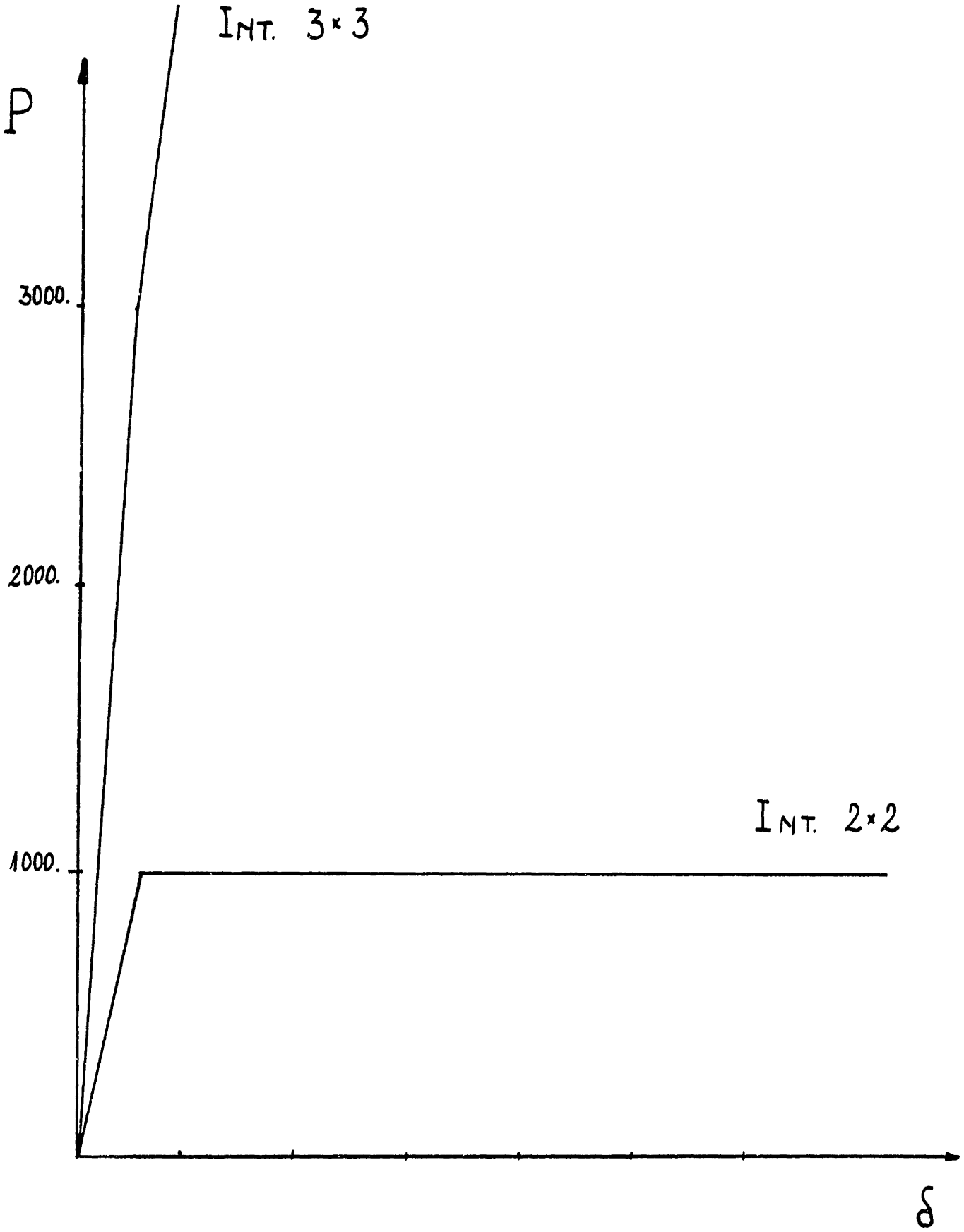


Figure A2.2 Response of the structure of Fig. A2.1

APPENDIX 3: The new four-node shell element does not contain spurious zero energy modes

The purpose of the present appendix is to discuss the fact that the new four-node shell element developed in Chapter 3 does not contain spurious zero energy modes.

First, let us assume that the element contains a spurious zero energy deformation mode, namely $\underline{U}_{KM}$. Then, with $\underline{K}$ the stiffness matrix of the element,

$$\underline{K}\,\underline{U}_{KM} = \underline{0} \tag{A3.1}$$

Since we calculate $\underline{K}$ using "normal integration", Eq. (A3.1) implies that

$$\underline{\tilde{B}}\,\underline{U}_{KM} = \underline{0} \tag{A3.2}$$

The matrix $\underline{\tilde{B}}$, is now decomposed into

$$\underline{\tilde{B}} = \underline{\tilde{B}}_1 + \underline{\tilde{B}}_2 + \underline{\tilde{B}}_3 \tag{A3.3}$$

where $\underline{\tilde{B}}_1$ is obtained from $\underline{\tilde{B}}$, by zeroing its 4th and 5th rows, $\underline{\tilde{B}}_2$ is obtained from $\underline{\tilde{B}}$ by zeroing all its rows but the 4th; and $\underline{\tilde{B}}_3$ is obtained from $\underline{\tilde{B}}$ by zeroing all its rows except the 5th row.

Therefore, Eq. (A3.2) implies

$$\underline{\tilde{B}}_1\,\underline{U}_{KM} = \underline{\tilde{B}}_2\,\underline{U}_{KM} = \underline{B}_3\,\underline{U}_{KM} = \underline{0} \tag{A3.4}$$

From Eq. (3.3),

$$\underline{\tilde{B}}_2 = \frac{1}{2}(1+\Gamma_1)\underline{\tilde{B}}_2^D + \frac{1}{2}(1-\Gamma_1)\underline{\tilde{B}}_2^B \qquad \text{(A3.5-a)}$$

$$\underline{\tilde{B}}_3 = \frac{1}{2}(1+\Gamma_2)\underline{\tilde{B}}_3^A + \frac{1}{2}(1-\Gamma_2)\underline{\tilde{B}}_3^C \qquad \text{(A3.5-b)}$$

For any given displacement vector $\underline{U}$

$$\underline{\tilde{B}}_2^D \underline{U} = \begin{bmatrix} 0 \\ 0 \\ 0 \\ 2\tilde{\epsilon}_{23}^D \\ 0 \end{bmatrix} \qquad \text{(A3.6)}$$

and a similar definition for all the other matrices in Eqs. (A3.5).

In this discussion, we now introduce for simplicity, a further limitation, the material of the element is isotropic elastic. Then we can define $\underline{U}_{KM}$ in the following way:

a) $\underline{U}_{KM}$ is not coincident with a true rigid body mode.

b) $\underline{\tilde{B}}_1 \underline{U}_{KM} = \underline{0}$

c) $\underline{\tilde{B}}_2^D \underline{U}_{KM} = \underline{\tilde{B}}_2^B \underline{U}_{KM} = \underline{\tilde{B}}_3^A \underline{U}_{KM} = \underline{\tilde{B}}_3^C \underline{U}_{KM} = \underline{0}$

d) $\tilde{\epsilon}_{13}^{DI} \not\equiv 0$ and/or $\tilde{\epsilon}_{23}^{DI} \not\equiv 0$ all over the element.

If we now consider a frame made of four 2-node iso-beam elements running along the sides of the shell element, the existence of a spurious zero energy mode in the shell element will necessarily imply the existence of a spurious zero energy mode in the frame; this mode will satisfy, at least, one of the equations stated above, in (c), and also (d).

Let us analyze first the beam 1-2; $\tilde{\epsilon}_{11}$ is calculated with the strain displacement relations and by (c) $\tilde{\epsilon}_{13}|_A = \tilde{\epsilon}_{13}^{D1}|_A$; this corresponds to an iso-beam in which, when calculating the stiffness matrix, the terms associated with $\tilde{\epsilon}_{13}$ are evaluated using one point Gauss integration (selective integration). The selectively integrated isobeam does not present spurious zero energy modes [80].

The same analysis can be made for the other 3 beam elements, therefore we conclude that neither the frame and, according to what we stated above, nor the shell element, contains spurious zero energy modes.

The above, rather than a formal mathematical proof, represents an interpretation of a fact that has been confirmed by extensive numerical experimentation with non-distorted and distorted elements.

APPENDIX 4: Matrices used in the new 4-node shell element

a) ${}^{t}_{0}\underline{\tilde{B}}_{L}$

By definition [29, Chapter 6],

$$ {}_{0}\underline{\tilde{e}} = {}^{t}_{0}\underline{\tilde{B}}\ \underline{U} \qquad \text{(A4.1)} $$

Therefore, ${}^{t}_{0}\underline{\tilde{B}}_{L}$ can be formed by inspection, using Eqs. (3.21-a), (3.22-a), (3.23-a), and (3.24-a).

b) ${}^{t}_{0}\underline{K}_{NL}$

Since we use different interpolations for the transverse shear strains and the other strain components, we can write

$$ {}^{t}_{0}\underline{K}_{NL} = {}^{t}_{0}\underline{\bar{K}}_{NL} + {}^{t}_{0}\underline{\bar{\bar{K}}}_{NL} \qquad \text{(A4.2)} $$

where ${}^{t}_{0}\underline{\bar{K}}_{NL}$ is function of ${}^{t}_{0}\tilde{S}^{11}$, ${}^{t}_{0}\tilde{S}^{22}$ and ${}^{t}_{0}\tilde{S}^{12}$, and ${}^{t}_{0}\underline{\bar{\bar{K}}}_{NL}$ is function of ${}^{t}_{0}\tilde{S}^{13}$ and ${}^{t}_{0}\tilde{S}^{23}$.

$$ {}^{t}_{0}\underline{\bar{K}}_{NL} = \int_{{}^{0}V} {}^{t}_{0}\underline{\tilde{B}}^{1}_{NL}{}^{T}\ {}^{t}_{0}\underline{\tilde{S}}^{1}\ {}^{t}_{0}\underline{\tilde{B}}^{1}_{NL}\ {}^{0}dV \qquad \text{(A4.3)} $$

where ${}^{t}_{0}\underline{\tilde{B}}^{1}_{NL}$ is formed in the standard way [29, Chapter 6], using (3.21-b) and (3.22-b) (see Table 1); and

$$
{}^{t}\tilde{\underline{B}}^{1}_{0\,NL} = \left[\begin{array}{ccccc}
 & h_{k,1} & 0 & 0 & -A_1\,{}^{t}V^{k}_{21} \quad A_1\,{}^{t}V^{k}_{11} \\
 & 0 & h_{k,1} & 0 & -A_1\,{}^{t}V^{k}_{22} \quad A_1\,{}^{t}V^{k}_{12} \\
 & 0 & 0 & h_{k,1} & -A_1\,{}^{t}V^{k}_{23} \quad A_1\,{}^{t}V^{k}_{13} \\
 & h_{k,2} & 0 & 0 & -A_2\,{}^{t}V^{k}_{21} \quad A_2\,{}^{t}V^{k}_{11} \\
 & 0 & h_{k,2} & 0 & -A_2\,{}^{t}V^{k}_{22} \quad A_2\,{}^{t}V^{k}_{12} \\
 & 0 & 0 & h_{k,2} & -A_2\,{}^{t}V^{k}_{23} \quad A_2\,{}^{t}V^{k}_{13}
\end{array}\right]
$$

node k

$$A_1 = h_{k,1}\,\partial_K\,\frac{\Gamma_3}{2}$$

$$A_2 = h_{k,2}\,\partial_K\,\frac{\Gamma_3}{2}$$

Table 1

$$
{}^{t}_{0}\underline{\tilde{S}}^{1} = \begin{bmatrix} {}^{t}_{0}\tilde{S}^{11}\,\underline{I}_3 & {}^{t}_{0}\tilde{S}^{12}\,\underline{I}_3 \\ \text{sym.} & {}^{t}_{0}\tilde{S}^{22}\,\underline{I}_3 \end{bmatrix} \qquad \text{(A4.4)}
$$

$$
\underline{I}_3 = \begin{bmatrix} 1 & 0 & 0 \\ & 1 & 0 \\ \text{sym.} & & 1 \end{bmatrix}
$$

Also,

$$
{}^{t}_{0}\underline{\bar{\bar{K}}}_{HL} = {}^{t}_{0}\tilde{S}^{13}\,{}^{t}_{0}\underline{\bar{\bar{K}}}^{1}_{HL} + {}^{t}_{0}\tilde{S}^{23}\,{}^{t}_{0}\underline{\bar{\bar{K}}}^{2}_{HL} \qquad \text{(A4.5)}
$$

It is immediate, by inspection, to determine ${}^{t}_{0}\underline{\bar{\bar{K}}}^{1}_{HL}$ and ${}^{t}_{0}\underline{\bar{\bar{K}}}^{2}_{HL}$ (see Tables 2 and 3).

$$
{}^{\tau}\bar{K}'_{NL} =
$$

$$
\begin{bmatrix}
\frac{1}{12}(1+\tau_2)\, a_1 \tau V'_{21} & \frac{1}{12}(1+\tau_2)\, a_1 \tau V'_{11} & 0 & 0 & 0 & 0 & 0 & 0 & 0 & 0 & 0 & 0 & 0 & 0 & 0 \\
\frac{1}{12}(1+\tau_2)\, a_1 \tau V'_{22} & \frac{1}{12}(1+\tau_2)\, a_1 \tau V'_{12} & 0 & 0 & 0 & 0 & 0 & 0 & 0 & 0 & 0 & 0 & 0 & 0 & 0 \\
\frac{1}{12}(1+\tau_2)\, a_1 \tau V'_{23} & \frac{1}{12}(1+\tau_2)\, a_1 \tau V'_{13} & 0 & 0 & 0 & 0 & 0 & 0 & 0 & 0 & 0 & 0 & 0 & 0 & 0 \\
0 & 0 & \frac{1}{12}(1+\tau_2)\, a_1 \tau V'_{21} & \frac{1}{12}(1+\tau_2)\, a_1 \tau V'_{22} & \frac{1}{12}(1+\tau_2)\, a_1 \tau V'_{23} & 0 & 0 & 0 & 0 & 0 & 0 & 0 & 0 & 0 & 0 \\
 & & \frac{1}{12}(1+\tau_2)\, a_1 \tau V'_{11} & \frac{1}{12}(1+\tau_2)\, a_1 \tau V'_{12} & \frac{1}{12}(1+\tau_2)\, a_1 \tau V'_{13} & 0 & 0 & 0 & 0 & 0 & 0 & 0 & 0 & 0 & 0 \\
 & & 0 & 0 & 0 & \frac{1}{12}(1+\tau_2)\, a_2 \tau V^2_{21} & \frac{1}{12}(1+\tau_2)\, a_2 \tau V^2_{22} & \frac{1}{12}(1+\tau_2)\, a_2 \tau V^2_{23} & 0 & 0 & 0 & 0 & 0 & 0 & 0 \\
 & & & & & \frac{1}{12}(1+\tau_2)\, a_2 \tau V^2_{11} & \frac{1}{12}(1+\tau_2)\, a_2 \tau V^2_{12} & \frac{1}{12}(1+\tau_2)\, a_2 \tau V^2_{13} & 0 & 0 & 0 & 0 & 0 & 0 & 0 \\
 & & & & & & & & \frac{1}{12}(1-\tau_2)\, a_3 \tau V^3_{21} & \frac{1}{12}(1-\tau_2)\, a_3 \tau V^3_{22} & \frac{1}{12}(1-\tau_2)\, a_3 \tau V^3_{23} & 0 & 0 & 0 & 0 \\
 & & & & & & & & \frac{1}{12}(1-\tau_2)\, a_3 \tau V^3_{11} & \frac{1}{12}(1-\tau_2)\, a_3 \tau V^3_{12} & \frac{1}{12}(1-\tau_2)\, a_3 \tau V^3_{13} & 0 & 0 & 0 & 0 \\
 & & & & & & & & & & & \frac{1}{12}(1-\tau_2)\, a_4 \tau V^4_{21} & \frac{1}{12}(1-\tau_2)\, a_4 \tau V^4_{22} & \frac{1}{12}(1-\tau_2)\, a_4 \tau V^4_{23} & 0 \\
 & & & & & & & & & & & \frac{1}{12}(1-\tau_2)\, a_4 \tau V^4_{11} & \frac{1}{12}(1-\tau_2)\, a_4 \tau V^4_{12} & \frac{1}{12}(1-\tau_2)\, a_4 \tau V^4_{13} & 0
\end{bmatrix}
$$

S Y M.

Table 2 ${}^{\tau}\bar{K}'_{NL}$

$$
{}^{\tau}\overline{K}^{2}_{NL} =
$$

$$
\begin{bmatrix}
\frac{1}{16}(1+\tau_i)\,a_1\tau V'_{21} & \frac{1}{16}(1+\tau_i)\,a_1\tau V'_{11} & 0 & 0 & 0 & 0 & 0 & 0 & 0 & 0 & 0 & 0 & 0 & 0 & 0 \\
-\frac{1}{16}(1+\tau_i)\,a_1\tau V'_{22} & \frac{1}{16}(1+\tau_i)\,a_1\tau V'_{12} & 0 & 0 & 0 & 0 & 0 & 0 & 0 & 0 & 0 & 0 & 0 & 0 & 0 \\
-\frac{1}{16}(1+\tau_i)\,a_1\tau V'_{23} & \frac{1}{16}(1+\tau_i)\,a_1\tau V'_{13} & 0 & 0 & 0 & 0 & 0 & 0 & 0 & 0 & 0 & 0 & 0 & 0 & 0 \\
0 & 0 & \frac{1}{16}(1+\tau_i)\,a_1\tau V'_{21} & \frac{1}{16}(1+\tau_i)\,a_1\tau V'_{11} & 0 & 0 & 0 & 0 & 0 & 0 & 0 & 0 & 0 & 0 & 0 \\
0 & 0 & -\frac{1}{16}(1+\tau_i)\,a_1\tau V'_{22} & \frac{1}{16}(1+\tau_i)\,a_1\tau V'_{12} & 0 & 0 & 0 & 0 & 0 & 0 & 0 & 0 & 0 & 0 & 0 \\
0 & 0 & -\frac{1}{16}(1+\tau_i)\,a_1\tau V'_{23} & \frac{1}{16}(1+\tau_i)\,a_1\tau V'_{13} & 0 & 0 & 0 & 0 & 0 & 0 & 0 & 0 & 0 & 0 & 0 \\
0 & 0 & 0 & 0 & -\frac{1}{16}(1-\tau_i)\,a_2\tau V^2_{21} & \frac{1}{16}(1-\tau_i)\,a_2\tau V^2_{11} & 0 & 0 & 0 & 0 & 0 & 0 & 0 & 0 & 0 \\
0 & 0 & 0 & 0 & -\frac{1}{16}(1-\tau_i)\,a_2\tau V^2_{22} & \frac{1}{16}(1-\tau_i)\,a_2\tau V^2_{12} & 0 & 0 & 0 & 0 & 0 & 0 & 0 & 0 & 0 \\
0 & 0 & 0 & 0 & -\frac{1}{16}(1-\tau_i)\,a_2\tau V^2_{23} & \frac{1}{16}(1-\tau_i)\,a_2\tau V^2_{13} & 0 & 0 & 0 & 0 & 0 & 0 & 0 & 0 & 0 \\
0 & 0 & 0 & 0 & 0 & 0 & -\frac{1}{16}(1-\tau_i)\,a_3\tau V^3_{21} & \frac{1}{16}(1-\tau_i)\,a_3\tau V^3_{11} & 0 & 0 & 0 & 0 & 0 & 0 & 0 \\
0 & 0 & 0 & 0 & 0 & 0 & -\frac{1}{16}(1-\tau_i)\,a_3\tau V^3_{22} & \frac{1}{16}(1-\tau_i)\,a_3\tau V^3_{12} & 0 & 0 & 0 & 0 & 0 & 0 & 0 \\
0 & 0 & 0 & 0 & 0 & 0 & -\frac{1}{16}(1-\tau_i)\,a_3\tau V^3_{23} & \frac{1}{16}(1-\tau_i)\,a_3\tau V^3_{13} & 0 & 0 & 0 & 0 & 0 & 0 & 0 \\
0 & 0 & 0 & 0 & 0 & 0 & 0 & 0 & \frac{1}{16}(1+\tau_i)\,a_4\tau V^4_{21} & \frac{1}{16}(1+\tau_i)\,a_4\tau V^4_{11} & 0 & 0 & 0 & 0 & 0 \\
0 & 0 & 0 & 0 & 0 & 0 & 0 & 0 & -\frac{1}{16}(1+\tau_i)\,a_4\tau V^4_{22} & \frac{1}{16}(1+\tau_i)\,a_4\tau V^4_{12} & 0 & 0 & 0 & 0 & 0 \\
0 & 0 & 0 & 0 & 0 & 0 & 0 & 0 & -\frac{1}{16}(1+\tau_i)\,a_4\tau V^4_{23} & \frac{1}{16}(1+\tau_i)\,a_4\tau V^4_{13} & 0 & 0 & 0 & 0 & 0
\end{bmatrix}
$$

S Y M.

Table 3 ${}^{\tau}\overline{K}^{2}_{NL}$

APPENDIX 5: Specialization of the new 4-node shell element, for a linear plate element

The formulation given in this appendix, similar to the one in Ref. [82-b], is a particular case of the shell element presented in Chapter 3 and [67], but it is important for two reasons. First, by concentrating on the linear analysis of plates we are able to very clearly and simply present the key ideas of our approach, and second, the plate element given here is more effective in plate analysis because no numerical integration is used through the element thickness.

a. Formulation of the element

As presented in detail in [29], the variational indicator of a Mindlin/Reissner plate is, in linear elastic analysis,

$$\Pi = \frac{1}{2}\int_A \underline{\varkappa}^T \underline{C}_b \underline{\varkappa}\, dA + \frac{1}{2}\int_A \underline{\gamma}^T \underline{C}_s \gamma\, dA - \int_A w p\, dA \qquad \text{(A5.1)}$$

where

$$\underline{\varkappa} = \begin{bmatrix} \beta_{x,x} \\ -\beta_{y,y} \\ \beta_{x,y} - \beta_{y,x} \end{bmatrix} \qquad \text{(A5.2)}$$

$$\underline{\gamma} = \begin{bmatrix} W,x + \beta_x \\ W,y - \beta_y \end{bmatrix} \qquad \text{(A5.3)}$$

$$\underline{C}_b = \frac{E\,h^3}{12(1-\nu^2)} \begin{bmatrix} 1 & \nu & 0 \\ \nu & 1 & 0 \\ 0 & 0 & \frac{1-\nu}{2} \end{bmatrix}; \underline{C}_s = \frac{E h k}{2(1+\nu)} \begin{bmatrix} 1 & 0 \\ 0 & 1 \end{bmatrix} \qquad \text{(A5.4)}$$

and, with reference to Fig. A5.1, β_x , β_y are the section rotations, W is the transverse displacement of the mid-surface of the plate, P is the distributed pressure loading, h is the thickness of the plate (assumed constant), and A is the area of the mid-surface of the plate. Also, E is Young's modulus, ν is Poisson's ratio and k is a shear correction factor (appropriately set to 5/6).

Perhaps the simplest way to formulate an element based on the variational indicator in Eq. (1) is to interpolate both the transverse displacements and the section rotations as follows

$$W = \sum_{i=1}^{7} h_i W_i$$

$$\beta_x = \sum h_i \theta_y^i \qquad \beta_y = \sum h_i \theta_x^i \qquad \text{(A5.5)}$$

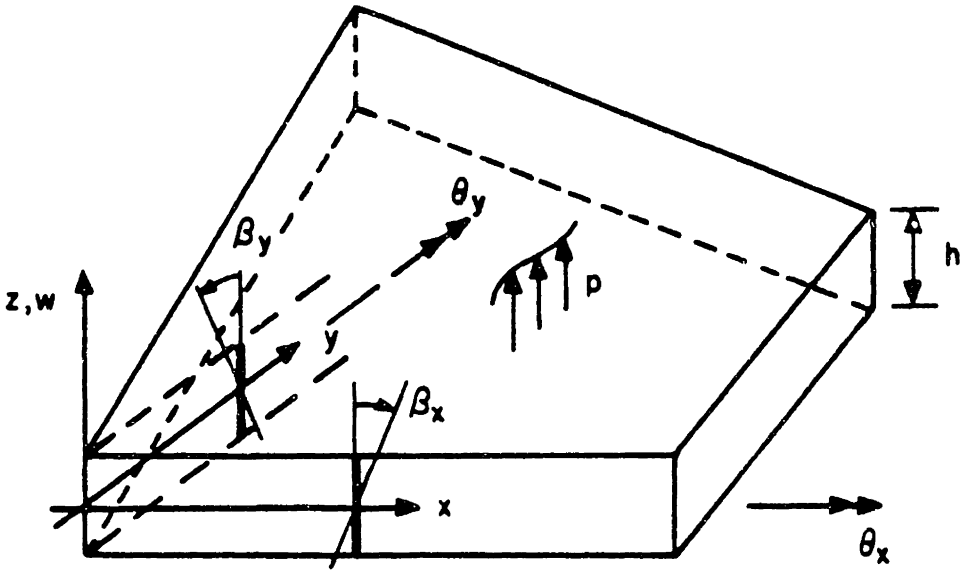
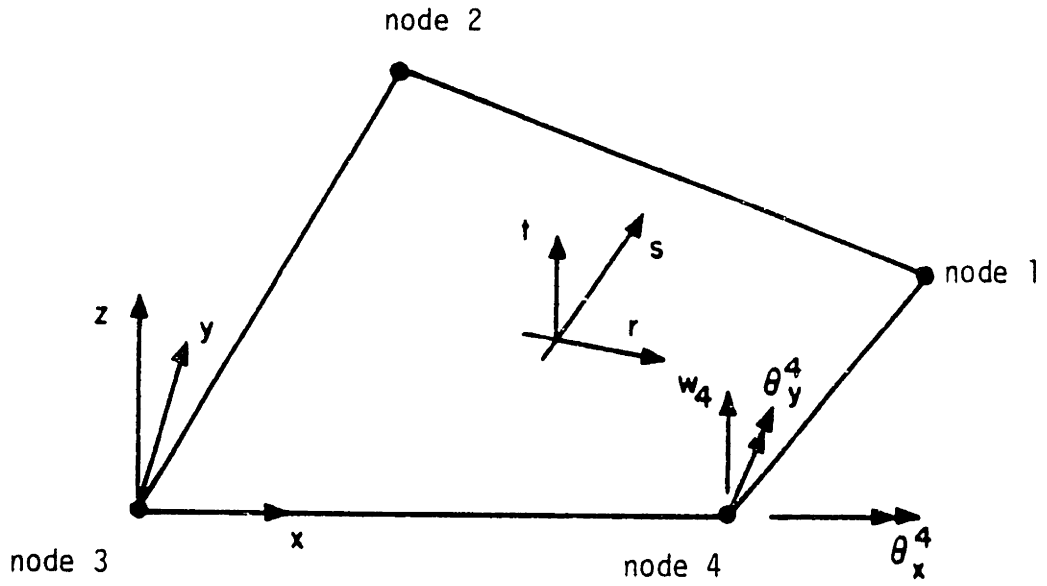


Figure A5.1 Notation used for Mindlin/Reissner plate theory

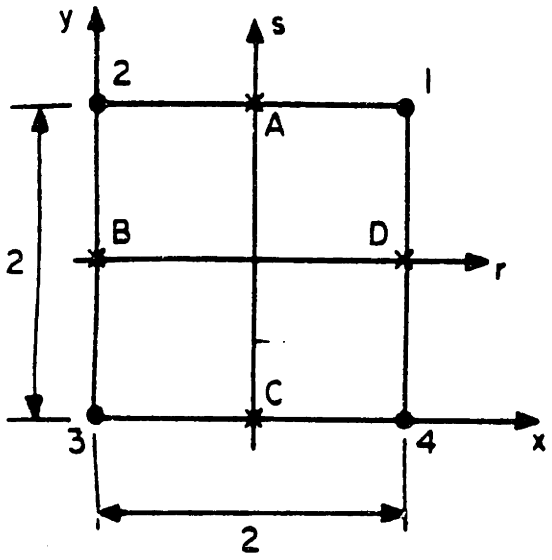
where the w_i , θ_y^i and θ_x^i are the nodal point values of the variables w, β_x and β_y , respectively, the $h_i(r,s)$ are the interpolation functions and q is the number of element nodes. A basic problem inherent in the use of the above interpolation is that when q is equal to four, see Fig. A5.2, the element "locks" when it is thin (assuming "full" numerical integration). This is due to the fact that with these interpolations the transverse shear strains cannot vanish at all points in the element when it is subjected to a constant bending moment. Hence, although the basic continuum mechanics assumptions contain the Kirchhoff plate assumptions, the finite element discretization is not able to represent these assumptions rendering the element not applicable to the analysis of thin plates or shells (see [29 , p. 240]). To solve this deficiency, various remedies based on selective and reduced integration have been proposed, but there is still much room for a more effective and reliable approach.

To circumvent the locking problem, we formulate the element stiffness matrix in our approach by including the bending effects and transverse shear effects through different interpolations, resulting in a mixed-formulation. To evaluate the section curvatures, $\underline{\kappa}$, we use Eq. (A5.2) and the interpolations in Eq. (A5.5). Hence, the element section curvatures are calculated as usual [29]; however, to evaluate the transverse shear strains we proceed differently.

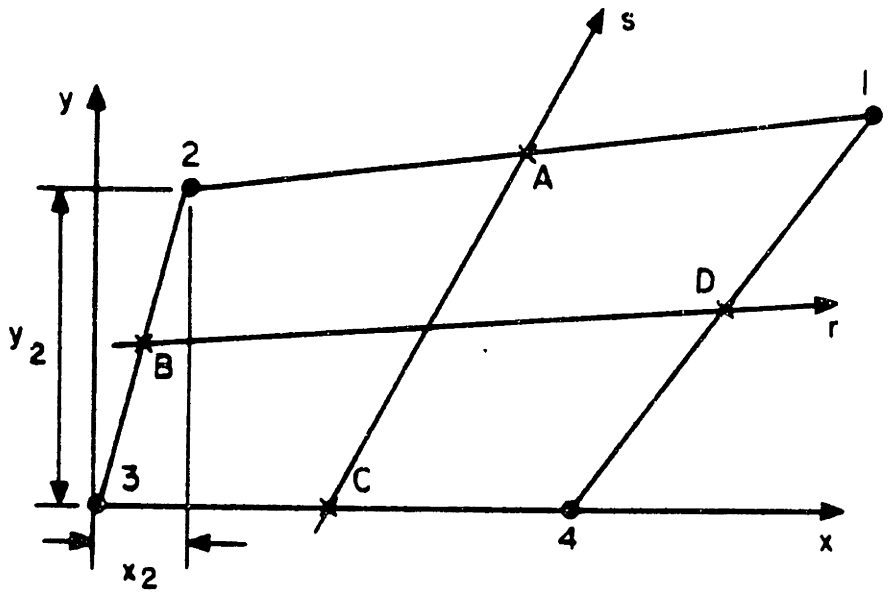
Consider first our element when it is of geometry 2 by 2 (for which the (x,y) coordinates could be taken to be equal to the (r,s) isoparametric coordinates). For this element we use the interpolation



View of general element



Special 2 by 2 element in the x-y plane



A general element in the x-y plane

Figure A5.2 Conventions used in formulation of 4 node plate bending element;
$h_1 = \frac{1}{4}(1+r)(1+s)$, $h_2 = \frac{1}{4}(1-r)(1+s)$, $h_3 = \frac{1}{4}(1-r)(1-s)$,
$h_4 = \frac{1}{4}(1+r)(1-s)$

$$\gamma_{rz} = \frac{1}{2}(1+s)\,\gamma_{rz}^{A} + \frac{1}{2}(1-s)\,\gamma_{rz}^{C}$$

$$\gamma_{sz} = \frac{1}{2}(1+r)\,\gamma_{sz}^{D} + \frac{1}{2}(1-r)\,\gamma_{sz}^{B} \qquad \text{(A5.6)}$$

where γ_{rz}^{A} , γ_{rz}^{C} , γ_{sz}^{D} and γ_{sz}^{B} are the (physical) shear strains at points A, B, C, and D. We evaluate these strains using the interpolations in Eq. (A5.5) to obtain

$$\gamma_{rz} = \frac{1}{2}(1+s)\left[\frac{w_1 - w_2}{2} + \frac{\theta_y^1 + \theta_y^2}{2}\right] + \frac{1}{2}(1-s)\left[\frac{w_4 - w_3}{2} + \frac{\theta_y^4 + \theta_y^3}{2}\right] \qquad \text{(A5.7-a)}$$

and

$$\gamma_{sz} = \frac{1}{2}(1+r)\left[\frac{w_1 - w_4}{2} - \frac{\theta_x^1 + \theta_x^4}{2}\right] + \frac{1}{2}(1-r)\left[\frac{w_2 - w_3}{2} - \frac{\theta_x^2 + \theta_x^3}{2}\right] \qquad \text{(A5.7-b)}$$

With these interpolations given, all strain-displacement interpolation matrices can directly be constructed and the stiffness matrix is formulated in the standard manner, see [29, p. 252].

Considering next the case of a general 4-node element, we use the same basic idea of interpolating the transverse shear strains, but - using Eq. (A5.6) - we interpolate the covariant tensor components measured in the (r,s) coordinate system. In this way we are directly taking account of the element distortion (from the 2 by 2 geometry). Using Eq. (A5.6) for the tensor shear strain components (as shown in [67]), we obtain

$$\gamma_{rz} = \frac{\sqrt{(C_x + r B_x)^2 + (C_y + r B_y)^2}}{8 \det \underline{J}}$$

$$\left\{(1+s)\left[\frac{w_1 - w_2}{2} + \frac{x_1 - x_2}{4}(\theta_y^1 + \theta_y^2) - \frac{(y_1 - y_2)}{4}(\theta_x^1 + \theta_x^2)\right]\right. \qquad \text{(A5.8-a)}$$

$$\left. + (1-s)\left[\frac{w_4 - w_3}{2} + \frac{x_4 - x_3}{4}(\theta_y^4 + \theta_y^3) - \frac{(y_4 - y_3)}{4}(\theta_x^4 + \theta_x^3)\right]\right\}$$

$$\gamma_{sz} = \frac{\sqrt{(A_x + s\,B_x)^2 + (A_y + s\,B_y)^2}}{8 \det \underline{J}}$$

$$\left\{ (1+\tau)\left[\frac{w_1 - w_4}{2} + \frac{x_1 - x_4}{4} (\theta_y^1 + \theta_y^4) - \frac{y_1 - y_4}{4} (\theta_x^1 + \theta_x^4) \right] \right.$$

$$+ (1-\tau)\left[\frac{w_2 - w_3}{2} + \frac{x_2 - x_3}{4} (\theta_y^2 + \theta_y^3) - \frac{y_2 - y_3}{4} (\theta_x^2 + \theta_x^3) \right] \qquad \text{(A5.8-b)}$$

where

$$\det \underline{J} = \begin{bmatrix} \frac{\partial x}{\partial \tau} & \frac{\partial y}{\partial \tau} \\ \frac{\partial x}{\partial s} & \frac{\partial y}{\partial s} \end{bmatrix} \qquad \text{(A5.9)}$$

and

$$A_x = x_1 - x_2 - x_3 + x_4 \qquad A_y = y_1 - y_2 - y_3 + y_4$$
$$B_x = x_1 - x_2 + x_3 - x_4 \qquad B_y = y_1 - y_2 + y_3 - y_4 \qquad \text{(A5.10)}$$
$$C_x = x_1 + x_2 - x_3 - x_4 \qquad C_y = y_1 + y_2 - y_3 - y_4$$

The above expressions for γ_{rz} and γ_{sz} give the (physical) shear strains corresponding to the r and s axes, and these components must be transformed to obtain γ_{xz} and γ_{yz}.

$$\gamma_{xz} = \gamma_{rz} \sin\beta - \gamma_{sz} \sin\alpha$$
$$\gamma_{yz} = -\gamma_{rz} \cos\beta + \gamma_{sz} \cos\alpha \qquad \text{(A5.11)}$$

where

$$\cos\alpha = \frac{A_x + s B_x}{\sqrt{(A_x + s B_x)^2 + (A_y + s B_y)^2}}$$

and (A5.12)

$$\cos\beta = \frac{C_x + r B_x}{\sqrt{(C_x + r B_x)^2 + (C_y + r B_y)^2}}$$

The formulation of the element is, in essence, a mixed formulation, in which the section rotations and transverse displacements are interpolated as given in Eq. (A5.5), the curvatures are obtained from the interpolated generalized displacements using Eq. (A5.2), and the shear strains are interpolated as given in Eq. (A5.6). For the use of Eq. (A5.6), the intensities of the transverse shear strains are constrained to equal the transverse shear strains derived from the displacements interpolation using the kinematic relations, at the points A, B, C, and D.

The element formulation can also be interpreted as based on a reduced penalty constraint between the transverse displacements and the section rotations, or the element can be viewed as based on a "discrete Mindlin/Reissner theory".

Since this plate element was directly derived from the general shell element, presented in Chapter 3, it also presents (assuming "full" numerical integration over r and s), the following properties:

- The element passes the patch test.
- The element can approximate the Kirchhoff hypothesis of negligible shear deformation effects and can be used for moderately thick and thin plates.

In practice, even for highly distorted elements we find that 2x2 Gauss integration is adequate.